

We are IntechOpen, the world's leading publisher of Open Access books Built by scientists, for scientists

6,300

Open access books available

171,000

International authors and editors

190M

Downloads

Our authors are among the

154

Countries delivered to

TOP 1%

most cited scientists

12.2%

Contributors from top 500 universities



WEB OF SCIENCE™

Selection of our books indexed in the Book Citation Index
in Web of Science™ Core Collection (BKCI)

Interested in publishing with us?
Contact book.department@intechopen.com

Numbers displayed above are based on latest data collected.
For more information visit www.intechopen.com



Accelerated Carbonation Curing as a Means of Reducing Carbon Dioxide Emissions

Hilal El-Hassan

Abstract

Globally, carbon dioxide concentration has immensely increased post the industrial revolution. With more greenhouse gases generated from human activities, more radiation is being absorbed by the Earth's atmosphere, causing an increase in global temperature. The phenomenon is referred to as the greenhouse gas effect. Alone, the cement industry contributes to approximately 5–8% of the global greenhouse gas emissions. Scientists and environmentalists have proposed different scenarios to alleviate such emissions. Among these, accelerated carbonation curing has been advocated as a promising mechanism to permanently sequester carbon dioxide. It has been applied to numerous construction applications, including concrete masonry blocks, concrete paving blocks, ceramic bricks, concrete pipes, and cement-bonded particleboards. Experimental results have shown that not only does it significantly reduce the carbon emissions, it also improves the mechanical and durability properties of carbonated products. The process enhances material performance, offers environmental benefits, and provides an excellent means to recycle carbon dioxide.

Keywords: carbonation curing, construction applications, mechanical properties, durability performance, environmental benefits

1. Introduction

Greenhouse gases are responsible for maintaining ecological balance and warmth on the planet. Of the total greenhouse gases, carbon dioxide is the main component comprising about 76% [1, 2]. With more CO₂ generated from industries, urbanization, and human activities, more radiation will be absorbed by the Earth's atmosphere, causing an increase in global temperature. The phenomenon is referred to as the greenhouse gas effect. In the 1990s, the rise in the planet's average temperature was 0.74°C. By the end of the 21st century, it is projected to increase by up to 6.4°C [3], instigating cataclysmic changes, as melting of polar ice, increase in sea levels, variations in rainfall and relative humidity (RH), and disappearance of fauna, among others [4].

Of the emitted carbon dioxide gas, the cement industry is responsible for about 5–8% [5]. Such emission is associated with the calcination of limestone (CaCO₃) to produce lime (CaO) and CO₂ and the burning of fossil fuels for clinkering and grinding. Indeed, it is estimated that the production of one ton of cement releases an equal weight of CO₂ gas [6]. Cement is the main constituent of concrete, the world's most

consumed man-made material with approximately one cubic meter being produced per capita [7]. With the rise in the human population, there is an ever-increasing demand for infrastructure and superstructures. Accordingly, more cement and concrete will be needed. As a result, cement production is becoming an increasing global pressing issue from an ecological, social, and environmental standpoint. To alleviate the emission of CO₂ associated with producing cement and concrete, scientists and environmentalists have proposed different schemes, including the replacement of cement with supplementary cementitious materials (SCMs), increase in energy efficiency, use of alternate fuels, and carbon sequestration [8].

The first scheme proposes modifications to the mixture proportions by replacing cement with SCMs, which are typically industrial waste materials. Cement kiln dust, a by-product of cement manufacturing, has been utilized in producing sustainable composites for construction applications with economic and environmental benefits [9–11]. Other industrial by-products, including fly ash, slag, rice husk ash, limestone filler, and silica fume, have also been used as partial cement replacement in the production of sustainable concrete [12–17]. The properties of so-produced concrete are equivalent, if not superior, to those of conventional cement-based counterparts. Furthermore, efforts have been made to fully replace cement in mortar and concrete. The resulting product has been denoted as alkali-activated or geopolymer mortar/concrete. Numerous studies have investigated the fresh and hardened properties of this novel material and have provided valuable input on its contribution to sustainable construction [18–43]. Nevertheless, the availability and innate compositional variability of the industrial by-products pose a challenge to the adoption and progression of this CO₂ mitigating strategy.

Cement-related carbon emissions could also be reduced by increasing energy efficiency or utilizing alternative fuels during cement production. The use of blended cements, high-activation grinding, and high-efficiency separators, driers, calciners, and clinker cools have been reported to significantly reduce the CO₂ emissions and energy requirements by the cement industry [44–47]. Yet, the suggested modifications in this scheme may not always be practical or economically feasible. Conversely, some studies aimed to alleviate the carbon emissions associated with the generated thermal energy by replacing fossil fuels with alternative fuels, including scrap tires, biomass residues, waste oils, plastics, slaughterhouse residues, spent pot lining, and sewage sludge [48–53]. The scenario is considered environment-friendly, as it conserves natural resources and recycles industrial wastes [54]. However, the different characteristics of these alternative fuels compared to fossil fuels have led to uneven heat distribution, unstable precalciner operation, and dusty kilns, among other complications [55].

While CO₂ emissions could be substantially reduced using the first three methods, they may not always be practical, feasible, or reliable. On the other hand, carbon sequestration or storage has been shown to be a more viable scheme due to its applicability to stationary point sources over the short term. Geological and ocean storage have been mainly practiced for the past few decades [56]. Nevertheless, mineral sequestration has shown great potential, specifically through the accelerated carbonation of hardened cement and concrete.

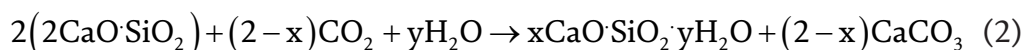
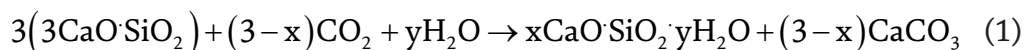
Carbonation is a curing mechanism applied to fresh concrete, i.e. within the first 24 hours after casting. It entails an exothermic chemical reaction between CO₂ and calcium-carrying compounds in cement. Its advantages are three-fold: 1) rapid strength gain, 2) enhanced durability performance, and 3) permanent sequestration of carbon dioxide gas [57, 58]. This chapter summarizes the research and experimental findings of collective studies that have utilized accelerated carbonation in construction applications, including concrete masonry blocks, concrete paving blocks, concrete pipes, reinforced concrete beams, cement-bonded particleboards,

and ceramic bricks. Other topics are also covered, comprising the fundamentals, processes, characterization techniques, and environmental benefits of carbonation of concrete. This work aims to shed light on the technical and environmental gains of accelerated carbonation and its applicability to different construction applications as a means of reducing cement-related carbon dioxide emissions.

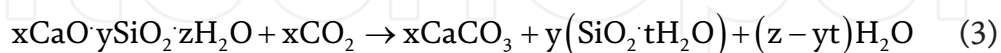
2. Fundamentals of carbonation

2.1 Reaction kinetics

Carbonation is a physicochemical reaction between cement and carbon dioxide gas in aqueous conditions. More specifically, it is the calcium silicates and their hydration products that undergo carbonation. At early age, calcium silicates, in the form of alite ($3\text{CaO}\cdot\text{SiO}_2$, or C_3S) and belite ($2\text{CaO}\cdot\text{SiO}_2$, or C_2S), react with CO_2 in the presence of water to produce calcium silicate hydrate ($x\text{CaO}\cdot\text{SiO}_2\cdot y\text{H}_2\text{O}$, or C-S-H) and calcium carbonate (CaCO_3). The reaction is primarily dependent on the rate of CO_2 diffusion, which, in turn, is controlled by the concentration of CO_2 and its pressure during carbonation [59]. The exothermic reactions are shown in Eq. (1) and (2) [60, 61].



Carbonation is an accelerated hydration reaction; yet, it is different than typical hydration of cement with water, as calcium carbonate formed instead of calcium hydroxide ($\text{Ca}(\text{OH})_2$) [60, 61]. In Eq. (1) and (2), the values of x and y depend on the extent of reaction, whereby the theoretical maximum degree of reactivity is 50% of the cement mass [62]. In the event of extensive carbonation exposure, CO_2 may decalcify the newly-formed C-S-H to produce silica gel (SiO_2) and calcium carbonate, as per Eq. (3) [63]. However, this reaction is not likely to occur in the short-term accelerated carbonation curing regimes employed in the studies addressed herein.



Moreover, the carbonation reaction does not consume all C_3S and C_2S particles, allowing for their subsequent hydration in a post-carbonation moist curing environment [64]. Accordingly, the end-result cementitious matrix is an intermix of C_2S , C_3S , CaCO_3 , C-S-H, and $\text{Ca}(\text{OH})_2$ [65–70].

2.2 Characterization of the reaction products

Carbonation of calcium silicates (C_3S and C_2S) is a form of mineral carbon sequestration that converts carbon dioxide gas into thermodynamically stable calcium carbonate. The calcium carbonate has been detected in three polymorph phases, namely aragonite, vaterite, and calcite [61]. Microstructure analysis showed that the first two polymorphs formed due to carbonation of C-S-H, while the third

one was a product of carbonating calcium silicates [71, 72]. Yet, among the three, calcite has been predominantly identified as the main reaction product of accelerated carbonation. In fact, thermogravimetric analysis (TGA) and X-ray diffraction (XRD) have shown that poorly crystalline aragonite and vaterite transformed into the more stable crystalline calcite polymorph during subsequent hydration [66, 73]. This phenomenon is shown in the XRD spectra of **Figure 1**.

While calcium carbonate has been highlighted as the main carbonation reaction product, C-S-H gel has been identified on fewer occasions. Using XRD, C-S-H was qualitatively detected as a slight increase in the baseline between 25 and 35°2θ [66, 73]. This C-S-H was similar in its amorphous morphology to that formed during typical C₃S hydration but different in that it was characterized by a lower

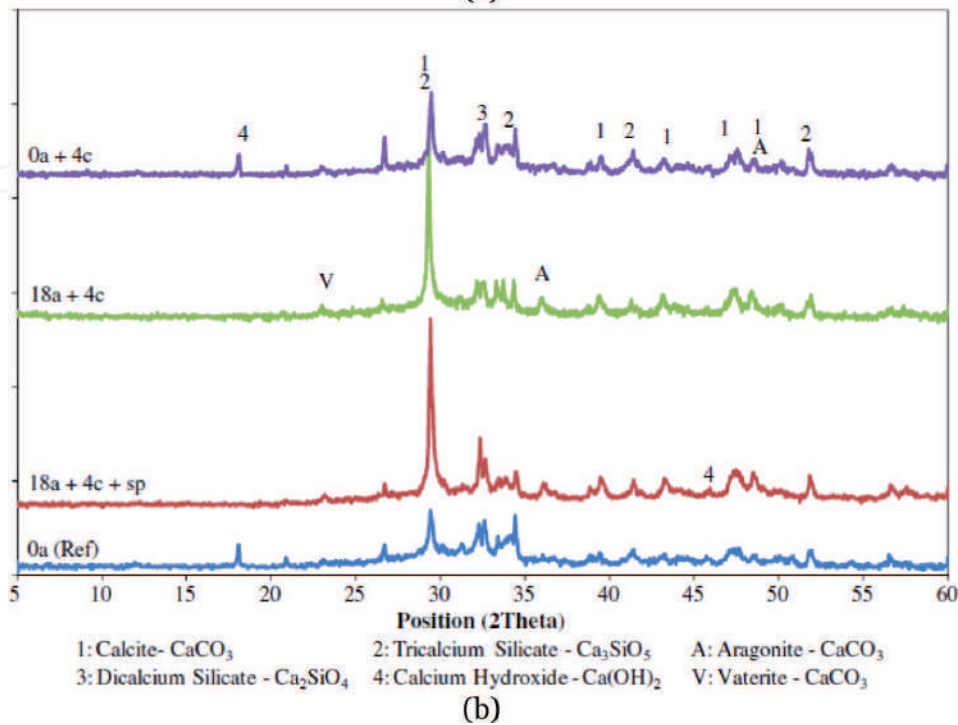
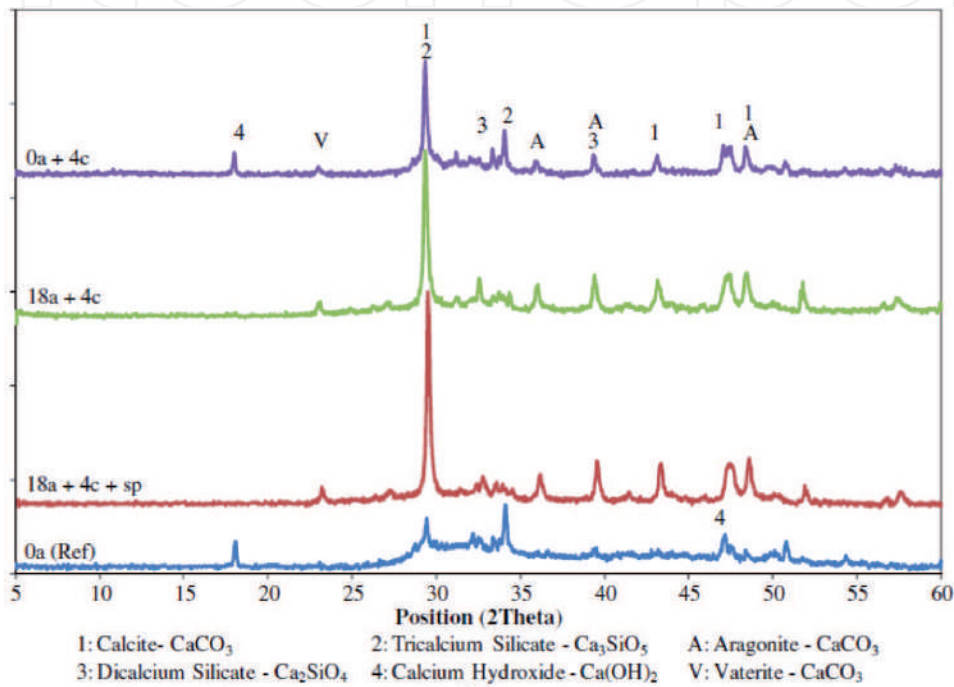


Figure 1. XRD pattern of concrete hydration- and carbonation-cured concrete at the age of (a) 1 day and (b) 28 days [66]. Reproduced with permission from the publisher.

CaO-to-SiO₂ ratio [71, 74, 75]. Actually, it was believed that a high degree of carbonation reaction (carbon uptake exceeding 18%, by cement mass) led to intermixing amorphous C-S-H with dominant CaCO₃ to form a calcium silicate hydrocarbonate product, rendering it difficult to be distinctively identifiable [66, 71]. Conversely, lower reactivity (carbon uptake below 10%, by cement mass) integrated small CaCO₃ crystals into a C-S-H-dominant nanostructure [65].

The morphology of these reaction products has also been studied. Calcium carbonate, in its three polymorphs, was reported in different shapes. Cubic, crystal shapes were identified, as depicted in **Figure 2**, when ordinary Portland cement (OPC) concrete was exposed to simultaneous carbonation and chloride ion ingress [76]. Successive preconditioning and carbonation curing of OPC paste and concrete presented amorphous C-S-H gel, calcium hydroxide hexagons, and amorphous calcium carbonate, as shown in **Figure 3a** [65]. A similar morphology is illustrated in **Figure 3b**, whereby OPC concrete made with drinking water treatment sludge was carbonated for 20 hours after 4 hours of preconditioning [77]. Further, an amorphous microstructure with a matrix comprising C-S-H and CaCO₃ was reported when OPC concrete was carbonated for 4 hours after 18 hours of preconditioning (**Figure 4a**). Similar findings have been reported in other studies [68, 78, 79]. Conversely, the morphology of Portland limestone cement (PLC) concrete exposed to a similar carbonation scheme encompassed ball-like forms covered with sharp crystals, as presented in **Figure 4b** [80]. Compared to carbonated OPC concrete, the microstructure of counterparts made with PLC was more porous with higher degree of crystallinity. It was believed that the presence of fine limestone in PLC may have served as nucleation sites for calcium carbonate crystal growth [80].

3. Carbonation process

With the advanced understanding of accelerated carbonation, more research has adopted carbonation curing for precast concrete products. The process promises to

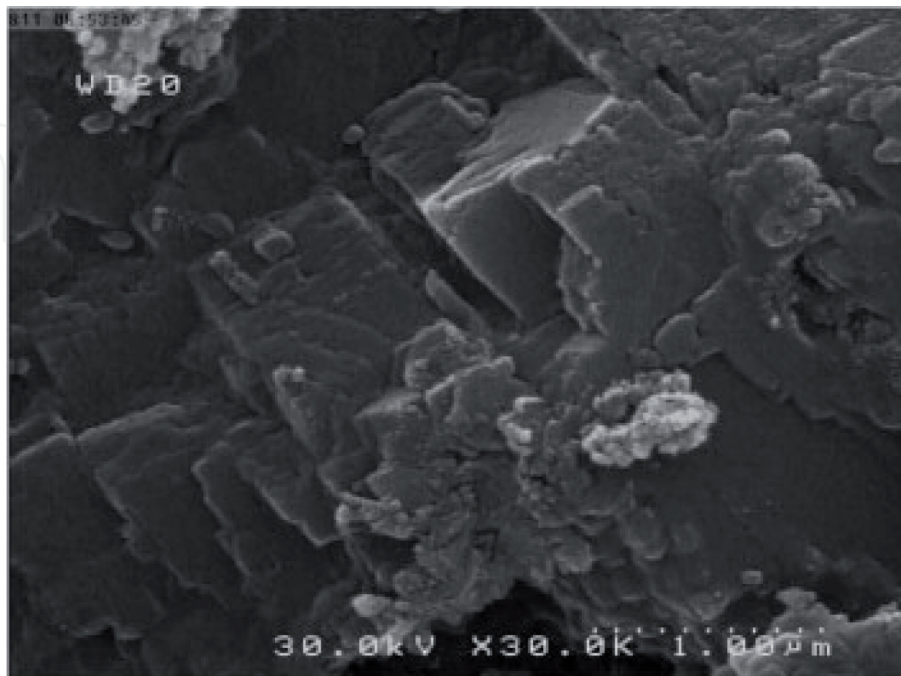
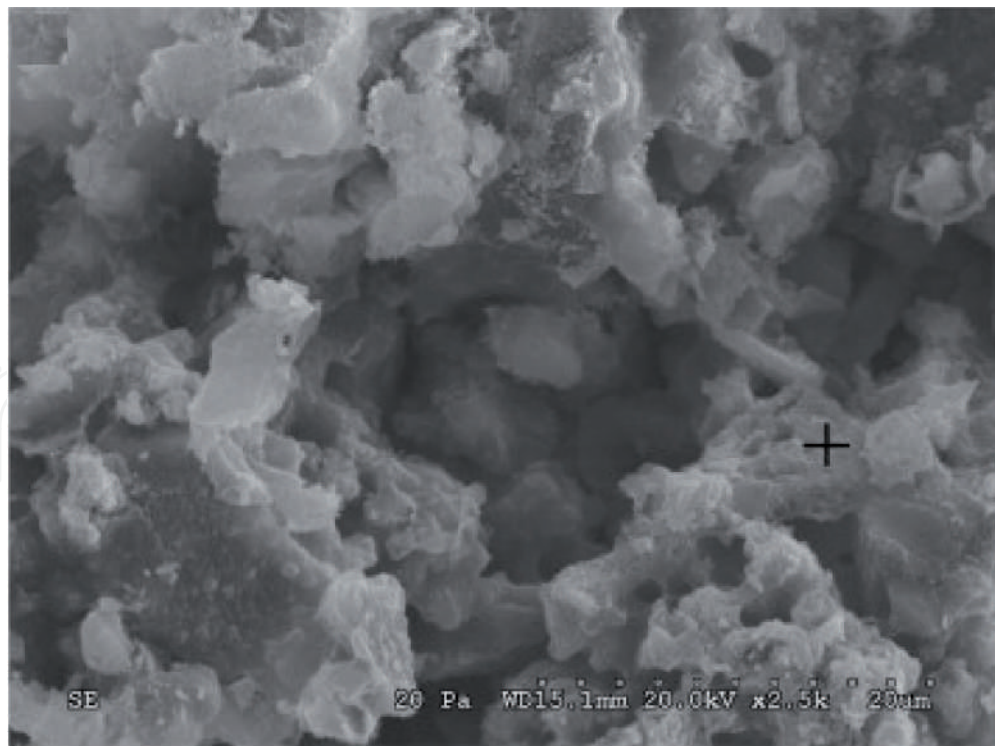
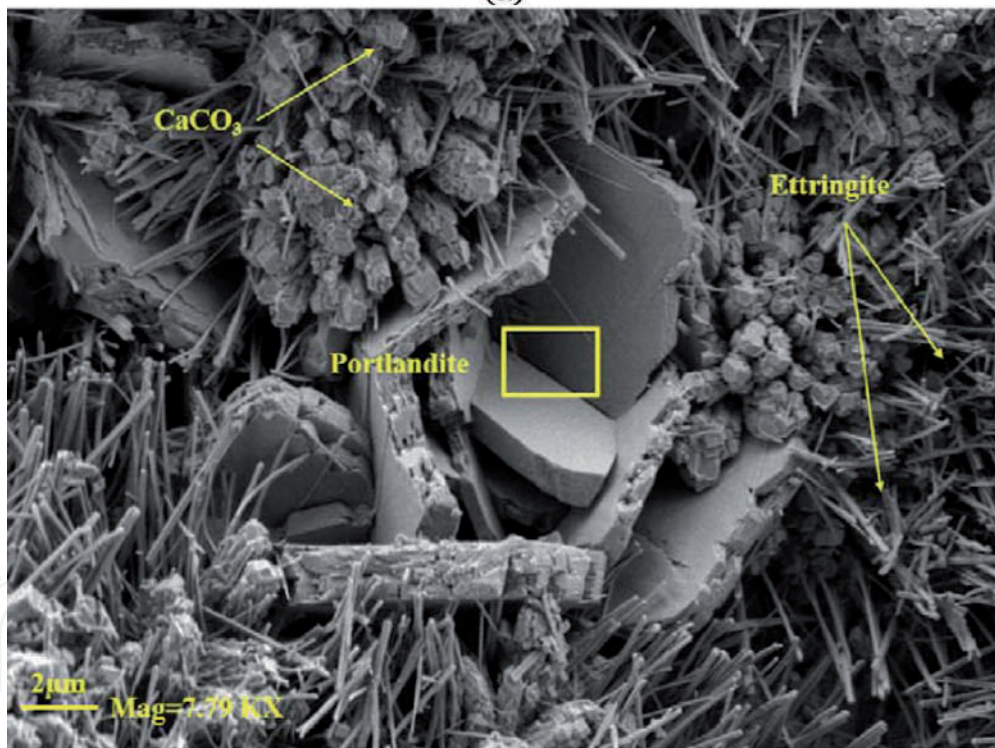


Figure 2.
*Morphology of cementitious matrix exposed to simultaneous carbonation and chloride ion ingress [76].
Reproduced with permission from the publisher.*



(a)



(b)

Figure 3. Morphology of cementitious matrix exposed to (a) 18-hour preconditioning and 2-hour carbonation [18], (b) 4-hour preconditioning and 18-hour carbonation [30]. Reproduced with permission from the publisher.

alleviate anthropogenic emissions through a mineral carbon sequestration technique. However, the environmental impact of carbonation is related to the degree of reaction, which is a function of the availability of water and pore precipitation sites. As such, different curing regimes have been adopted to optimize the amount of water for the highest reaction efficiency. These curing regimes were somewhat different in the adopted duration, temperature, and relative humidity. Yet, they had commonly implemented a three-phase curing process, namely preconditioning, carbonation curing, and post-carbonation hydration.

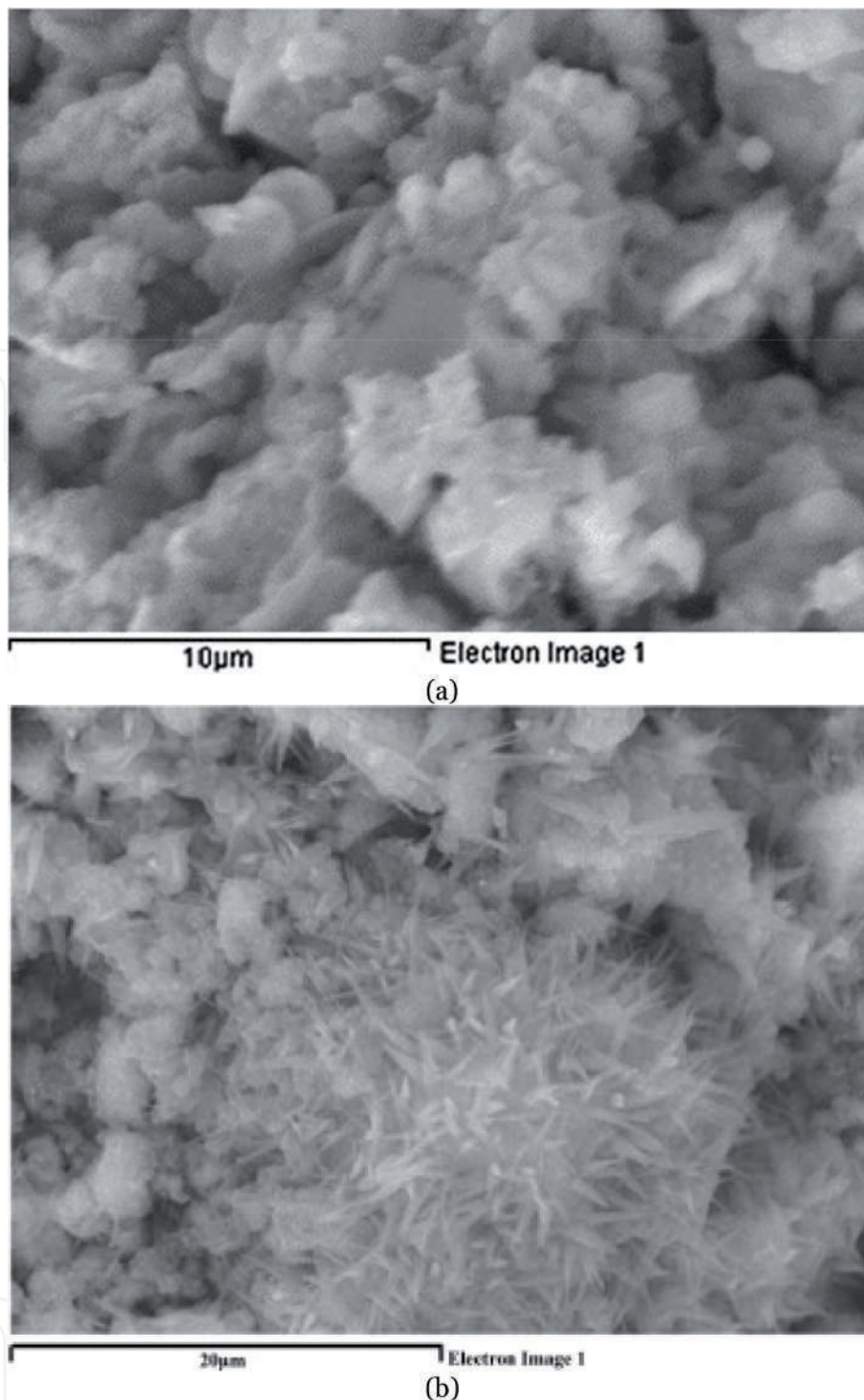


Figure 4.
SEM micrograph of carbonated (a) OPC concrete [66], (b) PLC concrete [80]. Reproduced with permission from the publisher.

3.1 Preconditioning

Past studies have reported that free water was necessary to facilitate the dissolution of CO_2 , however excess water obstructed its penetration through the available porous path [66]. As such, preconditioning was introduced to optimize the amount of water prior to exposing the designated samples to carbon dioxide gas. The adoption of such a process led to a superior carbonation degree and enhanced long-term hydration [81].

For dry mixes, preconditioning took place immediately after casting and before the initial setting of the mix [65, 70, 73, 80, 82]. Conversely, wet mixes were only

preconditioned after the initial setting [67, 83]. In general, the conditions comprised a duration, temperature, and relative humidity in the ranges of 2–24 hours, 20–25°C, and 40–60%, respectively [66, 67, 70, 73, 80, 82–86]. The effect of preconditioning at 25°C and 50% relative humidity on the water content during 14-day preconditioning is illustrated in **Figure 5**. To simulate industrial practice and limit the total curing time window to 24 hours, a maximum preconditioning duration of 18 hours was recommended [82]. At the end of the preconditioning phase, the cementitious matrix would include anhydrous and hydrated calcium silicate compounds.

3.2 Carbonation curing

Carbonation curing encompasses the time period in which concrete is exposed to carbon dioxide gas. Typically, CO₂ is released into a closed chamber and left for a certain duration and under specific conditions for the reaction to take place. A static carbonation system has been typically adopted by most researchers, as shown in **Figure 6a** [66, 70, 80, 82, 85, 87–93]. This carbonation scheme utilized a closed system, whereby the water that evaporated due to the exothermic reaction was included in the estimation of the degree of carbonation. Nevertheless, the reaction was hindered through the precipitation of calcium carbonate particles in the available porous space, leading to a decrease in porosity and retarded diffusivity. To overcome this challenge, a pseudo-dynamic carbonation setup was devised (**Figure 6b**) [73, 94]. This system removed surface free water in a controlled environment and enhanced carbon dioxide penetration by creating a route of capillaries through the sample. It is worth noting that both systems employed a vacuum prior to injecting 99%-pure CO₂ and the pressure was set to 1 bar. Several other researchers used a flue gas to enhance the environmental impact of carbonation, however, the degree of reaction was lesser [67, 95, 96]. Higher pressures of up to 5 bars were also employed [70, 84, 85, 97–99]. Although some promising results were reported when carbonation was utilized at higher pressure, the applicability and feasibility of adopting pressurized carbonation by the industry are yet to be evaluated.

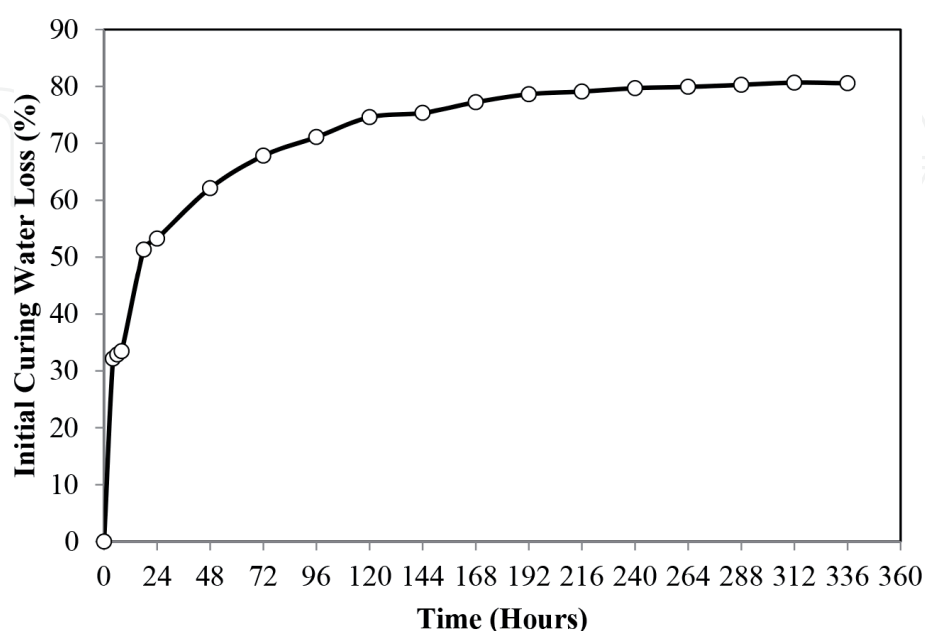


Figure 5. Water loss during preconditioning of lightweight concrete [82]. Reproduced with permission from the publisher.

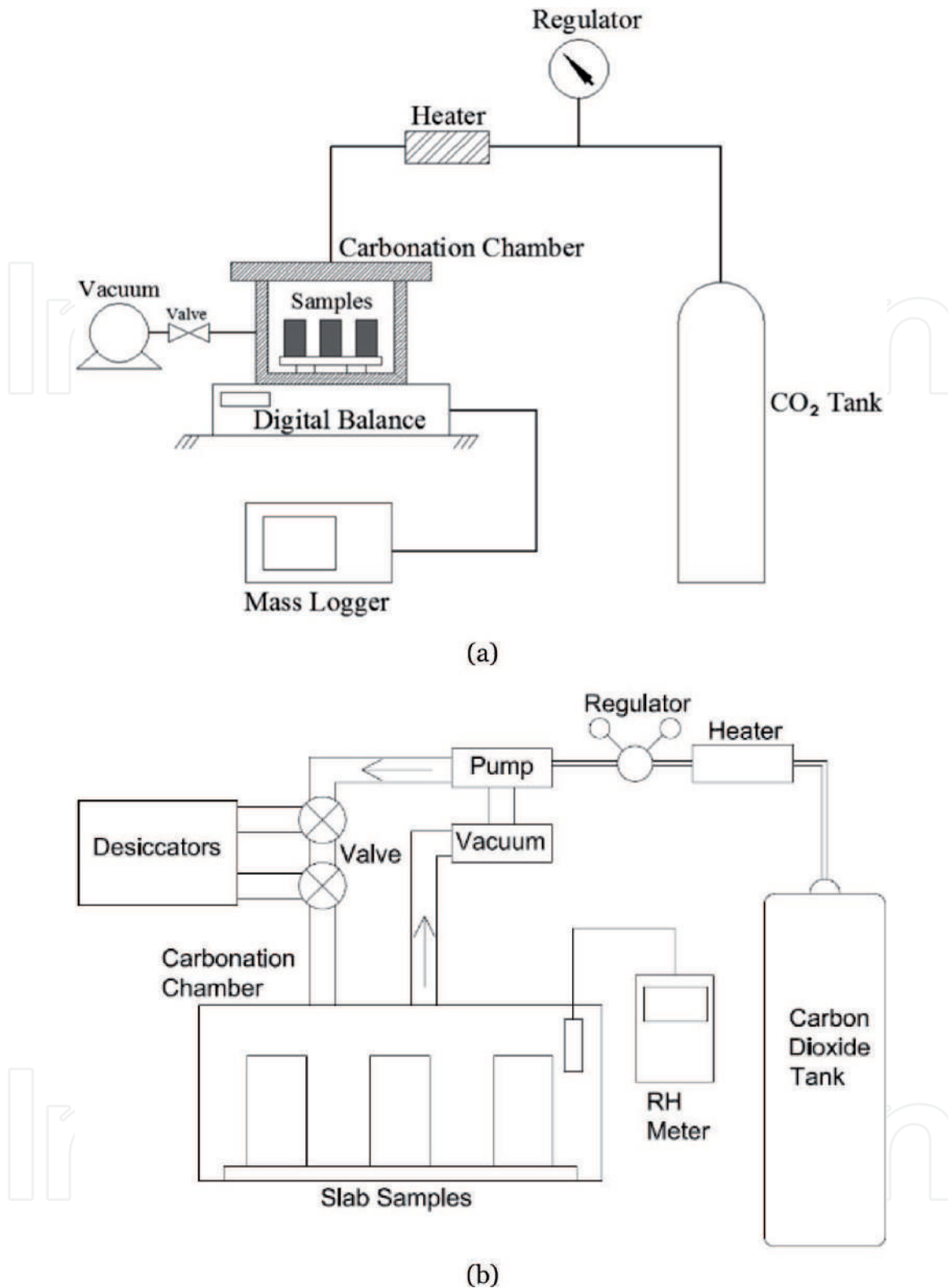


Figure 6.
(a) Static and (b) dynamic carbonation setups [73, 92]. Reproduced with permission from the publisher.

3.3 Post-carbonation hydration

The third phase of the carbonation process is the post-carbonation hydration. This step is critical to restore the water lost during preconditioning and the exothermic carbonation reaction and to promote subsequent hydration of unreacted hydraulic cement phases. Early research has reported up to 45% increase in the compressive strength when samples were placed in water for 3 days after

carbonation [64]. Other work incorporated spraying 4-hour carbonated concrete samples every other day until the age of 7 days [82]. The compressive strength increased by 20% compared to carbonated samples left to cure in open air. It is believed that such improvement in mechanical properties is primarily owed to the enhanced pore structure [84].

4. Carbonation degree and characterization techniques

Experimental research findings have provided evidence of the feasibility of utilizing carbonation curing for precast concrete products. Yet, the construction industry has not widely adopted it. To promote its utilization and adoption, most past studies aimed to augment the environmental benefit by maximizing the degree of carbonation reaction, which was typically characterized by the carbon uptake. One way to measure the carbon uptake was by examining the mass gained during the carbonation period, assuming homogeneous carbonation across the sample. Because the system was treated as a closed one, the water lost during the exothermic carbonation reaction was collected and added to the final sample mass. Based on Eq. (4), the carbon uptake is the difference in mass between before and after carbonation with the addition of the mass of water lost as a function of the mass of cement. This method has been implemented in several past studies [60, 66, 70, 73, 74, 80, 82, 89, 100–102].

$$\text{Carbon uptake (\%)} = \frac{\text{Final mass} - \text{Initial mass} + \text{water lost}}{\text{Mass of cement}} \times 100\% \quad (4)$$

Thermal analysis is another means of measuring the absolute carbon uptake. In this technique, a thermogravimetric analyzer (TGA) was utilized to monitor the mass loss of a powder sample of carbonated concrete with heat [103]. Alternatively, concrete chunks were decomposed in an electrical muffle furnace by raising the temperature from 25°C to approx. 1000°C. Within this range, multiple hydration and carbonation products were decomposed. The temperature ranges 105–200°C, 200–420°C, 420–550°C, 550–720°C, and 720–950°C were associated with the decomposition of low-temperature C-S-H and ettringite, well-formed C-S-H and C-A-H, calcium hydroxide, poorly crystalline calcium carbonate (vaterite and aragonite), and well crystalline calcite, respectively [66, 71, 73, 80, 81, 104, 105]. However, these ranges slightly differed depending on the type of binder used and the mixture proportions in general, and may even result in an overlap between carbonates and hydrates. To overcome this problem, Fourier transform infrared spectroscopy (FTIR) was employed alongside TGA, as shown in **Figure 7** [106]. It is a vibrational spectroscopic analytical technique that could detect calcium carbonate from the C-O characteristic peak at a wavelength of 1415 cm⁻¹ [106]. Other analytical tools have also been utilized together with TGA to identify carbonation products, including nuclear magnetic resonance (²⁹Si NMR) and XRD [65].

Carbon uptake was also determined by employing coulometric titration in a solution of hydrochloric acid [107]. The technique involved submerging a carbonated concrete powder in the acid solution and measuring the released carbon using the coulometer. The carbon uptake was then obtained using stoichiometric proportions. It is worth noting that thermal analysis and coulometric titration decompose all the carbonates present in the concrete. In an attempt to improve the sustainability of cement, some manufacturers have been replacing

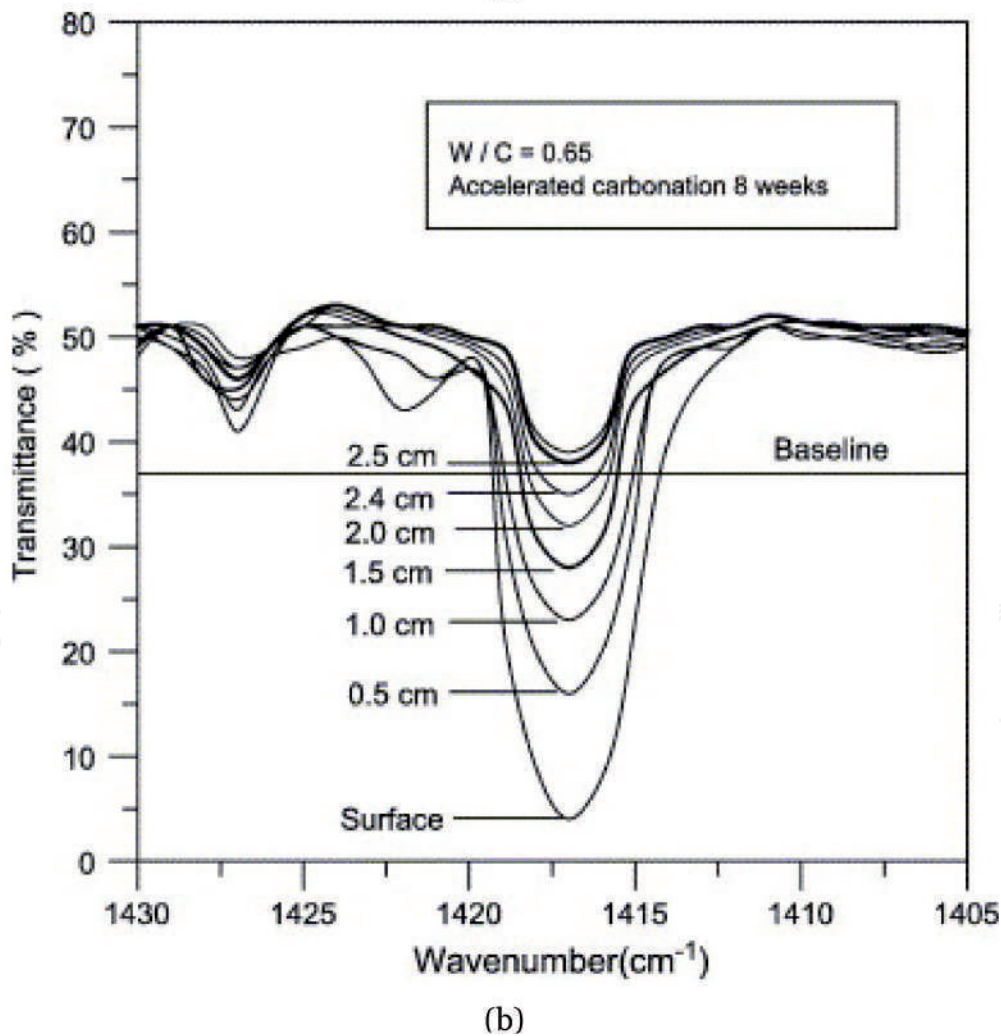
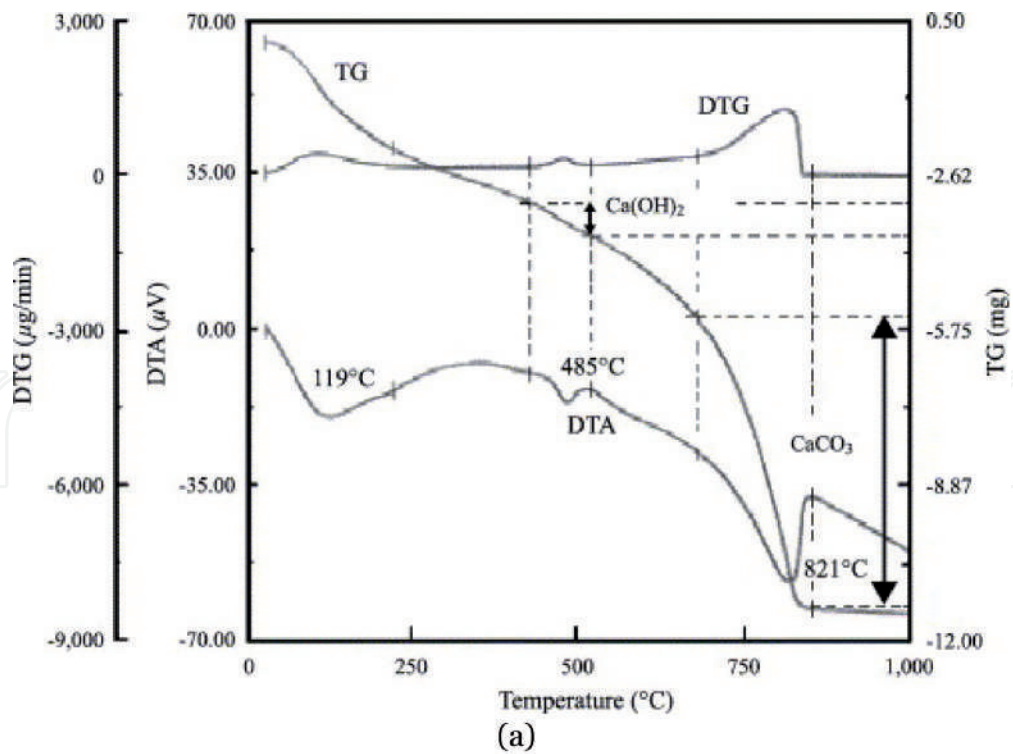


Figure 7.
(a) Thermogravimetric curves and (b) FTIR spectra of carbonated concrete [106]. Reproduced with permission from the publisher.

cement with certain amounts of limestone powder. Such limestone should be deducted from the overall measured carbon content to obtain the absolute carbon uptake [80, 108].

5. Carbonation in construction applications

Carbonation curing has been investigated for precast concrete products as a sustainable alternative curing regime to the more typically used steam and moist curing techniques. This section summarizes the collective studies that have examined the effect of accelerated carbonation on the performance of concrete masonry blocks, concrete paving blocks, concrete pipes, reinforced concrete beams, cement-bonded particleboards, and ceramic materials.

5.1 Concrete masonry blocks

Accelerated carbonation has been examined as a sustainable curing technique to replace steam curing for concrete blocks. Past studies have examined the mechanical and durability properties of concrete masonry units made with OPC and cured following 0- to 18-hour initial air curing and 2- to 4-hour static carbonation [82, 86, 87, 101, 109, 110]. The carbon uptake reached up to 24%, by cement mass, representing a 48% degree of reaction. The compressive strength within 1 day and at 28 days was comparable to that of steam- and moist-cured counterparts, with values reaching up to 10 and 39 MPa, respectively. It is worth noting that the highest carbon uptake and strength results were noted for samples that were preconditioned for 18 hours in open air prior to carbonation [82, 86, 109, 110]. Additionally, carbonation improved the resistance to chloride penetration by 1.4 and 6.2 times compared to the two conventionally-cured concrete, respectively, and enhanced resistance to sulfate attack by at least 1.5 times [101]. Also, carbonation-cured concrete (18a + 4c and 18a + 4c + sp) had 2 to 3 times better freeze-thaw resistance than concrete cured using steam (2a + 4s) or moist curing (0a), as shown in **Figure 8** [87].

When OPC was replaced by PLC, similar trends related to mechanical properties were noted, but the strength was ultimately lower due to a more porous and crystalline microstructure, as noted in **Figure 4** [66, 80]. Furthermore, concrete blocks

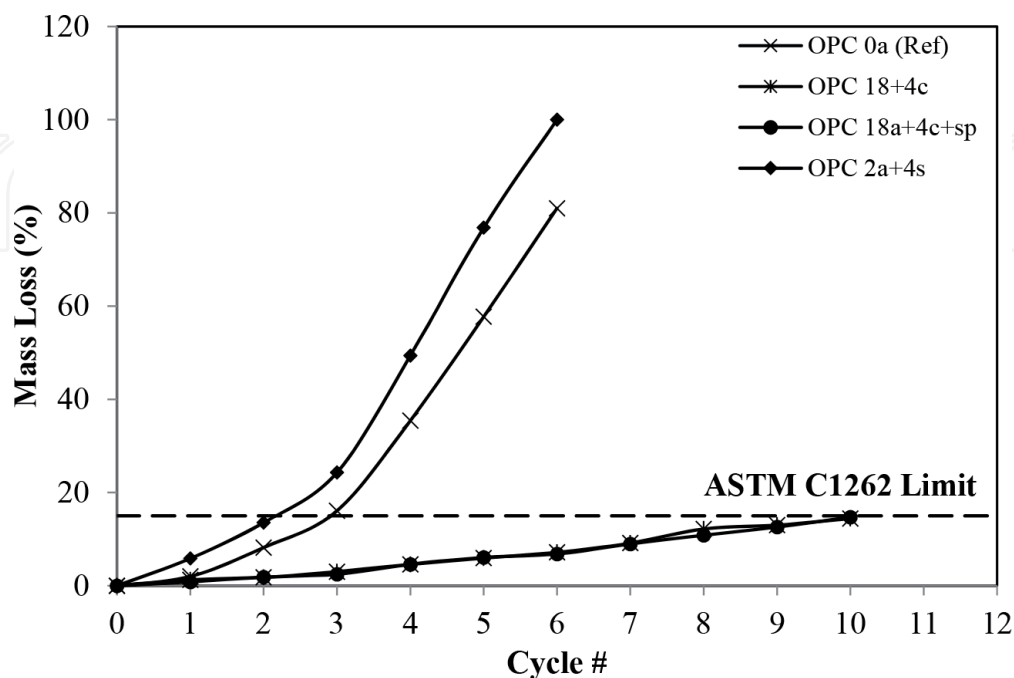


Figure 8. Freeze-thaw resistance of carbonated and hydrated concrete [87]. Reproduced with permission from the publisher.

were made with partial replacement of fine aggregates with drinking water treatment sludge and subjected to carbonation [77, 111]. The 1- and 28-day compressive strengths of carbonation-cured concrete blocks were up to 273 and 42% higher than those of normally-cured counterparts, respectively. Splitting tensile strength of the former was also higher than the latter but by no more than 45%. The durability of the concrete blocks was improved, evidenced by the reduction in water capillary absorption and better resistance to sulfate attack. It is believed that this enhancement in durability performance was owed to the pore-filling capacity of newly-formed calcium carbonate [77, 111]. The only detrimental effect of carbonation curing was the increased leaching of aluminum and copper ions, especially for the first 3 days. Nevertheless, the total 60-day leaching concentrations were within the acceptable range, indicating that carbonated concrete blocks made with drinking water treatment sludge were environment-friendly construction materials [111].

5.2 Concrete paving blocks

Paving blocks are precast non-reinforced concrete products used in construction applications, including pedestrian and vehicle pavements. With no steel reinforcement and the ability to mass-produce in a precast concrete plant, it is an ideal construction product that could sequester CO₂ through accelerated carbonation curing. In one study, Wang, Yeung [102] examined the use of CO₂ curing to create high performance, low-carbon paving blocks made with contaminated sediment and binary cement. Concrete samples were left to cure in a waterproof membrane until test age, after which they were placed in a drying chamber for 4 hours and cured with CO₂ gas for 24 hours at 0.1 bar above atmospheric pressure. Results of **Figure 9** show that the compressive strength of carbonation-cured concrete blocks was at least 2 times higher than that of air-cured counterparts. Evidently, carbonation curing accelerated the transformation of anhydrous phases into carbonates, while also promoting the formation of more hydrates during subsequent hydration.

Accelerated carbonation has also been employed to cure concrete paver blocks using pure CO₂ and flue gas [112–114]. After preconditioning, concrete samples were exposed to 2 to 4-hour carbonation and then, placed in a mist room to promote subsequent hydration up to 28 days. The CO₂ uptake was reported to be 3.29

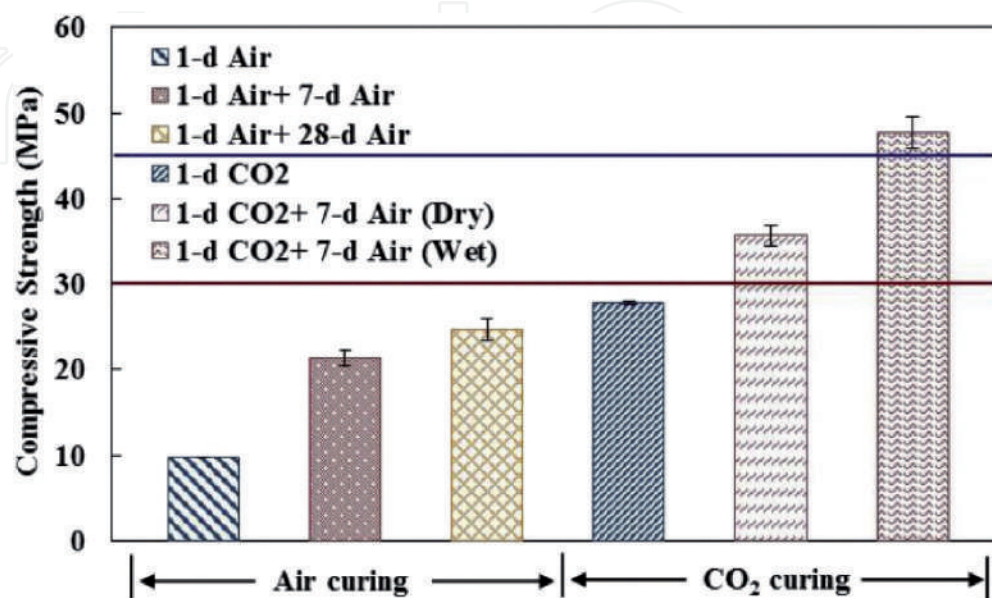


Figure 9. Compressive strength of concrete paving blocks with various curing methods [102]. Reproduced with permission from the publisher.

and 10.38%, by cement mass, for samples that were carbonated in 20 and 99% CO₂, respectively. Such lower uptake in the former was due to the lower CO₂ concentration, leading to less CaCO₃ formation and lower compressive strength than the latter. This also resulted in higher water absorption and inferior resistance to efflorescence [112, 113]. In addition, Shao and Lin [114] reported up to 60 times more freeze–thaw resistance when concrete paver blocks were carbonated rather than hydrated.

5.3 Concrete pipes

Past research has shown that carbonation curing is best applied to fresh concrete directly after casting to promote the chemical reaction between calcium silicates and CO₂ gas. Wet mixes are problematic when demolding within the first few minutes, while dry mixes are ideal for such applications. Concrete pipes are among the different types of concrete products that utilize dry mixes with zero slump. Accordingly, carbonation curing of concrete pipes has been investigated [114]. Samples were cast with a water-cement ratio (w/c) of 0.26 with cement, coarse aggregate, and fine aggregate contents of 426, 853, and 853 kg/m³. Directly after casting, they were demolded and placed in a carbonation chamber for 2 hours at a pressure of 1.5 bar and CO₂ purity of 99%. The average carbon uptake was found to be 11.3%, by cement mass. Compared to the hydrated control samples, the carbonated counterparts had a similar 28-day compressive strength of 16 MPa. As concrete pipes may be reinforced with steel, the pH of the carbonated concrete was measured. It was interesting to note that the pH remained above 12, indicating the ability to employ carbonation curing for concrete pipes even in the presence of steel reinforcement.

Other work investigated the feasibility of curing concrete pipes in combined steam and carbonation regime in an attempt to reduce the energy footprint of steam curing, while also sequestering CO₂ [70]. Based on the early-age strength results, concrete pipe samples cured in a combination of the two curing regimes, i.e. steam and carbonation, provided equivalent and superior results to those that were steam and carbonation-cured, respectively, and had a CO₂ uptake of approx. 9%, by cement mass. Compared to samples exposed to steam, those that underwent combined curing showed higher resistance to chloride penetration, sulfate attack, and acid attack, possibly due to the consumption of hydroxyl ions and the formation of calcium carbonate.

5.4 Reinforced concrete beams

Despite its adverse effect on reinforced concrete, carbonation of precast reinforced concrete products may be beneficial if performed at an early age. An early-age carbonation curing process was developed for precast reinforced concrete [90, 115]. The detailed curing regime encompassed i) 5-hour in-mold curing at 25°C and 60% RH, ii) 5–6-hour off-mold preconditioning at 25°C and 50 ± 5% RH, iii) 12-hour carbonation curing at a pressure of 5 bars, and iv) 27-day subsequent hydration at 25°C and 95% RH. Carbon sequestration potential was characterized by the CO₂ uptake. It increased from 8 to 15% as the pressure increased from 1 to 5 bar, respectively. This was also associated with an increase in carbonation depth from 8 to 17 mm. Although carbonation decreased the pH of the surface at early age to 9.2, it could recover to 12.3 after 27-day subsequent hydration, evident by the phenolphthalein color profile of **Figure 10**. Evidently, the pH of the area surrounding the steel reinforcement was not affected by carbonation. This indicated that the suggested carbonation curing process posed no risk of corrosion to the

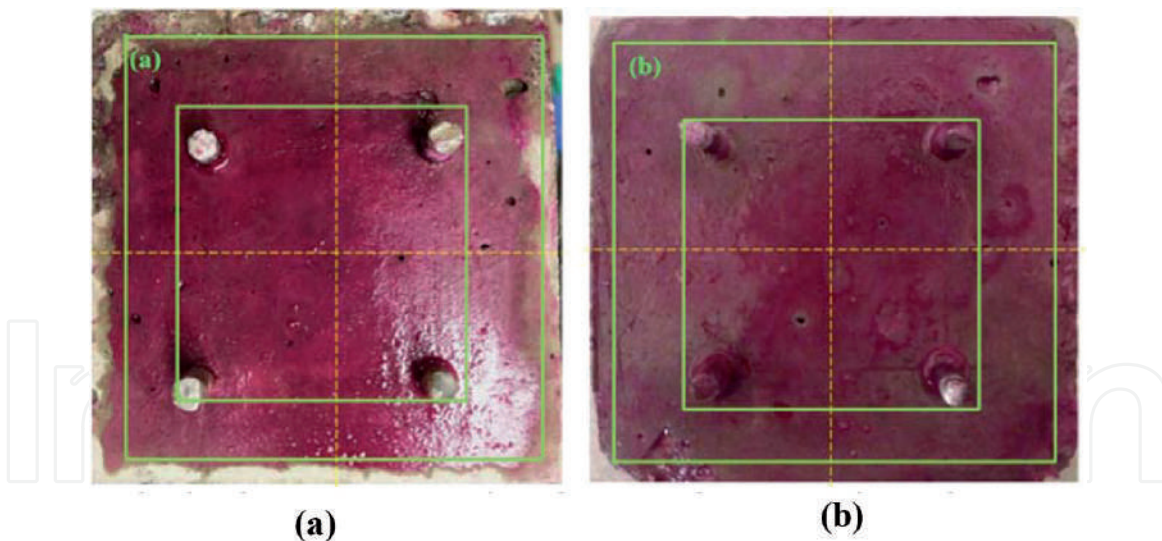


Figure 10. Depth of carbonation in a reinforced concrete beam: (a) after carbonation curing; (b) after carbonation curing and 28-day subsequent hydration [92]. Reproduced with permission from the publisher.

steel reinforcement and could be adopted for precast reinforced concrete products. Furthermore, carbonation-cured samples exhibited higher compressive strength, surface resistivity, resistance to chloride penetration, and resistance to weathering carbonation than hydration-cured counterparts. Apparently, carbonation curing reduced the pore size and volume due to calcium carbonate formation and precipitation within the cementitious matrix.

5.5 Cement-bonded particleboards

Cement-bonded particleboards are construction products that incorporate cement and fine wood chip fractions. As cement is the main binder in such products, past studies have investigated the use of carbonation curing as a replacement to typical hydration to expedite the production process, while also providing a sink for carbon sequestration. Early studies showed that 2-hour carbonation resulted in a carbon uptake of up to 24%, by cement mass, and compressive strength of 10.5 MPa, which was three times that of the hydrated reference [113, 116]. Nevertheless, prolonging carbonation to 24 hours enhanced the reaction efficiency to obtain an uptake of up to 28% [117]. The resulting flexural strength, freeze-thaw resistance, and wet-dry durability were higher than conventionally-cured counterparts.

Another study employed a wetting-drying-carbonation curing scheme for cellulose fiber-reinforced cement boards [69]. Experimental results showed that accelerated carbonation curing was beneficial to the performance of cement boards. Compared to conventional water curing, it provided superior flexural strength and toughness and reduced capillary porosity and microcracking in the autoclave. Similar findings were reported when cement-bonded particleboards were subjected to supercritical CO₂ curing [118, 119].

In addition to the utilization of carbonation curing to sequester carbon dioxide in cement-bonded particleboards, it has been employed to promote the recyclability of waste materials [120–123]. The mechanical, durability and physical properties of carbonated cement-bonded particleboards were comparable, if not superior, to those of air-cured and hydrated counterparts. Such performance enhancement is owed to the ability of carbonation curing to improve the intactness at the cement-fiber interface, limit the interfacial microcracks, and occupy the capillary space with newly-formed calcium carbonate.

5.6 Ceramic bricks

The applicability of accelerated carbonation curing has been explored in numerous construction applications. The common factor among these applications is the carbonation of calcium or magnesium silicates to produce carbonates. Ceramic materials are rich in such silicates and may be carbonated upon exposure to CO₂. As such, accelerated carbonation was applied to ceramic bricks from Andalusian factories in Spain [124]. The curing process entailed 24- to 720-hour exposure to CO₂ at a pressure of 10 bars. The authors noted that longer exposure led to higher carbon uptake, with values reaching up to 10%, by ceramic weight. These results highlight the possibility of employing carbonation curing to ceramic waste materials as a means of permanently sequestering carbon dioxide. Yet, more research is needed to validate the findings and evaluate the feasibility of adopting such a technique by the industry.

6. Environmental benefit

Concrete construction applications serve as a potential carbon dioxide sink for CO₂ sequestration. Rather than disposing of CO₂ in geological sites, it can be recycled into concrete with the added benefit of early-age strength and improved durability performance. Concrete products that are typically cured using the steam curing regime can be carbonated to relieve the dependency on high pressure and temperature steam. For instance, a concrete block can sequester nearly 0.5 kg of CO₂, at an uptake of 24%, by cement mass. At a global annual production of 1800 billion concrete blocks and bricks [125], it will be possible to sequester 900 million tons of CO₂, which is equivalent to carbon sequestration in approx. 900 geological sites. In comparison, a single concrete paver block could sequester 15.3 g of CO₂, characterized by an uptake of 10.4%, by cement mass. With 51.4 billion concrete paver blocks (assuming 20% cement content, a thickness of 80 mm, and a density of 2200 kg/m³) produced annually [126], these products could sequester up to 1.07 million tons of CO₂.

Concrete pipes are produced on the scale of 62 million tons per year [127]. At a carbon uptake of 20%, the concrete pipe industry can sequester up to 1.2 million tons of CO₂ per year. Further, precast concrete products in the form of railway ties can store a total of 0.1 million tons of CO₂ per year globally [128]. Conversely, the 9.5 billion m² of cement-bonded boards produced annually could sequester 10.8 million tons of CO₂, assuming 50% cement content, a thickness of 8 mm, a density of 1500 kg/m³, and CO₂ uptake of 19%, by cement mass [129]. Although ceramic tiles are different than cementitious concrete, they have also presented a 10% carbon uptake, by total weight. With the global production of 13.6 billion m², and assuming a typical thickness of 1.5 cm, the ceramic tile industry would be capable of sequestering 20.4 million tons of CO₂ [130]. Yet, it should be noted that only one study has been conducted in this research area, signifying the need for further investigation. On a global scale, if all producers of the concrete products presented herein were to adopt carbonation curing, a total of 934 million tons of CO₂ could be sequestered. With an annual global cement production of 4.2 billion tons [131], accelerated carbonation curing could reduce the carbon emissions associated with the cement industry by 22.2%. This capacity could further increase if carbonation were adopted for curing various precast reinforced concrete products.

While the environmental benefit in terms of CO₂ sequestration has been addressed in various research studies, the curing-related water consumption in carbonation curing compared to steam and moist counterparts has not been

investigated yet. Based on the work of El-Hassan, Shao [82], the only water required in accelerated carbonation curing is that for spraying the sample after carbonation. This water promoted subsequent hydration by compensating for the water lost due to preconditioning and the carbonation reaction. As such, the total water consumed in this curing regime was about 0.085 m³ per m³ of concrete. In contrast, moist and steam curing are estimated to consume about 3 and 1 m³ of water for the same volume of concrete, respectively [132]. Clearly, carbonation curing could be deemed more advantageous than moist and steam curing from a water preservation standpoint.

7. Conclusions

Accelerated carbonation is an innovative curing regime that promises to expedite strength gain, improve durability performance, and permanently sequester CO₂ gas in concrete products. Thus, it has the potential to enhance the sustainability of the construction industry.

Reaction kinetics, processes, and final products are comprehensively reviewed. The main chemical reactions occur between calcium silicates (C₃S and C₂S) in the cement and CO₂ gas to produce calcium silicate hydrate (C-S-H) gel and calcium carbonate (CaCO₃). Calcium carbonate was detected in its three polymorphic phases, aragonite, vaterite, and calcite, with the former two and latter being associated with the carbonation of C-S-H and calcium silicates, respectively. Their morphology was typical of amorphous, except for the case of carbonating PLC concrete, whereby sharp highly crystalline crystals formed. Conversely, C-S-H was not as easy to detect. In fact, it was intermixed with calcium carbonates to form an amorphous calcium silicate hydrocarbonate product.

The carbonation process was divided into three main stages, preconditioning, carbonation, and subsequent hydration. The utilization of preconditioning was found essential to optimize the water content and promote a higher degree of carbonation reaction. The optimum relative humidity employed in preconditioning was reported as 50–60%. As for carbonation curing, higher reactivity was noted when higher concentration and pressure of CO₂ were used, evidenced by the higher carbon uptake. Subsequent hydration was introduced afterward to enhance the late age mechanical and durability performance.

The applicability of accelerated carbonation to different construction applications has also been highlighted. Carbonated concrete masonry blocks showed comparable mechanical properties to those of steam- and moist-cured counterparts. Yet, the former's resistance to freeze-thaw damage and sulfate attack was greater than that of the latter. Furthermore, carbonation was applied to concrete paving blocks. The compressive strength and freeze-thaw resistance of carbonated samples were superior to those of hydration- and air-cured equivalents. Similarly, the mechanical and durability performance of concrete pipes and beams subjected to carbonation curing were superior to conventionally-cured counterparts. Also, it was interesting to note that there was no risk of corrosion to the steel reinforcement, as the pH of the surrounding 28-day concrete was above 12. Moreover, the feasibility of employing carbonation as a curing regime for cement-bonded particleboards was assessed. Carbonation curing improved the overall interfacial structure between the cement and fiber and led to the filling of capillary space with newly-formed CaCO₃. As a result, enhanced physical, mechanical, and durability properties were reported for carbonated samples compared to conventionally-cured samples. Lastly, carbonation was applied to ceramic bricks as a means of permanently sequestering carbon dioxide.

In addition to its evident improvement in the performance of construction applications, carbonation curing provides a carbon sink to beneficially recycle CO₂. Yet, its full potential can only be attained if it is adopted on a global scale. The application of carbonation curing to all globally-produced concrete blocks, concrete paving blocks, concrete pipes, cement-bonded particleboards, and ceramic bricks can store up to 934 million tons of CO₂, leading to a 22.2% reduction in cement-related carbon emissions. Additionally, it has the potential to reduce the water consumed in moist and steam curing by 97 and 91%, respectively. Evidently, the carbonation curing process enhances material performance, offers environmental benefits, and provides an excellent means to recycle carbon dioxide emitted by the cement industry.

Acknowledgements

This work was financially supported by the United Arab Emirates under grant number 31 N398.

Conflict of interest

The authors declare no conflict of interest.

Author details

Hilal El-Hassan
Civil and Environmental Engineering Department, United Arab Emirates
University, Al Ain, United Arab Emirates

*Address all correspondence to: helhassan@uaeu.ac.ae

IntechOpen

© 2020 The Author(s). Licensee IntechOpen. This chapter is distributed under the terms of the Creative Commons Attribution License (<http://creativecommons.org/licenses/by/3.0>), which permits unrestricted use, distribution, and reproduction in any medium, provided the original work is properly cited. 

References

- [1] Global greenhouse gas emissions data. <https://www.epa.gov/ghgemissions/globalgreenhouse-gas-emissions-data> [cited 2020].
- [2] Climate change indicators: greenhouse gases. <https://www.epa.gov/climateindicators/greenhouse-gases#ref3> [cited 2020].
- [3] IPCC. Projections of Future Changes in Climate. Intergovernmental Panel on Climate Change, 2007.
- [4] What is the greenhouse effect? <http://www.livescience.com/37743-greenhouseeffect.html> [cited 2020].
- [5] Pacheco-Torgal F, Abdollahnejad Z, Camões AF, Jamshidi M, Ding Y. Durability of alkali-activated binders: A clear advantage over Portland cement or an unproven issue? *Constr Build Mater.* 2012;30:400-5.
- [6] Chindapasirt P, Chareerat T, Sirivivatnanon V. Workability and strength of coarse high calcium fly ash geopolymer. *Cem Concr Compos.* 2007;29(3):224-9.
- [7] US Geological Survey. Minerals commodity summary - cement USA: USGS; 2016 [cited 2016 October 6].
- [8] An update on CO₂ capture from cement production. <http://www.globalccsinstitute.com/insights/authors/dennisvanpuyvelde/2013/02/20/update-co2-capturecement-production> [cited 2020].
- [9] Saleh HM, El-Saied FA, Salaheldin TA, Hezo AA. Macro- and nanomaterials for improvement of mechanical and physical properties of cement kiln dust-based composite materials. *J Clean Prod.* 2018;204:532-41.
- [10] Saleh HM, El-Saied FA, Salaheldin TA, Hezo AA. Influence of severe climatic variability on the structural, mechanical and chemical stability of cement kiln dust-slag-nanosilica composite used for radwaste solidification. *Constr Build Mater.* 2019;218:556-67.
- [11] Saleh HM, Salman AA, Faheim AA, El-Sayed AM. Sustainable composite of improved lightweight concrete from cement kiln dust with grated poly(styrene). *J Clean Prod.* 2020;277:123491.
- [12] Samad S, Shah A. Role of binary cement including Supplementary Cementitious Material (SCM), in production of environmentally sustainable concrete: A critical review. *International Journal of Sustainable Built Environment.* 2017;6(2):663-74.
- [13] Panesar DK, Zhang R. Performance comparison of cement replacing materials in concrete: Limestone fillers and supplementary cementing materials – A review. *Constr Build Mater.* 2020;251:118866.
- [14] Kayali O, Sharfuddin Ahmed M. Assessment of high volume replacement fly ash concrete – Concept of performance index. *Constr Build Mater.* 2013;39:71-6.
- [15] Hooton RD. Canadian use of ground granulated blast-furnace slag as a supplementary cementing material for enhanced performance of concrete. *Canadian Journal of Civil Engineering.* 2000;27(4):754-60.
- [16] Khatib JM, Hibbert JJ. Selected engineering properties of concrete incorporating slag and metakaolin. *Constr Build Mater.* 2005;19(6):460-72.
- [17] Juenger MCG, Siddique R. Recent advances in understanding the role of supplementary cementitious

- materials in concrete. *Cem Concr Res.* 2015;78:71-80.
- [18] Elahi MMA, Hossain MM, Karim MR, Zain MFM, Shearer C. A review on alkali-activated binders: Materials composition and fresh properties of concrete. *Constr Build Mater.* 2020;260:119788.
- [19] Nawaz M, Heitor A, Sivakumar M. Geopolymers in construction - recent developments. *Constr Build Mater.* 2020;260:120472.
- [20] Amran YHM, Alyousef R, Alabduljabbar H, El-Zeadani M. Clean production and properties of geopolymer concrete; A review. *J Clean Prod.* 2020;251:119679.
- [21] El-Hassan H, Ismail N. Effect of process parameters on the performance of fly ash/GGBS blended geopolymer composites. *J Sustain Cem Mater.* 2018;7(2):122-40.
- [22] Zhang P, Gao Z, Wang J, Guo J, Hu S, Ling Y. Properties of fresh and hardened fly ash/slag based geopolymer concrete: A review. *J Clean Prod.* 2020;270:122389.
- [23] Adesanya E, Ohenoja K, Kinnunen P, Illikainen M. Alkali Activation of Ladle Slag from Steel-Making Process. *Journal of Sustainable Metallurgy.* 2016;3:300-10.
- [24] El-Hassan H, Elkholy S. Performance Evaluation and Microstructure Characterization of Steel Fiber-Reinforced Alkali-Activated Slag Concrete Incorporating Fly Ash. *J Mater Civ Eng.* 2019;31(10):04019223.
- [25] Al-Majidi MH, Lampropoulos A, Cundy A, Meikle S. Development of geopolymer mortar under ambient temperature for in situ applications. *Constr Build Mater.* 2016;120:198-211.
- [26] Aydın S, Baradan B. Mechanical and microstructural properties of heat cured alkali-activated slag mortars. *Mater Des.* 2012;35:374-83.
- [27] Bernal S, De Gutierrez R, Delvasto S, Rodriguez E. Performance of an alkali-activated slag concrete reinforced with steel fibers. *Constr Build Mater.* 2010;24(2):208-14.
- [28] Bernal SA, Rodríguez ED, Mejía de Gutiérrez R, Provis JL, Delvasto S. Activation of Metakaolin/Slag Blends Using Alkaline Solutions Based on Chemically Modified Silica Fume and Rice Husk Ash. *Waste Biomass Valorization.* 2012;3(1):99-108.
- [29] Ismail N, El-Hassan H. Development and Characterization of Fly Ash/Slag-Blended Geopolymer Mortar and Lightweight Concrete. *J Mater Civ Eng.* 2018;30(4).
- [30] Choi S-J, Choi J-I, Song J-K, Lee BY. Rheological and mechanical properties of fiber-reinforced alkali-activated composite. *Constr Build Mater.* 2015;96(Supplement C):112-8.
- [31] Gu YM, Fang YH, Gong YF, Yan YR, Zhu CH. Effect of curing temperature on setting time, strength development and microstructure of alkali activated slag cement. *Materials Research Innovations.* 2014;18(sup2):S2-829-S2-32.
- [32] Gu Y-m, Fang Y-h, You D, Gong Y-f, Zhu C-h. Properties and microstructure of alkali-activated slag cement cured at below- and about-normal temperature. *Constr Build Mater.* 2015;79:1-8.
- [33] Islam A, Alengaram UJ, Jumaat MZ, Bashar II. The development of compressive strength of ground granulated blast furnace slag-palm oil fuel ash-fly ash based geopolymer mortar. *Mater Des.* 2014;56:833-41.
- [34] Islam A, Alengaram UJ, Jumaat MZ, Bashar II, Kabir SMA. Engineering properties and carbon footprint of

ground granulated blast-furnace slag-palm oil fuel ash-based structural geopolymer concrete. *Constr Build Mater.* 2015;101, Part 1:503-21.

[35] El-Hassan H, Shehab E, Al-Sallamin A. Influence of Different Curing Regimes on the Performance and Microstructure of Alkali-Activated Slag Concrete. *J Mater Civ Eng.* 2018;30(9):04018230.

[36] Karim MR, Hossain MM, Manjur A Elahi M, Mohd Zain MF. Effects of source materials, fineness and curing methods on the strength development of alkali-activated binder. *J Build Eng.* 2020;29:101147.

[37] Lee NK, Lee HK. Setting and mechanical properties of alkali-activated fly ash/slag concrete manufactured at room temperature. *Constr Build Mater.* 2013;47:1201-9.

[38] El-Hassan H, Ismail N, Al Hinaii S, Alshehhi A, Al Ashkar N. Effect of GGBS and curing temperature on microstructure characteristics of lightweight geopolymer concrete. *MATEC Web Conf.* 2017;120:03004.

[39] Li J, Liu S. Influence of Slag as Additive on Compressive Strength of Fly Ash-Based Geopolymer. *J Mater Civ Eng.* 2007;19(6).

[40] Ismail N, Mansour M, El-Hassan H. Development of a low-cost cement free polymer concrete using industrial by-products and dune sand. *MATEC Web Conf.* 2017;120:03005.

[41] Puertas F, Martiez-Ramirez S, Alonso S, Vazquez T. Alkali-activated fly ash/slag cement strength behaviour and hydration products. *Cem Concr Res.* 2000;30:1625-32.

[42] Provis JL. Alkali-activated materials. *Cem Concr Res.* 2018;114:40-8.

[43] Elkholy S, El-Hassan H, editors. *Mechanical and micro-structure*

characterization of steel fiber-reinforced geopolymer concrete. Interdependence between Structural Engineering and Construction Management; 2019; Chicago, IL: ISEC Press.

[44] Nidheesh PV, Kumar MS. An overview of environmental sustainability in cement and steel production. *J Clean Prod.* 2019;231:856-71.

[45] Hasanbeigi A, Price L, Lin E. Emerging energy-efficiency and CO₂ emission-reduction technologies for cement and concrete production: A technical review. *Renewable and Sustainable Energy Reviews.* 2012;16(8):6220-38.

[46] Scrivener K, Martirena F, Bishnoi S, Maity S. Calcined clay limestone cements (LC3). *Cem Concr Res.* 2018;114:49-56.

[47] Scrivener KL, John VM, Gartner EM. Eco-efficient cements: Potential economically viable solutions for a low-CO₂ cement-based materials industry. *Cem Concr Res.* 2018;114:2-26.

[48] Rahman A, Rasul MG, Khan MMK, Sharma S. Recent development on the uses of alternative fuels in cement manufacturing process. *Fuel.* 2015;145:84-99.

[49] Kääntee U, Zevenhoven R, Backman R, Hupa M. Cement manufacturing using alternative fuels and the advantages of process modelling. *Fuel Processing Technology.* 2004;85(4):293-301.

[50] Ghenai C, Inayat A, Shanableh A, Al-Sarairah E, Janajreh I. Combustion and emissions analysis of Spent Pot lining (SPL) as alternative fuel in cement industry. *Sci Total Environ.* 2019;684:519-26.

[51] Schneider M, Romer M, Tschudin M, Bolio H. *Sustainable*

- cement production—present and future. *Cem Concr Res.* 2011;41(7):642-50.
- [52] Madlool NA, Saidur R, Hossain MS, Rahim NA. A critical review on energy use and savings in the cement industries. *Renewable and Sustainable Energy Reviews.* 2011;15(4):2042-60.
- [53] Puertas F, Blanco-Varela MT. Use of alternative fuels in cement manufacture. Effect on clinker and cement characteristics and properties. *Materiales de Construcción.* 2004;54(274):51-64.
- [54] Trezza MA, Scian AN. Burning wastes as an industrial resource: Their effect on Portland cement clinker. *Cem Concr Res.* 2000;30(1):137-44.
- [55] Chinyama M. P. M. Alternative fuels in cement manufacturing. In: Manzanera M, editor. *Alternative Fuel.* Rijeka, Croatia: InTech; 2011.
- [56] Gluyas J, Mathias S. *Geological storage of carbon dioxide book.* 1st Edition ed: Woodhead Publishing; 2014.
- [57] Young JF, Berger RL, Breese J. Accelerated Curing Of Compacted Calcium Silicate Mortars On Exposure To CO₂. *Journal of the American Ceramic Society.* 1974;57(9):394-297.
- [58] Toennies HT, Shideler JJ. Plant Drying Carbonation of Concrete Block - NCMAPCA Cooperative Program. *Journal of the American Concrete Institute.* 1963;60(5):617-33.
- [59] Shi C, Liu M, He P, Ou Z. Factors affecting kinetics of CO₂ curing of concrete. *J Sustain Cem Mater.* 2012;1(1-2):24-33.
- [60] Berger RL, Young, J. F., and Leung, K. Accelerated curing of cementitious systems by carbon dioxide - Hydraulic calcium silicates and aluminates - Part II. *Cem Concr Res.* 1972;2:647-52.
- [61] Young JF, Berger, R. L., Breese, J. Accelerated Curing of Compacted Calcium Silicate Mortars on Exposure to CO₂. *Journal of the American Ceramic Society.* 1974;57(9):394-7.
- [62] Steinour H. Some Effects of Carbon Dioxide on Mortar and Concrete. *American Concrete Institute Journal.* 1956;30:905-7.
- [63] Papadakis VG, Vayenas, C. G., and Fardis, M. N. Fundamental Modeling and Experimental Investigation of Concrete Carbonation. *American Concrete Institute Materials Journal.* 1991;88(4):363-73.
- [64] Klemm WA, and Berger, R. L. Accelerated curing of cementitious systems by carbon dioxide - Part I - Portland Cement. *Cem Concr Res.* 1972;2:567-76.
- [65] Rostami V, Shao Y, Boyd AJ, He Z. Microstructure of cement paste subject to early carbonation curing. *Cem Concr Res.* 2012;42(1):186-93.
- [66] El-Hassan H, Shao Y, Ghoulleh Z. Reaction Products in Carbonation-Cured Lightweight Concrete. *J Mater Civ Eng.* 2013;25(6):799-809.
- [67] Jang JG, Lee HK. Microstructural densification and CO₂ uptake promoted by the carbonation curing of belite-rich Portland cement. *Cem Concr Res.* 2016;82:50-7.
- [68] Shah V, Scrivener K, Bhattacharjee B, Bishnoi S. Changes in microstructure characteristics of cement paste on carbonation. *Cem Concr Res.* 2018;109:184-97.
- [69] Soroushian P, Won J-P, Hassan M. Durability characteristics of CO₂-cured cellulose fiber reinforced cement

- composites. *Constr Build Mater.* 2012;34:44-53.
- [70] Rostami V, Shao, Y., and Boyd, A. J. Durability of concrete pipes subjected to combined steam and carbonation curing. *Constr Build Mater.* 2011;25:3345-55.
- [71] Goto S, Suenaga, K., and Kado, T. Calcium silicate carbonation products. *Journal of the American Ceramic Society.* 1995;78(11):2867-72.
- [72] Castellote M, and Fernandez, L. Chemical changes and phase analysis of OPC pastes carbonated at different CO₂ concentrations. *Mater Struct.* 2009;42(4):515-25.
- [73] El-Hassan H, Shao Y. Dynamic carbonation curing of fresh lightweight concrete. *Mag Concr Res.* 2014;66(14):708-18.
- [74] Goodbrake CJ, Young, J. F., and Berger, R. L. Reaction of hydraulic calcium silicates with carbon dioxide and water. *Journal of the American Ceramic Society.* 1979;62(9-10):488-91.
- [75] Berger RL. Stabilization of silicate structures by carbonation. *Cem Concr Res.* 1979;9(5):649-51.
- [76] Ramezani-pour AA, Ghahari SA, Esmaeili M. Effect of combined carbonation and chloride ion ingress by an accelerated test method on microscopic and mechanical properties of concrete. *Constr Build Mater.* 2014;58:138-46.
- [77] Liu Y, Zhuge Y, Chow CWK, Keegan A, Li D, Pham PN, et al. Properties and microstructure of concrete blocks incorporating drinking water treatment sludge exposed to early-age carbonation curing. *J Clean Prod.* 2020;261:121257.
- [78] Groves GW, and Brough, A. Progressive Changes in the Structure of Hardened C3S Cement Pastes Due to Carbonation. *Journal of the American Ceramic Society.* 1991;74(11):2891-6.
- [79] Mo L, Panesar DK. Effects of accelerated carbonation on the microstructure of Portland cement pastes containing reactive MgO. *Cem Concr Res.* 2012;42(6):769-77.
- [80] El-Hassan H, Shao Y. Early carbonation curing of concrete masonry units with Portland limestone cement. *Cem Concr Compos.* 2015;62:168-77.
- [81] Zhang D, Cai X, Jaworska B. Effect of pre-carbonation hydration on long-term hydration of carbonation-cured cement-based materials. *Constr Build Mater.* 2020;231:117122.
- [82] El-Hassan H, Shao Y, Ghouleh Z. Effect of Initial Curing on Carbonation of Lightweight Concrete Masonry Units. *ACI Mater J.* 2013;110(4):441-50.
- [83] Mo L, Zhang F, Deng M. Mechanical performance and microstructure of the calcium carbonate binders produced by carbonating steel slag paste under CO₂ curing. *Cem Concr Res.* 2016;88:217-26.
- [84] He P, Shi C, Tu Z, Poon CS, Zhang J. Effect of further water curing on compressive strength and microstructure of CO₂-cured concrete. *Cem Concr Compos.* 2016;72:80-8.
- [85] Zhang D, Cai X, Shao Y. Carbonation Curing of Precast Fly Ash Concrete. *J Mater Civ Eng.* 2016;28(11):04016127.
- [86] Shi C, He F, Wu Y. Effect of pre-conditioning on CO₂ curing of lightweight concrete blocks mixtures. *Constr Build Mater.* 2012;26(1):257-67.
- [87] El-Hassan H. Static and Dynamic Carbonation of Lightweight Concrete Masonry Units. Montreal, QC: McGill University; 2012.

- [88] Behfarnia K, Rostami M. An assessment on parameters affecting the carbonation of alkali-activated slag concrete. *J Clean Prod.* 2017;157:1-9.
- [89] Monkman S, MacDonald M. Carbon dioxide upcycling into industrially produced concrete blocks. *Constr Build Mater.* 2016;124:127-32.
- [90] Zhang D, Shao Y. Early age carbonation curing for precast reinforced concretes. *Constr Build Mater.* 2016;113:134-43.
- [91] Matsushita F, Aono, Y., and Shibata, S. Carbonation degree of autoclaved aerated concrete. *Cem Concr Res.* 2000;30:1741-5.
- [92] El-Hassan H, Shao Y. Carbonation Curing of Concrete Blocks to Mitigate Carbon Emission. *The Conference on Carbon Capture, Utilization, and Storage, Annual CCUS 2015 Conference; Pittsburgh, PA, USA.* 2015.
- [93] El-Hassan H, Shao Y. Carbon Storage through Concrete Block Carbonation. *Journal of Clean Energy Technologies.* 2014;2(3):287-91.
- [94] El-Hassan H, Shao Y. Carbon Storage through Dynamic Carbonation of Fresh Lightweight Concrete. *American Institute of Chemical Engineers (AIChE) 2016 Spring Meeting; Houston, TX, USA* 2016.
- [95] He Z, Wang S, Mahoutian M, Shao Y. Flue gas carbonation of cement-based building products. *Journal of CO2 Utilization.* 2020;37:309-19.
- [96] Neves Junior A, Toledo Filho RD, de Moraes Rego Fairbairn E, Dweck J. The effects of the early carbonation curing on the mechanical and porosity properties of high initial strength Portland cement pastes. *Constr Build Mater.* 2015;77:448-54.
- [97] Xuan D, Zhan B, Poon CS. Development of a new generation of eco-friendly concrete blocks by accelerated mineral carbonation. *J Clean Prod.* 2016;133:1235-41.
- [98] Ahmad S, Assaggaf RA, Maslehuddin M, Al-Amoudi OSB, Adekunle SK, Ali SI. Effects of carbonation pressure and duration on strength evolution of concrete subjected to accelerated carbonation curing. *Constr Build Mater.* 2017;136:565-73.
- [99] Monkman S, Shao Y. Carbonation Curing of Slag-Cement Concrete for Binding CO₂ and Improving Performance. *J Mater Civ Eng.* 2010;22(4):296-304.
- [100] Monkman S, Shao Y. Assessing the carbonation behavior of cementitious materials. *J Mater Civ Eng.* 2006;November/December:768-76.
- [101] Rostami V, Shao Y, Boyd AJ. Carbonation Curing versus Steam Curing for Precast Concrete Production. *J Mater Civ Eng.* 2012;24(9):1221-9.
- [102] Wang L, Yeung TLK, Lau AYT, Tsang DCW, Poon C-S. Recycling contaminated sediment into eco-friendly paving blocks by a combination of binary cement and carbon dioxide curing. *J Clean Prod.* 2017;164:1279-88.
- [103] Scrivener K, Snellings R, Lothenbach B. *A Practical Guide to Microstructural Analysis of Cementitious Materials*: CRC Press; 2015.
- [104] Ramachandran VS, Beaudoin JJ. *Handbook of Analytical Techniques in Concrete Science and Technology*: William Andre Publishing/Noyes; 2001.
- [105] Bukowski JM, and Berger, R. L. Reactivity and strength development of CO₂ activated non-hydraulic calcium silicates. *Cem Concr Res.* 1979;9(1):57-68.

- [106] Chang C, and Chen, J. The experimental investigation of concrete carbonation depth. *Cem Concr Res.* 2006;36:1760-7.
- [107] Huffman EWD. Performance of a new automatic carbon dioxide coulometer. *Microchemical Journal.* 1977;22(4):567-73.
- [108] El-Hassan H, Shao Y. Innovative CO₂ Utilization By Carbonation Curing of Lightweight Concrete Made with Portland Limestone Cement. American Institute of Chemical Engineers (AIChE) 2016 Annual Meeting; San Francisco, CA, USA.2016.
- [109] Shao Y, El-Hassan H, editors. CO₂ Utilization in Concrete Block Production. American Institute of Chemical Engineers (AIChE) Annual Meeting 2012; 2012; Pittsburgh, PA, USA.
- [110] Shao Y, El-Hassan H. CO₂ Utilization in Concrete. Third International Conference on Sustainable Construction Materials and Technologies (SCMT3), ; Kyoto, Japan2013.
- [111] Liu Y, Zhuge Y, Chow CWK, Keegan A, Pham PN, Li D, et al. Recycling drinking water treatment sludge into eco-concrete blocks with CO₂ curing: Durability and leachability. *Sci Total Environ.* 2020;746:141182.
- [112] Zhang S, Ghoulah Z, Shao Y. Effect of Carbonation Curing on Efflorescence Formation in Concrete Paver Blocks. *J Mater Civ Eng.* 2020;32(6):04020127.
- [113] Shao Y, Monkman S, Wang S. Market Analysis of CO₂ Sequestration in Concrete Building Products. Second International Conference on Sustainable Construction Materials and Technologies; Acona, Italy2010.
- [114] Shao Y, Lin X. Early-Age Carbonation Curing of Concrete Using Recovered CO₂. *Concrete International.* 2011;33(9):50-6.
- [115] Zhang D, Shao Y. Enhancing Chloride Corrosion Resistance of Precast Reinforced Concrete by Carbonation Curing. *ACI Mater J.* 2019;116(3):3-12.
- [116] Shao Y, Wang S. Carbonation Curing of Cement Bonded Fiberboard Made by Slurry-Dewatering Process. ACI Symposium Publication. 2009;260:125-38.
- [117] He Z, Jia Y, Wang S, Mahoutian M, Shao Y. Maximizing CO₂ sequestration in cement-bonded fiberboards through carbonation curing. *Constr Build Mater.* 2019;213:51-60.
- [118] Maaail RS, Umemura K, Aizawa H, Kawai S. Curing and degradation processes of cement-bonded particleboard by supercritical CO₂ treatment. *Journal of Wood Science.* 2011;57(4):302-7.
- [119] Maaail RS. Degradation Analysis on Manufacture of Cement-bonded Particleboard Using Supercritical CO₂. 2017.
- [120] Soroushian P, Aouadi F, Chowdhury H, Nossoni A, Sarwar G. Cement-bonded straw board subjected to accelerated processing. *Cem Concr Compos.* 2004;26(7):797-802.
- [121] Wang L, Chen SS, Tsang DCW, Poon C-S, Dai J-G. CO₂ curing and fibre reinforcement for green recycling of contaminated wood into high-performance cement-bonded particleboards. *Journal of CO₂ Utilization.* 2017;18:107-16.
- [122] Soroushian P, Hassan M. Evaluation of cement-bonded strawboard against alternative cement-based siding products. *Constr Build Mater.* 2012;34:77-82.
- [123] Wang L, Chen SS, Tsang DCW, Poon C-S, Shih K. Recycling contaminated wood into eco-friendly particleboard using green cement and carbon dioxide curing. *J Clean Prod.* 2016;137:861-70.

[124] Martín D, Aparicio P, Galán E. Accelerated carbonation of ceramic materials. Application to bricks from Andalusian factories (Spain). *Constr Build Mater.* 2018;181:598-608.

[125] Transparency Market Research. Global Concrete Block and Brick Manufacturing Market Estimated to Surpass 2700 Billion Units by 2027. Albany, NY, USA: Transparency Market Research, 2018.

[126] Concrete Manufacturers Association. Concrete Block Paving. 5th Edition ed. Midrand, South Africa: Concrete Manufacturers Association; 2009. 30 p.

[127] Lucintel. Concrete Pipe Market Report: Trends, Forecast and Competitive Analysis. Dallas, TX, USA: 2020.

[128] Railway Tie Association. <https://www.rta.org/faqs#:~:text=Currently%2C%20the%20industry%20has%20the,just%20over%2019%20million%20ties>. Georgia, USA: Railway Tie Association; 2020 [cited 2020].

[129] Saunders A, Davidson E. Cement Boards. *Global Cement.* 2014:32-8.

[130] ACIMAC. World Production and Consumption of Ceramic Tiles. Italy: Association of Italian Manufacturers of Machinery and Equipment for Ceramics, 2018.

[131] Cement production worldwide from 1995 to 2019. <https://www.statista.com/statistics/1087115/global-cement-production-volume/> [cited 2020].

[132] El-Dieb AS. Self-curing concrete: Water retention, hydration and moisture transport. *Constr Build Mater.* 2007;21(6):1282-7.

Cement-Based Piezoelectricity Application: A Theoretical Approach

*Daniel A. Triana-Camacho, Jorge H. Quintero-Orozco
and Jaime A. Perez-Taborda*

Abstract

The linear theory of piezoelectricity has widely been used to evaluate the material constants of single crystals and ceramics, but what happens with amorphous structures that exhibit piezoelectric properties such as cement-based? In this chapter, we correlate the theoretical and experimental piezoelectric parameters for small deformations after compressive stress–strain, open circuit potential, and impedance spectroscopy on cement-based. Here, in detail, we introduce the theory of piezoelectricity for large deformations without including a functional for the energy; also, we show two generating equations in terms of a free energy's function for later it will be reduced to constitutional equations of piezoelectricity for infinitesimal deformations. Finally, here is shown piezoelectric and electrical parameters of gold nanoparticles mixed to cement paste: the axial elasticity parameter $Y = 323.5 \pm 75.3 [kN/m^2]$, the electroelastic parameter $\gamma = -20.5 \pm 6.9 [mV/kN]$, and dielectric constant $\epsilon = (939.6 \pm 82.9)\epsilon_0 [F/m]$, which have an interpretation as linear theory parameters s_{ijkl}^D , g_{kij} and ϵ_{ik}^T discussed in the chapter.

Keywords: piezoelectricity, cement-based, nano-composites, constitutional equations, impedance spectroscopy

1. Introduction

The direct piezoelectric effect creates an electric polarization on a continuum medium due to applied stress. The polarization can be macroscopic (effect over continuum medium) and nanoscopic and microscopy scales (effect over atoms, molecules, and electrical domains). Once the Curie brothers discovered the piezoelectric effect in 1880 [1], piezoelectricity investigations led to more data and constructed models based on crystallography to explain the electricity generation since electro-optics and thermodynamic. Voigt in 1894 proposed a piezoelectric parameter related to the strain of material; since the thermodynamic theory, he constructed a non-linear model and expressed the free energy of a piezoelectric crystal in terms of the electric field, strain, electric and elastic deformation potentials, temperature, pyroelectric and piezoelectric parameters [2]. Currently, we can see these constants in the constitutive equations of piezoelectricity. During 1956 and 1963, Toupin and Eringen used a variational formulation to construct a functional in

terms of internal energy and derive the constitutive equations [3, 4]. Then, in 1971 Tiersten proposed to use the conservation equations of mass, electrical charge, linear momentum, angular momentum, and energy, adding a Legendre transformation to include a thermodynamic functional in terms of the free energy, achieving a reduction of the number of constitutive equations from 7 to 4 to facilitate theoretical calculations [5]. These constitutional equations and their linear approach gave support to the theoretical calculus of piezoelectric parameters of crystalline structures, e.g., zinc-blende [6, 7], zinc oxide [8, 9], and other crystals with similar symmetric of quartz [10, 11]. Finally, between 1991 and 2017, Yang has proposed modifications for the Legendre transformation of Tiersten, and he has included two models to describe the polarization in a deformable continuum medium [12, 13].

According to electrostatic theory, the macroscopic polarization \vec{P} can be written in terms of electric charge distribution likewise with the electric field \vec{E} induced into the continuum medium. Besides, the polarization starts with continuum medium deformation \vec{S} for applied stress. Considering: (i) Uniqueness for the parameters that relate the polarization and the electric field, (ii) Stress produces equal deformations in each cell of crystal, (iii) The deformations lead dipole and quadrupole moments affecting the piezoelectric parameters directly. Based on the above considerations, the linear constitutive equations of piezoelectricity can be written, as Martin said [6].

This chapter book is thought to be a working example that connects the piezoelectricity theory and experimental data of electromechanical and electrical properties. These data were obtained on cement paste mixed with gold nanoparticles.

2. Constitutional equations in detail and correlation with the piezoelectricity of cement-based composites

In this section, we have selected Yang's differential approach to obtain the constitutional equations of piezoelectricity. The differential derivation shows the physics involved in the conservation laws differently. For example, it shows that the electric body couple and the Cauchy stress tensor are asymmetric. Also, it relates the local electric field with the electric interaction between the differential elements of the lattice continuum and the electronic continuum.

2.1 Conservation laws applied to a polarized continuum from differential approximation

Regarding the study of the piezoelectric properties of cement paste, it is necessary to describe the material separately as two continua medium, as from the piezoelectric phenomenon, the crystal and their symmetry would have a lattice (positive charge) and an electronic component (negative charge) Those continua can be separated by mechanical stress. Their physical properties could change according to the coordinate systems or states. Therefore, the body will study in two states (reference state and current state), as is shown in **Figure 1**.

2.1.1 Electric charge conservation

The conservation electric charge in the body takes importance with an infinitesimal displacement on the medium's current state to get polarization. For this reason, the phenomenon described in the above state is known as the two continuum medium model. The electronic continuum comes under an infinitesimal

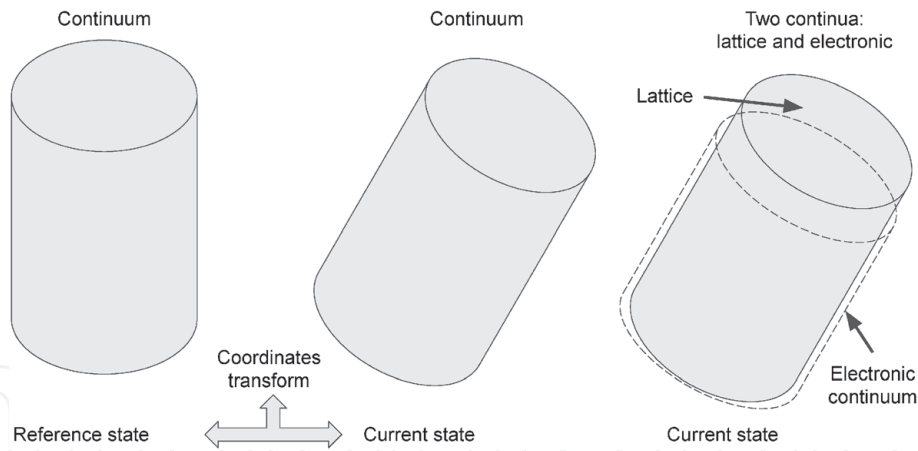


Figure 1.
 States of a deformable and polarizable continuum.

displacement η respect to the lattice. It is produced by body deformation, as described in **Figure 2**. From the assumption of the lattice and electronic continuum, the medium have equal volumes, some variation of infinitesimal displacement respect coordinates in the current state should be zero and can be written as

$$\eta_{k,k} = \frac{\partial \eta_k(\vec{y})}{\partial y_k} = 0 \quad (1)$$

Furthermore, if it is taken the two continuous mediums, the electric charge density must be neutral to consider only the piezoelectric effect.

$$\mu^l(\vec{y}) + \mu^e(\vec{y} + \vec{\eta}) = 0 \quad (2)$$

We can show that the gradient of infinitesimal displacement Eq. (1) and the neutrality condition of electric charge density Eq. (2) are sufficient to explain the polarization in a deformable continuum

$$\vec{P} = \mu^l(\vec{y}) [-\vec{\eta}(\vec{y})] = \mu^e(\vec{y} + \vec{\eta}) \vec{\eta} \approx \mu^e(\vec{y}) \vec{\eta} \quad (3)$$

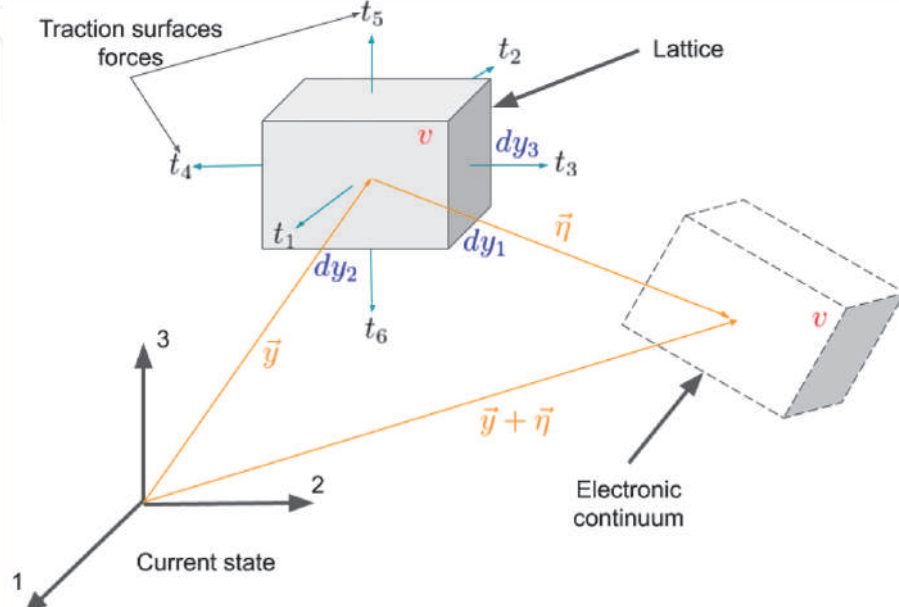


Figure 2.
 Volume elements of electronic and lattice continuum medium.

2.1.2 Energy conservation

Once the body is deformed, electronic and lattice continua electric charges apply a quasi-static electric field. Tiersten et al. called it Maxwellian electric field E_k . It is interacting on two continuum mediums producing an electrical force on each one. The other forces acting on the body are traction and body forces. The traction force t_k per unit, the area is working on the surfaces of volume elements of the lattice (see **Figure 2**). Also, it can be written in terms of Cauchy stress tensor τ_{jk} as $t_k = n_j \tau_{jk}$, where n_j is the normal vector. Moreover, body force refers to an external force acting on the body, for example, gravity. The previous three forces are necessary to get the conservation laws, including energy.

From the three forces above, it is possible to construct the Eqs. (4) and (5), linear and angular momentum conservation, respectively.

$$\rho \dot{u}_k = f_k^E + \tau_{mk,m} + \rho f_k \quad (4)$$

$$c_i^E + \varepsilon_{ijk} \tau_{jk}(\vec{y}) = 0 \quad (5)$$

where f_k^E is the electric force on the body and start from the dot product of polarization P_j with the electric field gradient $E_{k,i}$; Besides, c_i^E is called electric coupling, and it is the cross product of P_j with E_k ; finally, f_k is the external force on the body per unit mass.

Then, replacing the electric coupling c_i^E by the cross product between P_j and E_k , we can rewrite Eq. (5) as follow

$$\varepsilon_{ijk} P_j E_k(\vec{y}) + \varepsilon_{ijk} \tau_{jk}(\vec{y}) = 0 \quad (6)$$

Factoring the permutation tensor ε_{ijk}

$$\varepsilon_{ijk} [P_j E_k + \tau_{jk}] = 0 \quad (7)$$

The term in square brackets from Eq. (7) is a symmetry tensor that can be written as

$$\tau_{jk}^S = P_j E_k + \tau_{jk} \quad (8)$$

The term $P_j E_k$ is called the Maxwell stress tensor T_{jk}^E . On the other hand, multiplying Eq. (5) by ε_{iqr} is obtain

$$\begin{aligned} \varepsilon_{iqr} c_i^E + \varepsilon_{iqr} \varepsilon_{ijk} \tau_{jk}(\vec{y}) &= 0 \\ \delta_{jq} \delta_{kr} \tau_{jk}(\vec{y}) - \delta_{jr} \delta_{kq} \tau_{jk}(\vec{y}) &= -\varepsilon_{iqr} c_i^E \\ \tau_{qr}(\vec{y}) - \tau_{rq}(\vec{y}) &= -\varepsilon_{iqr} c_i^E \end{aligned} \quad (9)$$

From Eq. (9) we can conclude that the Cauchy stress tensor ($t_k = n_j \tau_{jk}$) is asymmetry. Now, we get the total energy inside the continuum medium as a combination of kinetic and internal energy ε^{in} [13], both per mass unit. Here is performed the powers added due to the three forces above.

$$\begin{aligned} \frac{d}{dt} \left(\frac{1}{2} u_k u_k \rho dv + \varepsilon^{in} \rho dv \right) &= \mu^l(\vec{y}) E_k(\vec{y}) u_k(\vec{y}) dv \\ &+ \mu^e(\vec{y} + \vec{\eta}) E_k(\vec{y} + \vec{\eta}) \left[u_k(\vec{y}) + \dot{\eta}_k \right] dv + t_k u_k ds \\ &+ \rho f_k u_k dv \end{aligned} \quad (10)$$

The following steps from Eq. (10) conduct to develop conservation energy law. **In the first step**, we work on the **total energy term**. Then, the product rule to the total energy term is applied:

$$\begin{aligned} \frac{d}{dt} \left(\frac{1}{2} u_k u_k \rho dv + \varepsilon^{in} \rho dv \right) &= \rho dv \frac{d}{dt} \left(\frac{1}{2} u_k u_k + \varepsilon^{in} \right) + \left(\frac{1}{2} u_k u_k + \varepsilon^{in} \right) \frac{d}{dt} (\rho dv) \\ &= \rho dv \frac{d}{dt} \left(\frac{1}{2} u_k u_k + \varepsilon^{in} \right) + \left(\frac{1}{2} u_k u_k + \varepsilon^{in} \right) \frac{d}{dt} (\rho dv) \end{aligned} \quad (11)$$

The term $\frac{d}{dt}(\rho dv)$ represents the mass conservation. Therefore, this term is null in Eq. (11).

$$\frac{d}{dt} \left(\frac{1}{2} u_k u_k \rho dv + \varepsilon^{in} \rho dv \right) = \rho dv \frac{d}{dt} \left(\frac{1}{2} u_k u_k + \varepsilon^{in} \right) \quad (12)$$

Then, here is writes the add of derivatives from kinetic and internal energies

$$\frac{d}{dt} \left(\frac{1}{2} u_k u_k \rho dv + \varepsilon^{in} \rho dv \right) = \rho dv u_k \frac{d}{dt} (u_k) + \rho dv \frac{d}{dt} (\varepsilon^{in}) \quad (13)$$

In the second step, the **electric power term** will be developed by Taylor's expansion.

$$\begin{aligned} &\mu^l(\vec{y}) E_k(\vec{y}) u_k(\vec{y}) dv + \mu^e(\vec{y} + \vec{\eta}) E_k(\vec{y} + \vec{\eta}) \left[u_k(\vec{y}) + \dot{\eta}_k \right] dv \\ &\approx \mu^l(\vec{y}) E_k(\vec{y}) u_k(\vec{y}) dv + \mu^e(\vec{y} + \vec{\eta}) \left[E_k(\vec{y}) + E_{k,i}(\vec{y}) \eta_i \right] \left[u_k(\vec{y}) + \dot{\eta}_k \right] dv \end{aligned} \quad (14)$$

From Eq. (14), it will solve the dot product between the electric field and velocity,

$$\begin{aligned} &= \mu^l(\vec{y}) E_k(\vec{y}) u_k(\vec{y}) dv \\ &+ \mu^e(\vec{y} + \vec{\eta}) \left[E_k(\vec{y}) u_k(\vec{y}) + E_k(\vec{y}) \dot{\eta}_k + E_{k,i}(\vec{y}) \eta_i u_k(\vec{y}) + E_{k,i}(\vec{y}) \eta_i \dot{\eta}_k \right] dv \end{aligned} \quad (15)$$

The second-order term $\eta_i \dot{\eta}_k = \eta_i \dot{\eta}_i = \frac{1}{2} \frac{d}{dt} \eta_i^2 \approx 0$ is zero, taking into account the infinitesimal displacement. Then, factorize $E_k(\vec{y}) u_k(\vec{y}) dv$ in Eq. (15), it takes a form:

$$= \left[\mu^l(\vec{y}) + \mu^e(\vec{y} + \vec{\eta}) \right] E_k(\vec{y}) u_k(\vec{y}) dv + \left[E_k(\vec{y}) \dot{\eta}_k + E_{k,i}(\vec{y}) \eta_i u_k(\vec{y}) \right] dv \quad (16)$$

Replacing Eq. (2) in Eq. (16), we obtain:

$$= \mu^e (\vec{y} + \vec{\eta}) E_k(\vec{y}) \dot{\eta}_k dv + \mu^e (\vec{y} + \vec{\eta}) E_{k,i}(\vec{y}) \eta_i u_k(\vec{y}) dv \quad (17)$$

With Eq. (3), Eq. (17) takes the form:

$$= \mu^e (\vec{y} + \vec{\eta}) E_k(\vec{y}) \dot{\eta}_k dv + P_i E_{k,i}(\vec{y}) u_k(\vec{y}) dv \quad (18)$$

In Eq. (18), the term $\mu^e (\vec{y} + \vec{\eta}) E_k(\vec{y}) \dot{\eta}_k$ is called the electric power of the body w^E . And the term $P_i E_{k,i}$ is the electric force between the lattice and electronic volume elements. It was defined in Eq. (4) above.

$$\mu^l (\vec{y}) E_k(\vec{y}) u_k(\vec{y}) dv + \mu^e (\vec{y} + \vec{\eta}) E_k(\vec{y} + \vec{\eta}) [u_k(\vec{y}) + \dot{\eta}_k] dv = w^E dv + f_k^E u_k(\vec{y}) dv \quad (19)$$

In the third step, we will solve the **traction force** in terms of Cauchy stress tensor. Then, the power due to the traction force takes the form:

$$\begin{aligned} t_k u_k ds &= \tau_{mk} n_m u_k ds \\ &= \tau_{1k} \left(\vec{y} + \frac{1}{2} dy_1 \hat{i}_1 \right) u_k \left(\vec{y} + \frac{1}{2} dy_1 \hat{i}_1 \right) dy_2 dy_3 \\ &\quad - \tau_{1k} \left(\vec{y} - \frac{1}{2} dy_1 \hat{i}_1 \right) u_k \left(\vec{y} - \frac{1}{2} dy_1 \hat{i}_1 \right) dy_2 dy_3 \\ &\quad + \tau_{2k} \left(\vec{y} + \frac{1}{2} dy_2 \hat{i}_2 \right) u_k \left(\vec{y} + \frac{1}{2} dy_2 \hat{i}_2 \right) dy_3 dy_1 \\ &\quad - \tau_{2k} \left(\vec{y} - \frac{1}{2} dy_2 \hat{i}_2 \right) u_k \left(\vec{y} - \frac{1}{2} dy_2 \hat{i}_2 \right) dy_3 dy_1 \\ &\quad + \tau_{3k} \left(\vec{y} + \frac{1}{2} dy_3 \hat{i}_3 \right) u_k \left(\vec{y} + \frac{1}{2} dy_3 \hat{i}_3 \right) dy_1 dy_2 \\ &\quad - \tau_{3k} \left(\vec{y} - \frac{1}{2} dy_3 \hat{i}_3 \right) u_k \left(\vec{y} - \frac{1}{2} dy_3 \hat{i}_3 \right) dy_1 dy_2 \end{aligned} \quad (20)$$

Now, we apply Taylor's expansion to Cauchy stress tensor τ_{1k} and velocity u_k . Next, the last result will be implemented in the components: two τ_{2k} and three τ_{3k}

$$\begin{aligned} &\tau_{1k} \left(\vec{y} + \frac{1}{2} dy_1 \hat{i}_1 \right) u_k \left(\vec{y} + \frac{1}{2} dy_1 \hat{i}_1 \right) dy_2 dy_3 - \tau_{1k} \left(\vec{y} - \frac{1}{2} dy_1 \hat{i}_1 \right) u_k \left(\vec{y} - \frac{1}{2} dy_1 \hat{i}_1 \right) dy_2 dy_3 \\ &\approx \left[\tau_{1k}(\vec{y}) + \frac{1}{2} dy_1 \tau_{1k,1}(\vec{y}) \right] \left[u_k(\vec{y}) + \frac{1}{2} dy_1 u_{k,1}(\vec{y}) \right] dy_2 dy_3 \\ &\quad - \left[\tau_{1k}(\vec{y}) - \frac{1}{2} dy_1 \tau_{1k,1}(\vec{y}) \right] \left[u_k(\vec{y}) - \frac{1}{2} dy_1 u_{k,1}(\vec{y}) \right] dy_2 dy_3 \end{aligned} \quad (21)$$

The products give

$$\begin{aligned} & \approx \left[\tau_{1k} u_k + \tau_{1k} \frac{1}{2} dy_1 u_{k,1} + \frac{1}{2} dy_1 \tau_{1k,1} u_k + \frac{1}{4} dy_1^2 \tau_{1k,1} u_{k,1} \right] dy_2 dy_3 \\ & - \left[\tau_{1k} u_k - \tau_{1k} \frac{1}{2} dy_1 u_{k,1} - \frac{1}{2} dy_1 \tau_{1k,1} u_k + \frac{1}{4} dy_1^2 \tau_{1k,1} u_{k,1} \right] dy_2 dy_3 \end{aligned} \quad (22)$$

Adding similar terms:

$$\approx \left[\tau_{1k}(\vec{y}) dy_1 u_{k,1}(\vec{y}) + dy_1 \tau_{1k,1}(\vec{y}) u_k(\vec{y}) \right] dy_2 dy_3 \quad (23)$$

Factorizing dy_1 that multiply to dy_2 and dy_3 it will transform into the volume element dv .

$$\approx \tau_{1k}(\vec{y}) u_{k,1}(\vec{y}) dv + \tau_{1k,1}(\vec{y}) u_k(\vec{y}) dv \quad (24)$$

Reply the proceeding since Eq. (21) to Eq. (24) for the components τ_{2k} and τ_{3k} yield

$$\begin{aligned} t_k u_k ds &= \tau_{1k}(\vec{y}) u_{k,1}(\vec{y}) dv + \tau_{1k,1}(\vec{y}) u_k(\vec{y}) dv + \tau_{2k}(\vec{y}) u_{k,2}(\vec{y}) dv \\ &+ \tau_{2k,2}(\vec{y}) u_k(\vec{y}) dv + \tau_{3k}(\vec{y}) u_{k,3}(\vec{y}) dv + \tau_{3k,3}(\vec{y}) u_k(\vec{y}) dv \end{aligned} \quad (25)$$

Each one of the components has information about two opposite faces of the volume element. Then, adding index m it reduces the Eq. (25) to:

$$t_k u_k ds = \tau_{mk}(\vec{y}) u_{k,m}(\vec{y}) dv + \tau_{mk,m}(\vec{y}) u_k(\vec{y}) dv \quad (26)$$

From the results of Eq. (13), Eq. (19), and Eq. (26) into Eq. (10), we obtain

$$\begin{aligned} \rho dv u_k \frac{d}{dt}(u_k) + \rho dv \frac{d}{dt}(\epsilon^{in}) &= w^E dv + f_k^E u_k(\vec{y}) dv + \tau_{mk}(\vec{y}) u_{k,m}(\vec{y}) dv \\ &+ \tau_{mk,m}(\vec{y}) u_k(\vec{y}) dv + \rho f_k u_k dv \end{aligned} \quad (27)$$

Here is factoring the terms that contain $u_k(\vec{y}) dv$ to the left side and the terms with the volume differential dv to the right side.

$$\left[\rho \frac{d}{dt}(u_k) + f_k^E + \tau_{mk,m}(\vec{y}) + \rho f_k \right] u_k(\vec{y}) dv = \left\{ w^E - \rho \frac{d}{dt}[\epsilon^{in}] + \tau_{mk}(\vec{y}) u_{k,m}(\vec{y}) \right\} dv \quad (28)$$

From Eq. (28), the term in the square bracket is null by Eq. (4). Then, we obtain Eq. (29) for energy conservation that depends on internal energy.

$$\rho \dot{\epsilon}^{in} = w^E + \tau_{mk}(\vec{y}) u_{k,m}(\vec{y}) \quad (29)$$

Remember from Eq. (19) that electric power can be written as:

$$w^E = \mu^e(\vec{y} + \vec{\eta}) E_m(\vec{y}) \frac{d\eta_m}{dt} = E_m(\vec{y}) \left\{ \frac{d}{dt} [\mu^e(\vec{y} + \vec{\eta}) \eta_m] - \frac{d\mu^e(\vec{y} + \vec{\eta})}{dt} \eta_m \right\}$$

$$w^E = E_m(\vec{y}) \left\{ \dot{P}_m - \dot{\mu}^e(\vec{y} + \vec{\eta}) \eta_m \right\} \quad (30)$$

Another form of electric charge conservation is $\dot{\mu}^e(\vec{y} + \vec{\eta}) + \mu^e(\vec{y} + \vec{\eta}) u_{i,i} = 0$, it will simplify the Eq. (30) to:

$$w^E = E_m(\vec{y}) \left\{ \dot{P}_m + \mu^e(\vec{y} + \vec{\eta}) u_{i,i} \eta_m \right\} \quad (31)$$

The mass conservation $\dot{\rho} + \rho u_{i,i} = 0$ has a similar mathematical structure as charge conservation. Therefore, the gradient of the speed $u_{i,i}$ in Eq. (31) was replaced

$$\begin{aligned} w^E &= E_m(\vec{y}) \dot{P}_m + E_m(\vec{y}) \mu^e(\vec{y} + \vec{\eta}) \frac{-\dot{\rho}}{\rho} \eta_m = E_m \dot{P}_m - \frac{\dot{\rho}}{\rho} E_m P_m \\ w^E &= \frac{E_m}{\rho} [\rho \dot{P}_m - \dot{\rho} P_m] \end{aligned} \quad (32)$$

Eq. (32) has been used on Eq. (29)

$$\rho \dot{\varepsilon}^{in} = \frac{E_m}{\rho} [\rho \dot{P}_m - \dot{\rho} P_m] + \tau_{mk}(\vec{y}) u_{k,m}(\vec{y}) \quad (33)$$

With Legendre transformation showing in Eq. (34), Tiersten replaced the internal energy ε^{in} by free energy χ [5]. This transformation diminishes the number of constitutional equations. Besides, it offers a quantitative interpretation that can not get from the internal energy resulting in more useful for those who perform piezoelectricity experiments. After Section 2.3, we could see the χ will depend on the gradient of potential in the reference state and deformation tensor.

$$\chi = \varepsilon^{in} - E_m \frac{P_m}{\rho} \quad (34)$$

Upon differentiating respect to time the Eq. (34).

$$\dot{\chi} = \dot{\varepsilon}^{in} - \dot{E}_m \frac{P_m}{\rho} - E_m \frac{\dot{P}_m}{\rho} + E_m \frac{P_m}{\rho^2} \dot{\rho} \quad (35)$$

Clear the term $\rho \dot{\varepsilon}^{in}$

$$\rho \dot{\varepsilon}^{in} = \rho \dot{\chi} + \dot{E}_m P_m + E_m \dot{P}_m - E_m \frac{P_m}{\rho} \dot{\rho} \quad (36)$$

Using Eq. (36) on Eq. (29), we obtain:

$$\begin{aligned} \rho \dot{\chi} + \dot{E}_m P_m + E_m \dot{P}_m - E_m \frac{P_m}{\rho} \dot{\rho} &= \frac{E_m}{\rho} [\rho \dot{P}_m - \dot{\rho} P_m] + \tau_{mk}(\vec{y}) u_{k,m}(\vec{y}) \\ \rho \dot{\chi} + \dot{E}_m P_m + E_m \dot{P}_m - E_m \dot{\rho} \frac{P_m}{\rho} &= E_m \dot{P}_m - E_m \dot{\rho} \frac{P_m}{\rho} + \tau_{mk}(\vec{y}) u_{k,m}(\vec{y}) \end{aligned} \quad (37)$$

The similar terms $E_m \dot{P}_m$ and $-E_m \dot{\rho} \frac{P_m}{\rho}$ in Eq. (37), are clear. Finally, we have rewritten **energy conservation** in terms of free energy, electrical (electric field and

polarization vector), and mechanical (Cauchy stress tensor) components, as is shown in Eq. (38).

$$\rho\dot{\chi} = \tau_{mk}(\vec{y})u_{k,m}(\vec{y}) - \dot{E}_m P_m \quad (38)$$

2.2 Transformation of fundamental physical quantities in piezoelectricity to the reference state

There are several reasons to consider two coordinate systems (reference and current state) for continuum. Firstly, it is not mathematically simple to describe the movement of each particle that compounds a continuum as seen on the gradient of velocity $u_{k,m}$ in Eq. (38); it is more appropriate to propose a coordinate system that describes the continuum in the reference system. The material behavior could be affected by the characteristics of the current state, too. For example, fluids and solids can change their mechanical behavior while changing the shape [14]. Hence, we refer to our study material (cement-based composites) whom we know the physical properties in the reference state X_L . To explain the behavior of a material, we must include physical quantities respect the reference state X_L : potential gradient W_K , polarization P_L , electric displacement D_L , volume free charge density ρ^E , mass density ρ^0 and the second Piola-Kirchhoff stress T^S_{KL} [15]. It raises by the transformation of symmetric tensor τ^S_{mk} in the current state to reference state, and relate the traction force with areas, both in the reference state. While the first Piola-Kirchhoff stress is connecting the traction force and electric force in the current state with regions in the reference state.

This section will describe the **transformation of energy conservation from the current state to the reference state**, using Eq. (8), the symmetric tensor modifies Eq. (38).

$$\rho\dot{\chi} = \tau^S_{mk}u_{k,m} - P_m E_k u_{k,m} - \dot{E}_m P_m \quad (39)$$

2.2.1 Electric field and gradient of potential

To transform the electric field to a reference state, here will use follow:

$$W_K = E_m y_{m,K} \quad (40)$$

The gradient of the potential W_K is multiplying both sides by $X_{K,m}$

$$W_K X_{K,m} = E_m y_{m,K} X_{K,m} = E_m \frac{\partial y_m}{\partial X_K} \frac{\partial X_K}{\partial y_m} \quad (41)$$

Therefore,

$$E_m = W_K X_{K,m} \quad (42)$$

The derivative respect to time of E_m becomes

$$\dot{E}_m = \frac{d}{dt} [W_K X_{K,m}] = \frac{d}{dt} (W_K) X_{K,m} + W_K \frac{d}{dt} (X_{K,m}) \quad (43)$$

The term $X_{K,m}$ from Eq. (43) is developed as follow

$$X_{K,m} = \delta_{KL}X_{L,m} = \frac{\partial y_k}{\partial X_L} \frac{\partial X_K}{\partial y_k} X_{L,m} \quad (44)$$

Derivative $X_{K,m}$ respect to time

$$\frac{d}{dt}(X_{K,m}) = \frac{d}{dt} \left(\frac{\partial y_k}{\partial X_L} \frac{\partial X_K}{\partial y_k} X_{L,m} \right) = \frac{d}{dt} (y_{k,L} X_{K,k} X_{L,m}) \quad (45)$$

$$\frac{d}{dt}(X_{K,m}) = \frac{d}{dt} (y_{k,L}) X_{K,k} X_{L,m} + \frac{d}{dt} (X_{K,k}) y_{k,L} X_{L,m} + \frac{d}{dt} (X_{L,m}) y_{k,L} X_{K,k}$$

Partial derivate of y and X are written in Leibniz notation.

$$\frac{d}{dt}(X_{K,m}) = u_{k,L} X_{K,k} X_{L,m} + \frac{d}{dt} (X_{K,k}) \frac{\partial y_k}{\partial X_L} \frac{\partial X_L}{\partial y_m} + \frac{d}{dt} (X_{L,m}) \frac{\partial y_k}{\partial X_L} \frac{\partial X_K}{\partial y_k} \quad (46)$$

The products of partial derivate are reduced to Kronecker delta.

$$\frac{d}{dt}(X_{K,m}) = u_{k,L} X_{K,k} X_{L,m} + \frac{d}{dt} (X_{K,k}) \delta_{km} + \frac{d}{dt} (X_{L,m}) \delta_{KL} \quad (47)$$

The index into $X_{K,k}$ and $X_{L,m}$ were exchanging due to commutation Kronecker deltas.

$$\frac{d}{dt}(X_{K,m}) = u_{k,L} X_{K,k} X_{L,m} + \frac{d}{dt} (X_{K,m}) + \frac{d}{dt} (X_{K,m}) \quad (48)$$

In Eq. (48) was delete the term $\frac{d}{dt} (X_{K,m})$ in both sides

$$0 = u_{k,L} X_{K,k} X_{L,m} + \frac{d}{dt} (X_{K,m}) \quad (49)$$

Clearing $\frac{d}{dt} (X_{K,m})$ we obtain

$$\frac{d}{dt} (X_{K,m}) = -u_{k,L} X_{K,k} X_{L,m} \quad (50)$$

Substituting Eq. (50) into Eq. (43) becomes

$$\dot{E}_m = \frac{d}{dt} [W_K X_{K,m}] = \dot{W}_K X_{K,m} - u_{k,L} X_{K,k} X_{L,m} W_K \quad (51)$$

Then, we replace the Eq. (51) into Eq. (39).

$$\rho \dot{\chi} = \tau^S_{mk} u_{k,m} - P_m E_k u_{k,m} - P_m (\dot{W}_K X_{K,m} - u_{k,L} X_{K,k} X_{L,m} W_K) \quad (52)$$

The index L was changed by k , into $u_{k,L}$, due to $X_{L,m}$

$$\rho \dot{\chi} = \tau^S_{mk} u_{k,m} - P_m E_k u_{k,m} - P_m (\dot{W}_K X_{K,m} - u_{k,m} X_{K,k} W_K) \quad (53)$$

In Eq. (53), the term $X_{K,k} W_K$ is the electric field concerning the current state.

$$\rho \dot{\chi} = \tau^S_{mk} u_{k,m} - P_m E_k u_{k,m} - P_m \dot{W}_K X_{K,m} + P_m u_{k,m} E_k \quad (54)$$

From Eq. (54) the term $P_m E_k u_{k,m}$ was removed to get

$$\rho \dot{\chi} = \tau^S_{mk} u_{k,m} - P_m \dot{W}_K X_{K,m} \quad (55)$$

2.2.2 Polarization vector

In this subsection, we will perform the transformation of the polarization vector to the reference state.

$$P_L = J X_{L,i} P_i \quad (56)$$

Where J is the Jacobian, multiplying Eq. (56) by $J^{-1} y_{m,L}$ we obtain

$$J^{-1} y_{m,L} P_L = J^{-1} y_{m,L} J X_{L,i} P_i = \delta_{mi} P_i \quad (57)$$

To get

$$P_m = J^{-1} y_{m,L} P_L \quad (58)$$

From Eq. (58) into Eq. (55) results in

$$\begin{aligned} \rho \dot{\chi} &= \tau^S_{mk} u_{k,m} - J^{-1} y_{m,L} P_L \dot{W}_K X_{K,m} \\ \rho \dot{\chi} &= \tau^S_{mk} u_{k,m} - J^{-1} P_L \dot{W}_K \frac{\partial y_m}{\partial X_L} \frac{\partial X_K}{\partial y_m} \\ \rho \dot{\chi} &= \tau^S_{mk} u_{k,m} - J^{-1} P_L \dot{W}_K \delta_{KL} \\ \rho \dot{\chi} &= \tau^S_{mk} u_{k,m} - J^{-1} P_K \dot{W}_K \end{aligned} \quad (59)$$

Until now, in Eq. (59), we have obtained a partial transformation, and still missing transform the symmetric Cauchy stress tensor τ^S_{mk} .

2.2.3 Second Piola-Kirchhoff stress

The symmetric tensor τ^S_{mk} is related with second Piola-Kirchhoff stress T^S_{KL} through a reverse transformation as follow:

$$\tau^S_{mk} = J^{-1} y_{m,K} y_{k,L} T^S_{KL} \quad (60)$$

Eq. (60) into Eq. (59) results in

$$\rho \dot{\chi} = J^{-1} y_{m,K} y_{k,L} T^S_{KL} u_{k,m} - J^{-1} P_K \dot{W}_K \quad (61)$$

The gradient of velocity $u_{k,m}$ can be separated on antisymmetric tensor $\omega_{mk} = \frac{1}{2}(u_{k,m} - u_{m,k})$ plus a symmetric tensor $d_{mk} = \frac{1}{2}(u_{k,m} + u_{m,k})$.

$$\rho \dot{\chi} = J^{-1} y_{m,K} y_{k,L} T^S_{KL} (\omega_{mk} + d_{mk}) - J^{-1} P_K \dot{W}_K \quad (62)$$

$$\rho \dot{\chi} = J^{-1} y_{m,K} y_{k,L} T^S_{KL} \omega_{mk} + J^{-1} y_{m,K} y_{k,L} T^S_{KL} d_{mk} - J^{-1} P_K \dot{W}_K$$

From Eq. (61), the product between symmetric tensor T^S_{KL} and antisymmetric tensor ω_{mk} result be null

$$\rho\dot{\chi} = J^{-1}y_{m,K}y_{k,L}T^S_{KL}d_{mk} - J^{-1}P_K\dot{W}_K \quad (63)$$

The term $y_{m,K}y_{k,L}d_{mk}$ will be solved as following

$$\begin{aligned} y_{m,K}y_{k,L}d_{mk} &= y_{m,K}y_{k,L} \frac{1}{2}(u_{k,m} + u_{m,k}) = \frac{1}{2}(u_{k,m}y_{m,K}y_{k,L} + u_{m,k}y_{m,K}y_{k,L}) \\ y_{m,K}y_{k,L}d_{mk} &= \frac{1}{2} \left(\frac{\partial u_k}{\partial y_m} \frac{\partial y_m}{\partial X_K} \frac{\partial y_k}{\partial X_L} + \frac{\partial u_m}{\partial y_k} \frac{\partial y_m}{\partial X_K} \frac{\partial y_k}{\partial X_L} \right) = \frac{1}{2} \left(\frac{\partial u_k}{\partial X_K} \frac{\partial y_k}{\partial X_L} + \frac{\partial u_m}{\partial X_L} \frac{\partial y_m}{\partial X_K} \right) \\ y_{m,K}y_{k,L}d_{mk} &= \frac{1}{2}(u_{k,K}y_{k,L} + u_{m,L}y_{m,K}) \end{aligned} \quad (64)$$

We interchange the index k to m in $u_{k,K}$.

$$\begin{aligned} y_{m,K}y_{k,L}d_{mk} &= \frac{1}{2}(u_{m,K}y_{k,L} + u_{m,L}y_{m,K}) = \frac{1}{2}(\dot{y}_{m,K}y_{k,L} + \dot{y}_{m,L}y_{m,K}) \\ y_{m,K}y_{k,L}d_{mk} &= \frac{1}{2} \frac{d}{dt}(y_{m,K}y_{k,L}) = \frac{d}{dt} \left[\frac{1}{2}(y_{m,K}y_{k,L} - \delta_{KL}) \right] \end{aligned} \quad (65)$$

With $m = k$ the term $\frac{1}{2}(y_{m,K}y_{k,L} - \delta_{KL})$ is known as the finite strain tensor E_{KL} in the reference state, and \dot{E}_{KL} with an uppercase index will represent the electric field vector in the reference state. Then, we reduce $y_{m,K}y_{k,L}d_{mk}$ to:

$$y_{m,K}y_{k,L}d_{mk} = \frac{d}{dt}(E_{KL}) = \dot{E}_{KL} \quad (66)$$

Substituting Eq. (66) into Eq. (63), we obtain

$$\rho\dot{\chi} = J^{-1}T^S_{KL}\dot{E}_{KL} - J^{-1}P_K\dot{W}_K \quad (67)$$

Factoring the inverse of Jacobian, we get

$$\rho\dot{\chi} = J^{-1}(T^S_{KL}\dot{E}_{KL} - P_K\dot{W}_K) \quad (68)$$

Multiplying both sides into Eq. (68) by the Jacobian gives

$$J\rho\dot{\chi} = JJ^{-1}(T^S_{KL}\dot{E}_{KL} - P_K\dot{W}_K) \quad (69)$$

Using mass transformation to the reference state $\rho^0 = \rho J$ into Eq. (69), we get a new equation for energy conservation in terms of physical quantities in the reference state. Symmetric tensor T^S_{KL} , strain tensor E_{KL} , polarization P_K and gradient of potential W_K .

$$\rho^0\dot{\chi} = T^S_{KL}\dot{E}_{KL} - P_K\dot{W}_K \quad (70)$$

2.3 Constitutional equations from free energy

The conservation laws are valid for any piezoelectric material, including cement-based composites. However, a specific material's piezoelectric properties are determined by a set of functions that describes free energy, symmetric tensor, and polarization. Once we replace these functions into Eq. (70), we will get the

piezoelectricity's constitutional equations. Take into account Eq. (70), we can propose the next dependence to the functions

$$\begin{aligned}\chi &= \chi(E_{KL}, W_K) \\ T^S_{KL} &= T^S_{KL}(E_{KL}, W_K) \\ P_K &= P_K(E_{KL}, W_K)\end{aligned}\quad (71)$$

Derivation respect to time the free energy into Eq. (71) as follow

$$\dot{\chi} = \frac{\partial \chi}{\partial E_{KL}} \dot{E}_{KL} + \frac{\partial \chi}{\partial W_K} \dot{W}_K \quad (72)$$

Substituting Eq. (72) into Eq. (70), we obtain

$$\rho^0 \frac{\partial \chi}{\partial E_{KL}} \dot{E}_{KL} + \rho^0 \frac{\partial \chi}{\partial W_K} \dot{W}_K = T^S_{KL} \dot{E}_{KL} - P_K \dot{W}_K \quad (73)$$

Both sides of Eq. (73) were compared to deduce two transformations, which resulting symmetric tensor T^S_{KL} and polarization P_K . The transformations use free energy as a generating function, as shown in Eq. (75).

$$T^S_{KL} = \rho^0 \frac{\partial \chi}{\partial E_{KL}} \quad (74)$$

$$P_K = -\rho^0 \frac{\partial \chi}{\partial W_K} \quad (75)$$

The mathematical structure of the free energy function will define the order of constitutional equations. There are functions for the free energy of piezoelectric materials from order 1 to order 3 [15]. It means that piezoelectric material behavior depends on the free energy function and its parameters. Here is an example of free energy function with order three

$$\begin{aligned}\rho^0 \chi &= \frac{1}{2} c_{ABCD} E_{AB} E_{CD} - e_{ABC} W_A E_{BC} - \frac{1}{2} \chi^E_{AB} W_A W_B + \frac{1}{6} c_{ABCDEF} E_{AB} E_{CD} E_{EF} \\ &+ \frac{1}{2} d_{ABCDE} W_A E_{BC} E_{DE} - \frac{1}{2} b_{ABCD} W_A W_B E_{CD} - \frac{1}{6} \chi^E_{ABC} W_A W_B W_C \\ &+ \frac{1}{24} c_{ABCDEFGH} E_{AB} E_{CD} E_{EF} E_{GH} + \frac{1}{6} d_{ABCDEFG} W_A E_{BC} E_{DE} E_{FG} \\ &+ \frac{1}{4} a_{ABCDEF} W_A W_B E_{CD} E_{EF} + \frac{1}{6} d_{ABCDE} W_A W_B W_C E_{DE} \\ &- \frac{1}{24} \chi^E_{ABCD} W_A W_B W_C W_D + \dots,\end{aligned}\quad (76)$$

The parameters are called elasticity c , piezoelectric e , electric permeability χ^E , odd electrolytic d , electrostrictive b , and electroelastic force even a .

2.3.1 The linear approach of piezoelectricity

We take on order one approach from Eq. (76) to free energy χ . Then, replacing it in Eq. (74) and Eq. (75) to obtain

$$T_{AB}^S = \frac{\partial}{\partial E_{AB}} \left(\frac{1}{2} c_{ABCD} E_{AB} E_{CD} - e_{ABC} W_A E_{BC} - \frac{1}{2} \chi_{AB}^E W_A W_B \right) \quad (77)$$

$$P_A = - \frac{\partial}{\partial W_A} \left(\frac{1}{2} c_{ABCD} E_{AB} E_{CD} - e_{ABC} W_A E_{BC} - \frac{1}{2} \chi_{AB}^E W_A W_B \right) \quad (78)$$

The approximation is possible if we consider an infinitesimal deformation, weak electric field, and low amplitude displacements around the reference state. Hence, it approaches require a nomenclature exchange for physical quantities. Thus, second Piola-Kirchhoff stress will be replaced by infinitesimal Cauchy stress tensor $T_{KL}^S \rightarrow T_{ij}$; finite strain tensor will be exchanged by infinitesimal strain tensor $E_{KL} \rightarrow S_{kl}$; potential gradient, polarization, and displacement electric vector are similar either reference or current state: $W_K \rightarrow E_k$, $P_L \rightarrow P_i$, and $D_L \rightarrow D_i$. Then, Eqs. (77) and (78) follow:

$$T_{ij} = \frac{\partial}{\partial S_{ij}} \left(\frac{1}{2} c_{ijkl} S_{ij} S_{kl} - e_{ijk} E_i S_{jk} - \frac{1}{2} \chi_{ij}^E E_i E_j \right) \quad (79)$$

$$P_i = - \frac{\partial}{\partial E_i} \left(\frac{1}{2} c_{ijkl} S_{ij} S_{kl} - e_{ijk} E_i S_{jk} - \frac{1}{2} \chi_{ij}^E E_i E_j \right) \quad (80)$$

Here is considering symmetry to parameters elastic c_{ijkl} , piezoelectric e_{kij} , and electric χ_{ik} when they have odd permutations. Differentiating the Eq. (79) and Eq. (80), we obtain

$$T_{ij} = c_{ijkl} S_{kl} - e_{kij} E_k \quad (81)$$

$$P_i = e_{ikl} S_{kl} + \chi_{ik}^E E_k \quad (82)$$

The polarization can be written in terms of electric displacement vector too.

$$P_i = D_i - \varepsilon_0 E_i \quad (83)$$

From Eq. (83) into Eq. (82) gives

$$D_i - \varepsilon_0 E_i = e_{ikl} S_{kl} + \chi_{ik}^E E_k \quad (84)$$

Solving D_i ,

$$D_i = e_{ikl} S_{kl} + \varepsilon_0 E_i + \chi_{ik}^E E_k = e_{ikl} S_{kl} + \varepsilon_0 \delta_{ik} E_i + \chi_{ik}^E E_k \quad (85)$$

Factoring E_k ,

$$D_i = e_{ikl} S_{kl} + (\varepsilon_0 \delta_{ik} + \chi_{ik}^E) E_k \quad (86)$$

where the term $\varepsilon_0 \delta_{ik} + \chi_{ik}^E$ is defined as dielectric constant ε_{ik} . Finally, we have the linear constitutional equation for the electric displacement vector.

$$D_i = e_{ikl} S_{kl} + \varepsilon_{ik} E_k \quad (87)$$

We have seen several forms to present the linear constitutional equations in piezoelectricity. Next, we include another form of constitutional equations shown in the IEEE standard for piezoelectricity. It can be obtained inverting the matrix formed by Eq. (81) and Eq. (82).

$$D_i = d_{ikl}S_{kl} + \varepsilon_{ik}^T E_k \quad (88)$$

$$S_{ij} = s_{ijkl}^D T_{kl} + g_{kij} D_k \quad (89)$$

The electromechanical properties are defined by piezoelectric charge d_{ikl} and voltage g_{kij} constants. Unlike parameters c_{ijkl} and e_{ikl} These new piezoelectric constants are taken out directly from experiments, as shown in the next section.

2.4 Electromechanical and electrical properties of cement-based composites

Incorporating piezoelectric nanocomposites into cement paste improves its piezoelectric and mechanical properties [16] due to increased deformable crystal structures. Zeolites, oxides, and carbon nanotubes are the most used cement-based composites to improve these properties [17]. Chen et al. also report some piezoelectric parameters of cement-based composites such as piezoelectric charge d_{33} , voltage g_{33} . And the coupling factor K_t . As was mentioned in the previous section, these piezoelectric parameters come from linear piezoelectricity theory. However, the crystalline structure of Calcium Silicate Hydrate (C-S-H) that compose the cement is a complex system described by linear theory. It could also be combined with statistical physics and mean-field homogenization theory tools to get the macroscale properties [18]. Here are show piezoelectric and electrical parameters of gold nanoparticles mixed to cement paste, which we hope to lead to our system's constitutional equations.

Next, we introduce a brief description of the gold nanoparticles' physical synthesis [19, 20]. They are produced by laser ablation at 532 nm. A gold plate at 99.9999% purity is put inside a beaker filled with 50 mL of ultrapure water. Then, the pulse laser spot with an energy of 30 mJ beats the gold plate by 10 minutes, as shown in **Figure 3**.

At the time, the gold nanoparticles were brought to be characterized by dynamical light scattering (DLS). If not done quickly, the gold nanoparticles were agglomerated. These measures are required because the gold nanoparticles directly affect the piezoelectric properties of cement cylinders. Some results of gold nanoparticle sizes are shown in **Figure 4**.

Also, the gold nanoparticles in water must be mixed quickly with the cement. The ratio of water/cement used was 0.47 mL/g. Then, the admixture was poured into cylindrical molds that contained copper wires as follows in **Figure 5**.

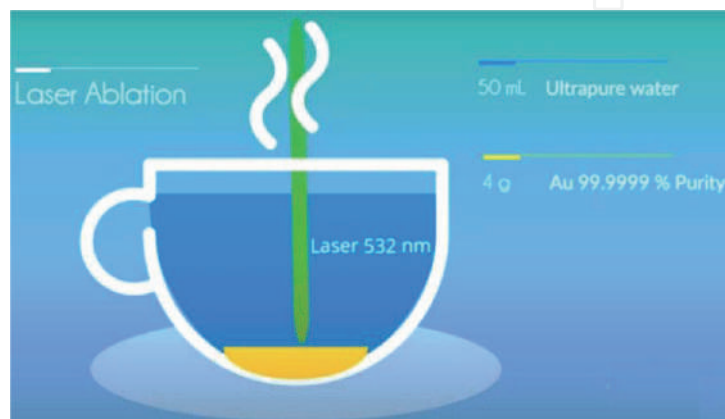


Figure 3.
 Scheme of nanoparticle physical synthesis by laser ablation.

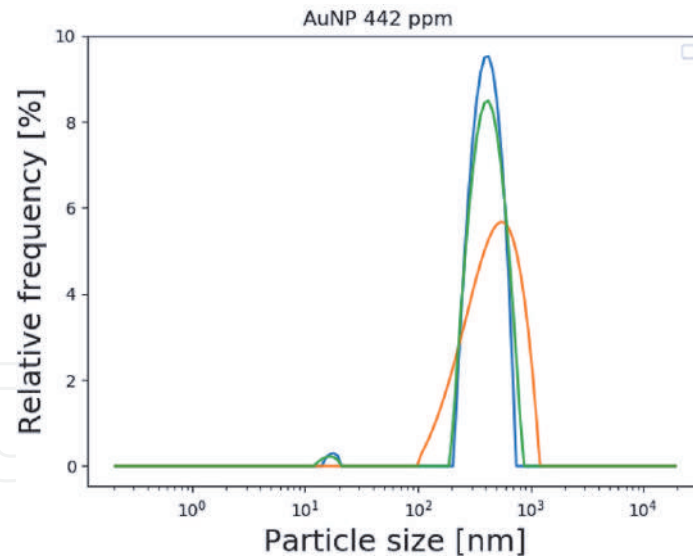


Figure 4.
The particle size distribution of gold nanoparticles suspended in water to concentration 442 ppm.



Figure 5.
Molds and dimensions of cement cylinders.

The cement cylinders were dried one day. Then it leaves curing for 28 days and finally to thermal treatment one day more. After 14 days, electromechanical measurements were performed, as shown in **Figure 6**.

Electromechanical measurements consist of two measurements performed in parallel: the cement cylinders under compressive strength test in the axial direction, open circuit potential (OCP) measurements in the electrodes of cement cylinders. From mechanical and electrical data, we calculated an electroelastic parameter with units $[mV/kN]$, it has the same interpretation of piezoelectric parameter e in linear theory. From **Figure 7**, an example of voltage-force curves for identically cement samples with gold nanoparticles is shown. We did get from the above measurements the axial elasticity parameter:

$$Y = 323.5 \pm 75.3 [kN/m^2] \quad (90)$$

The axial piezoelectric parameter:

$$\gamma = -20.5 \pm 6.9 [mV/kN]. \quad (91)$$

For a total deformation $S = 0.57 \pm 0.09 [mm]$ in the axial direction.

The electrical properties of cement cylinders were obtained from the imaginary part of impedance; an example of these curves in **Figure 8**. From impedance data

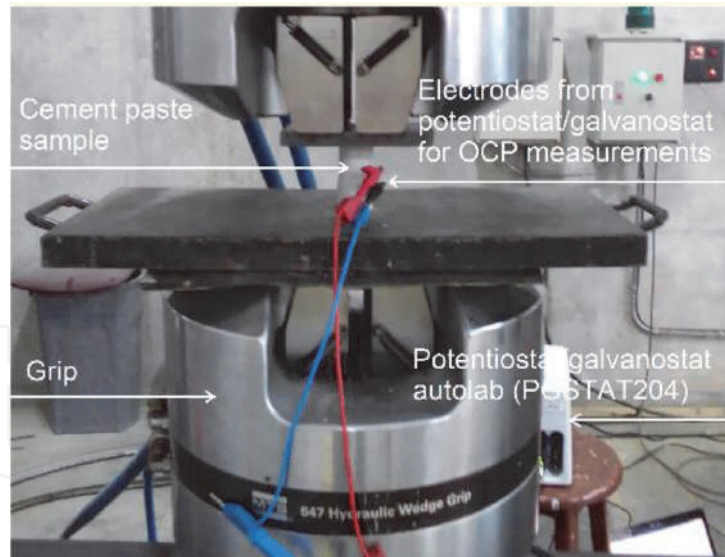


Figure 6.
 Experimental setup of electromechanical measurements.

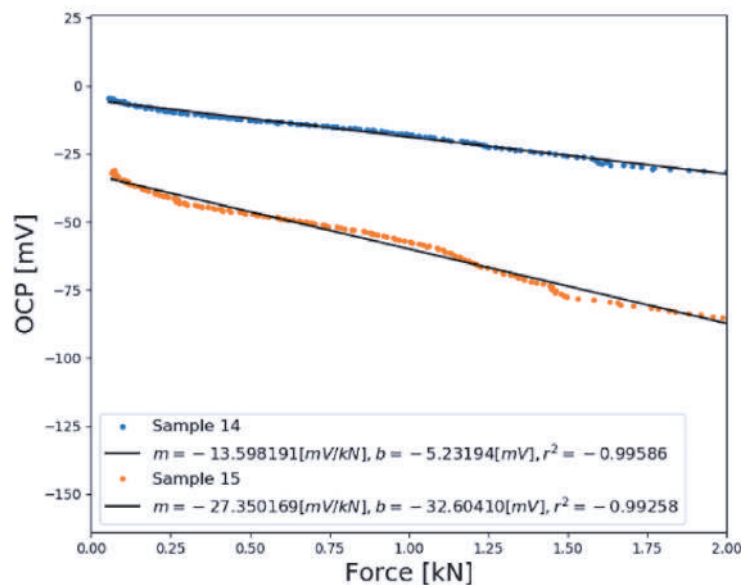


Figure 7.
 OCP-force curves from cement cylinders with gold nanoparticles concentrated to 658 ppm.

can perform a transformation to get a real part of the capacitance C' . It has frequency dependence as follow

$$C'(\omega) = \frac{1}{\omega Z''} \quad (92)$$

The geometry of copper electrodes (an approximation to parallel plates) is related to capacitance. Therefore, we can calculate the dielectric parameter ϵ since 1 MHz; this parameter is a real number that depends on the frequency and is given by

$$\epsilon(\omega)\epsilon_0 = \frac{d * C'}{A} \quad (93)$$

where ϵ_0 is the electric permittivity of free space, A is the transversal section, and d is the thickness between electrodes.

From the data in **Figure 8** and Eq. (92) and Eq. (93), we obtain the dielectric constant:

$$\varepsilon = (939.6 \pm 82.9)\varepsilon_0 \quad (94)$$

Where ε_0 has unit $[F/m]$. The piezoelectric and electrical properties of cement paste mixed with gold nanoparticles exhibit reproducibility and linearity of the piezoelectric parameter.

2.5 Future studies and remarks

The Piezoelectric parameters are an initial point to beginning a new connection with piezoelectricity theory by inverse modeling and constructing new free energy functions and constitutional equations. To catch out with researchers in this scope, we suggest thinking about the next research questions; how is the piezoelectric parameter presented related to the piezoelectric parameter formulated by linear theory for piezoelectricity? Is the free energy function of order one sufficient to describe cement paste's piezoelectric with gold nanoparticles? How to develop a new function for free energy that models cement paste's piezoelectric behavior of cement paste with gold nanoparticles?

In this chapter, we have intended to contribute to the theory of piezoelectricity for large deformations without including an energy function. **Figure 9** shows a possible use around IoT as intelligent sensing of devices based on cement-based composites' piezoresistivity. Without reaching into depth in the technical and engineering aspect that smart construction, active sensing system entails; we highlight how the Eqs. (88) and (89) that relate the electromechanical properties and that are defined by piezoelectric charge d_{ikl} and voltage g_{kij} constants are present as indicators to improve the detection resolution in large structures with large deformations.

The sensors analyze the deformations, temperature, relative humidity, and other critical parameters of the concrete in real-time. This data is captured via wireless communication (WAN/BLE) and deployed on a secure and scalable platform (Cloud) capable of collecting data to facilitate remote decision making with

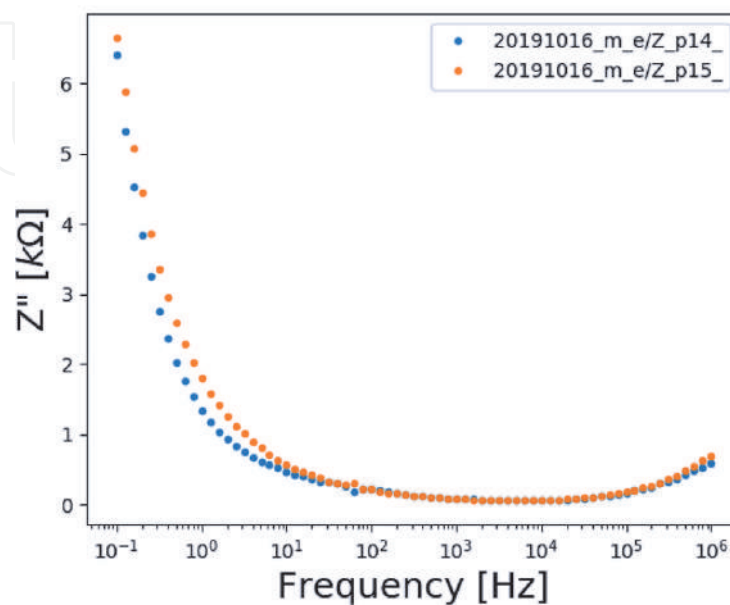


Figure 8.

The imaginary part of electrical impedance represented in a Bode plot was performed on two cement cylinders with gold nanoparticles concentrated to 658 ppm.

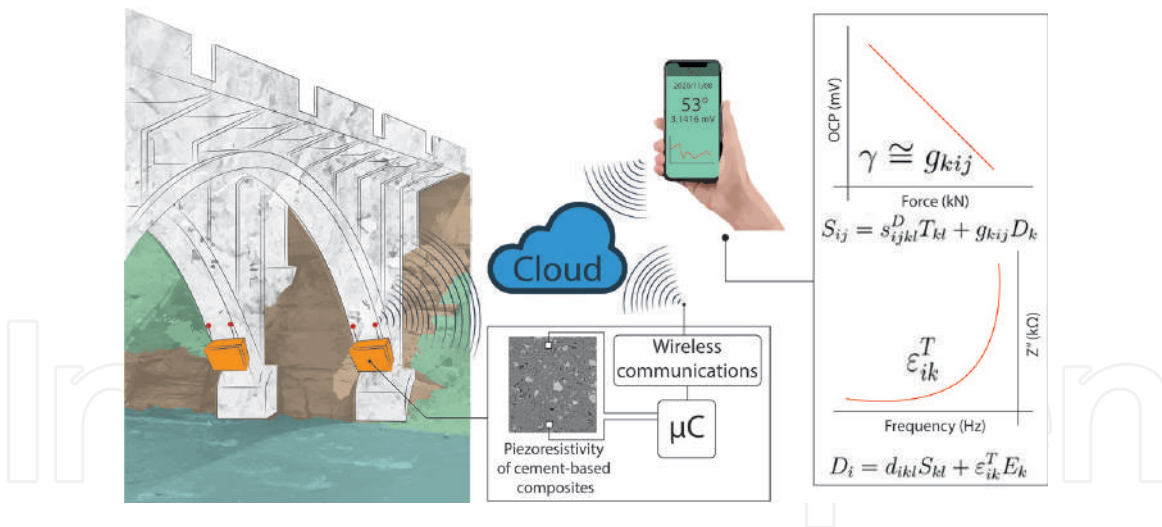


Figure 9.
 The image shows a network of IoT sensors based on cement-based composites piezoresistivity as an active part of smart construction.

information from deep within the concrete. The experimental control of the NPs embedded within the cement paste's dispersions and piezoresistive responses is essential to have a good signal-to-noise ratio within the sensing. Knowing the coupling between the electromechanical equations from a theoretical approach is another crucial factor in making viable these technological solutions.

3. Conclusions

This chapter proposed a mathematical physicist construction of the linear theory of piezoelectricity since classical movement laws and the conservation of their physical quantities (mass, charge, linear momentum, angular momentum, and energy) over time. This construction takes parts of Eringen, Tiersten, and Yang's research without including the variational formulation or energy functional to deduce the constitutional equations. We have also presented some results of piezoelectric and dielectric constants obtained for cement mixed to gold nanoparticles. We got the axial elasticity parameter $Y = 323.5 \pm 75.3 [kN/m^2]$, the electroelastic parameter $\gamma = -20.5 \pm 6.9 [mV/kN]$, and dielectric constant $\epsilon = (939.6 \pm 82.9)\epsilon_0 [F/m]$, which can be compared with parameters s_{ijkl}^D , g_{kij} and ϵ_{ik}^T respectively presents into constitutional equations discussed in the chapter.

Acknowledgements

We would like to thank the Vice-rector for research in project N 2676 of the Universidad Industrial de Santander, the CIMBIOS research group for the ablation laser system (Universidad Industrial de Santander), and the CA Perez-Lopez for his support in the editing of images of the Department of Electrical and Electronic Engineering of the Universidad de los Andes Colombia.

Conflict of interest

The authors declared no potential conflicts of interest concerning the research, authorship, and/or publication of this book chapter.

Appendices and nomenclature

In the reference state, the continuum has a volume V , and mass density ρ^0 .

In the current state, the continuum has a volume v , mass density ρ , electronic charge density μ^e and lattice charge density μ^l . Besides, In the current state with infinitesimal displacement η , the electronic charge does not change its volume.

The capital letter in the index is for the reference state X_K And the lowercase letters to the current state y_i . Also, the index in the physics quantities can denote a vector. For example X_K, y_i, u_i ; or a tensor, for example E_{KL}, τ_{jk} . Another form to present a vector quantity is the right-pointing arrow \vec{y} .

The velocity of the continuum is denoted by lower case letter u , and just makes sense in the current state.

The partial derivate is denoted by comma separation in the indexes. For example $y_{i,i}$.

Author details

Daniel A. Triana-Camacho¹, Jorge H. Quintero-Orozco¹
and Jaime A. Perez-Taborda^{2*}

¹ CIMBIOS Group, Physics Department, Universidad Industrial de Santander, Bucaramanga, Colombia

² Department of Electrical and Electronic Engineering, Universidad de los Andes, Bogotá, Colombia

*Address all correspondence to: jaimeandres@protonmail.com

IntechOpen

© 2021 The Author(s). Licensee IntechOpen. This chapter is distributed under the terms of the Creative Commons Attribution License (<http://creativecommons.org/licenses/by/3.0>), which permits unrestricted use, distribution, and reproduction in any medium, provided the original work is properly cited. 

References

- [1] Katzir, S. The beginnings of piezoelectricity: A study in mundane physics. Springer Science & Business Media; 2007. 273 p. DOI: 10.1007/978-1-4020-4670-4
- [2] Voigt, W. Piezo-und pyroelectricität, dielectriche influenz und electrostriction bei krystallen ohne symmetriecentrum. *Annalen Der Physik*. 1985;291(8):701-731. DOI: 10.1002/andp.18952910812
- [3] Eringen, A. C. On the foundations of electroelastostatics. 1963;1(1):127-153. DOI: 10.1016/0020-7225(63)90028-4
- [4] Toupin, R. A. The elastic dielectric. *Journal of Rational Mechanics and Analysis*. 1956;5(6):849-915. Retrieved from <http://www.jstor.org/stable/24900192>
- [5] Tiersten, H. F. On the non-linear equations of thermo-electroelasticity. *International Journal of Engineering Science*. 1972;9(7):587-604. DOI: 10.1016/0020-7225(71)90062-0
- [6] Martin, R. M. Piezoelectricity. *Physical Review B*. 1972;5(4):1607-1613. DOI: 10.1103/PhysRevB.5.1607
- [7] Casamento, J., Chang, C. S., Shao, Y. T., Wright, J., Muller, D. A., Xing, H., & Jena, D. Structural and piezoelectric properties of ultra-thin ScxAl1-xN films grown on GaN by molecular beam epitaxy. *Applied Physics Letters*. 2020; 117(11):112101. DOI: 10.1063/5.0013943
- [8] Auld, B. A. *Acoustic fields and waves in solids* Рипол Классик. John Wiley & Sons, New York. 1973.
- [9] Ma, J., Ren, J., Jia, Y., Wu, Z., Chen, L., Haugen, N. O., ... & Liu, Y. High efficiency bi-harvesting light/vibration energy using piezoelectric zinc oxide nanorods for dye decomposition. *Nano Energy*. 2019;62:376-383. DOI: 10.1016/j.nanoen.2019.05.058
- [10] Bechmann, R. Elastic and piezoelectric constants of alpha-quartz. *Physical Review*, 1958;110(1): 1060-1061. DOI: 10.1103/PhysRev.110.1060
- [11] Tiersten, H. F. *Linear piezoelectric plate vibrations: Elements of the linear theory of piezoelectricity and the vibrations piezoelectric plates*. Springer, Boston, MA. 2013. DOI: 10.1007/978-1-4899-6453-3
- [12] Yang, J. On the derivation of electric body force, couple and power in an electroelastic body. *Acta Mechanica Solida Sinica*. 2015;28(6):613-617.
- [13] Yang, J. Differential derivation of momentum and energy equations in electroelasticity. *Acta Mechanica Solida Sinica*. 2017;30(1), 21-26.
- [14] Abeyaratne, R., & Knowles, J. K. A continuum model of a thermoelastic solid capable of undergoing phase transitions. *Journal of the Mechanics and Physics of Solids*. 1993;41(3): 541-571. DOI: 10.1016/0022-5096(93)90048-K
- [15] Tiersten, H. F. Non-linear electroelastic equations cubic in the small field variables. *The Journal of the Acoustical Society of America*. 1975;57(3):660-666. DOI:10.1121/1.380490
- [16] Chen, J., Qiu, Q., Han, Y., & Lau, D. Piezoelectric materials for sustainable building structures: Fundamentals and applications. *Renewable and Sustainable Energy Reviews*. 2019;101:14-25. DOI: 10.1016/j.rser.2018.09.038
- [17] Paul, S. C., van Rooyen, A. S., van Zijl, Gideon P. A. G., & Petrik, L. F. Properties of cement-based composites using nanoparticles: A comprehensive review. *Construction and Building Materials*. 2018;189:1019-1034. DOI: 10.1016/j.conbuildmat.2018.09.062

[18] Qomi, M. J. A., Ulm, F. J., & Pellenq, R. J. M. Physical origins of thermal properties of cement paste. *Physical Review Applied*. 2015;3(6): 064010. DOI: 10.1103/PhysRevApplied.3.064010

[19] Yan, Z., & Chrisey, D. B. Pulsed laser ablation in liquid for micro-/ nanostructure generation. *Journal of Photochemistry and Photobiology C: Photochemistry Reviews*. 2012;13(3): 204-223. DOI:10.1016/j.jphotochemrev.2012.04.004

[20] Huang, H., Lai, J., Lu, J., & Li, Z. Pulsed laser ablation of bulk target and particle products in liquid for nanomaterial fabrication. *AIP Advances*. 2019;9(1):015307. DOI: 10.1063/1.5082695

IntechOpen

Sustainable Recycling of Marble Dust as Cement Replacement in Concrete: Advances and Recent Trends

Ahed Habib and Maan Habib

Abstract

In recent years, many researchers in the construction industry had taken up the challenge to incorporate non-biodegradable wastes as partial replacement of cement and/or natural aggregates in the daily production of cement-based materials. Various efforts were intended to understand the influence of using marble dust in concrete due to its availability and a relatively high volume of the generation that causes serious environmental problems. Previous studies have utilized marble dust as a replacement of cement, fine aggregate, or total paste in the concrete and mortar mixtures. In general, several investigations have shown that up to a certain cement replacement ratio, marble dust can positively impact on the strength and micro-structure properties of concrete. Furthermore, the results have indicated that the considerably high degree of fineness in the marble dust provides sufficient cohesiveness of mortar and concrete even in low w/c ratio conditions. Hence, this powder can be utilized as a filler to improve the flowability of cement-based materials. Consequently, this chapter aims to summarize recent investigations on the properties of concrete incorporating marble waste as cement replacement materials, highlight the potential gaps in the literature, and propose a prediction model for estimating the compressive and flexural strengths of concrete with marble dust using regression analysis.

Keywords: sustainable materials, marble dust, cement-based materials, cement replacement, mechanical properties

1. Introduction

Throughout the last few decades, considerable efforts in the scientific community were focused on providing sustainable solutions for minimizing non-biodegradable wastes by suggesting innovative waste management plans. Recently, the construction industry has started taking an active role in recycling these materials by utilizing them as a partial replacement of the constituents in cement-based productions, aiming to come up with a green alternative for conventional construction materials.

Stone marble industrial activities, including mining, processing, and finishing, have contributed to the development of several major environmental risks [1].

One of these risks is the disposal of marble wastes that are raised during the production of marble slabs. Currently, the availability and the reasonably high volume of a generation of marble dust has attracted several researchers to conduct investigations on the possibility of utilizing this waste material as a partial replacement of cement [2–4], fine aggregates [5, 6], or total paste in concrete, mortar, and asphaltic mixtures [7, 8]. The main benefit of replacing cement by marble dust comes from the reduction in the cost of the mixture, and CO₂ emission related to the production of cement [9].

Previous studies have illustrated that incorporating this material in concrete affects its fresh, mechanical, durability, and porosity properties [10–12]. Its main impact on the strength carrying capacity of concrete is generally considered such that when replacing a low percentage of the cement with marble dust, the strength is improved. However, at high replacement ratios, beyond 10% to 15%, the compressive and tensile strengths of the concrete reduce. Another importance of this material, in addition to its sustainable benefits, comes from the high degree of fineness that allows utilizing it as filler in cement-based mixtures.

Therefore, this chapter is intended to offer a brief review of the utilization and mechanical properties of cement-based materials incorporating marble dust with emphasis on concrete mixtures with marble wastes cement replacement. Another aim of the study is to propose estimation models using multiple regression analysis for the compressive and flexural strengths of marble dust concrete and highlight some observations on the influence of marble dust content and properties on the change in the concrete strength capacity.

2. Engineering properties marble dust

Marble is defined scientifically as a metamorphic rock composed of recrystallized calcite (CaCO₃) or dolomite (CaMg(CO₃)₂), while commercially as any limestone or dolomite processed and taking a polish, **Figure 1** [13]. During cutting and polishing these stones in the marble factories, a product composed of the marble dust mixed with water referred to in the literature as marble waste slurry is generated. Usually, marble dust is obtained by chemically processing the marble waste slurry to separate the wastewater from the marble dust.

The X-ray powder diffraction (XRD) pattern of marble dust is exhibited in **Figure 2**, which shows calcite (CaCO₃) as the main mineral component of this material. Also, **Figure 3** presents an example of a scanning electron microscope (SEM) micrographs of marble dust particles.

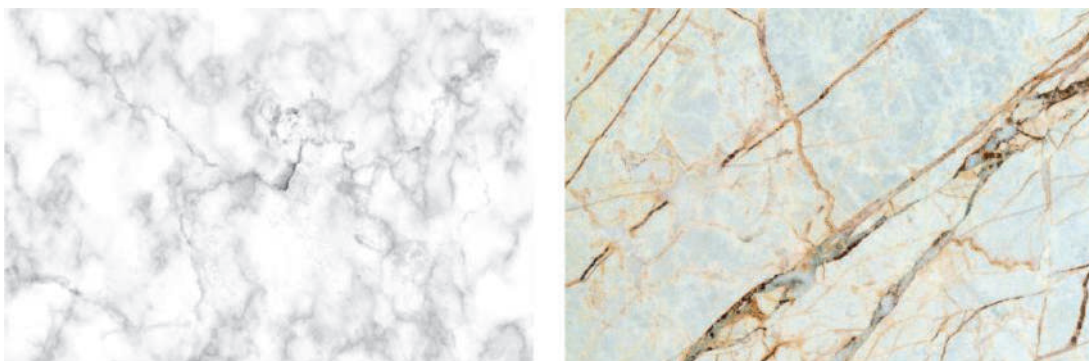


Figure 1.
Typical types of polished marbles.

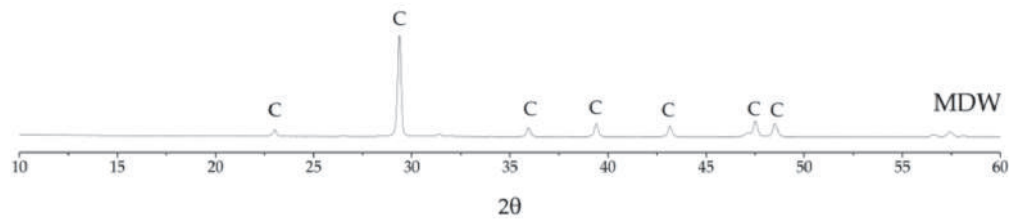


Figure 2.
 XRD pattern of marble dust waste as discussed in Julphunthong & Joyklad [14] study.

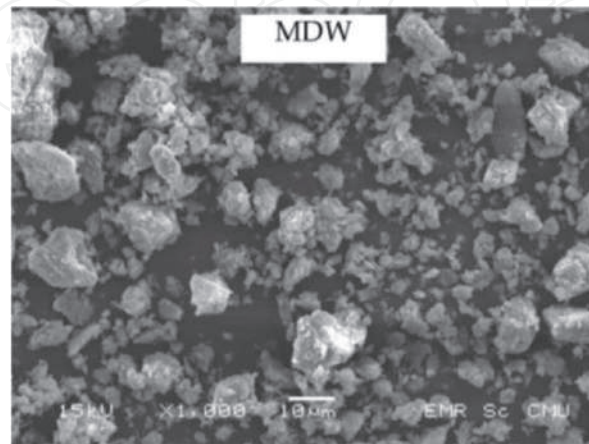


Figure 3.
 SEM image of marble dust as given by Julphunthong & Joyklad [14].

Author/s	Chemical analysis (wt. %)							
	CaO	SiO ₂	Fe ₂ O ₃	Al ₂ O ₃	MgO	Na ₂ O	K ₂ O	SO ₃
[16]	52.45	1.29	0.78	0.39	0.54	-	0.11	-
[17]	40.73	6.01	0.8	0.6	15.21	0.06	0.05	0.09
[18]	41.83	8.38	0.65	0.67	10.36	0.60	0.07	0.33

Table 1.
 Chemical compositions of marble dust as reported in the literature.

As reported previously, the specific gravity of this material varies over a wide range between 2.39 and 3.16 due to the difference in the structural and chemical properties of the marble stones [15]. Similarly, the chemical compositions of marble dust varies based on the type of stone used. Some examples of the chemical compositions from Gesoğlu et al. [16], Vardhan et al. [17], and Ashish [18] studies can be seen in **Table 1**.

The cutting one-meter cube of marble block into slabs of 2 cm thickness each, 25% of the total amount will turn into fine particles [19]. Previous studies, Gesoğlu et al. [16], Singh et al. [20], and Li et al. [21] presented the particle size distribution of marble wastes as demonstrated in **Figure 4**, in which it depends mainly on the method of cutting the marbles and the size of the produced layer.

3. Types of marble waste utilizations and potential applications

Over the last few years, marble dust has been introduced to various kinds of cement-based materials as a partial replacement of cement [2, 5], fine aggregate [22],

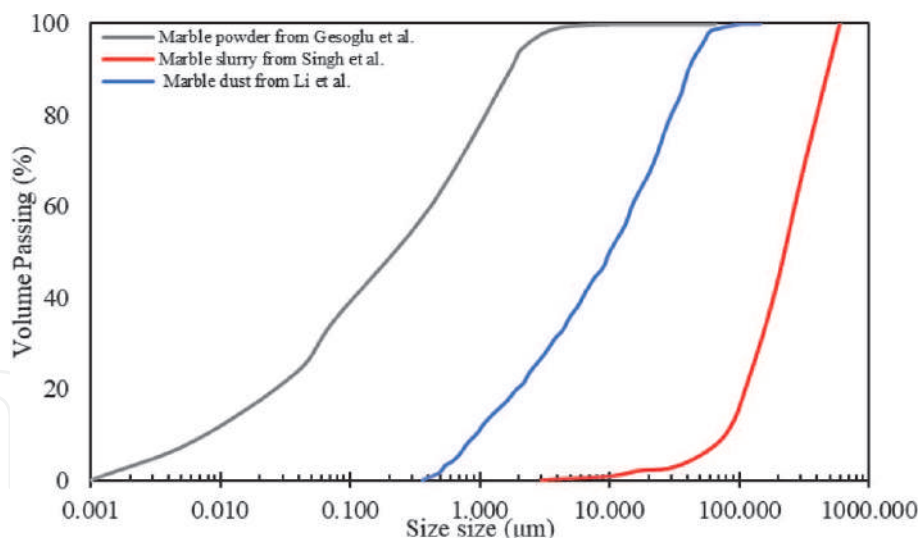


Figure 4.
Particle size distribution of marble wastes used in the literature.

Author/s	Mixture type	Type of replacement
[2–4]	Concrete	Cement
[1]	Concrete	Cement and fine aggregate
[23–25]	Self-compacting concrete	Cement
[26]	High-performance concrete	Cement
[5]	Concrete paving blocks	Fine aggregate
[27]	Concrete	Fine aggregate
[28]	Mortar	Cement
[6]	Mortar	Fine aggregate
[21]	Mortar	Total paste
[29]	Cement composites	Cement

Table 2.
A brief summary of the utilization of marble wastes in the literature.

or total paste [21]. The essential types of mixtures in which marble dust has been utilized can be epitomized as concrete, mortar, cement composites. A summary of the types of marble wastes utilization in cement-based materials can be seen in **Table 2**.

Previously Singh et al. [30] have discussed some of the potential applications of marble wastes in the construction industry. Some of these applications are presented as follows:

- It can be used as a filler for roads and embankment materials where water bound macadam can be laid.
- It can be implemented in the manufacturing process of bricks due to the existence of very fine particles in marble slurry.
- It can be utilized as a partial replacement of cement in concrete due to its capability of being used as a filler to improve the concrete's properties.

- It can be used in the production of hollow blocks and wall tiles in addition to other clay-based products.
- It can be utilized as a substitute of limestone in various construction materials and industrial applications.

4. Mechanical properties of concrete utilizing marble waste

In this section, the mechanical properties of a concrete mixture incorporating marble waste as partial replacement of cement will be introduced. Previous studies showed, **Figure 5**, that the mechanical properties of concrete mixtures are influenced when marble waste is incorporated. Ergün [3] observed that replacing 5% of the cement content by marble powder results in increasing the compressive strength of concrete by almost 12%. Also, he reported that at the same replacement ratio, a 5% increase in the flexural strength of concrete was achieved. In contrast, higher marble dust content indicated a negative effect on the flexural capacity. Moreover, Munir et al. [31] measured a slight increase in the compressive strength of concrete when 10% of its cement was replaced by marble powder. Vardhan et al. [17] reported that utilizing marble powder as a partial substitution of up to 10% of the cement content in concrete does not have a significant negative influence on the compressive strength. A similar observation was mentioned by Rana et al. [32].

Furthermore, Rana et al. [32] reported a slight reduction in the flexural capacity of concrete when marble wastes replaced up to 10% of the cement. In contrast, higher replacement ratios caused a considerable fall in flexural strength. The modulus of elasticity of concrete with marble powder as substitution of cement was investigated by Soliman [33]. In general, they concluded that up to a 5% ratio, the modulus of elasticity is positively impacted, and beyond this value, the parameter starts to drop slightly. Nevertheless, Usysal & Yilmaz [25] clarified that an increase in the modulus of elasticity when up to 20% of the cement was changed by marble powder in a self-compacting concrete mixture, but a slight decline is observed at 30% replacement ratio. Kumar and Kumar [2] measured an increase in the splitting tensile and flexural strengths by 9.21% and 7.5%, respectively, at 15% cement substitution, while the compressive strength was reduced by 9.06%. On the other hand, using a 20% replacement ratio caused a lowering in the compressive and tensile strengths as compared to the control specimens. This reduction in the strength properties of concrete incorporating high content of marble wastes, beyond 10% in most cases, as a substitution of cement, can be attributed to the decrease in the cement content [3].

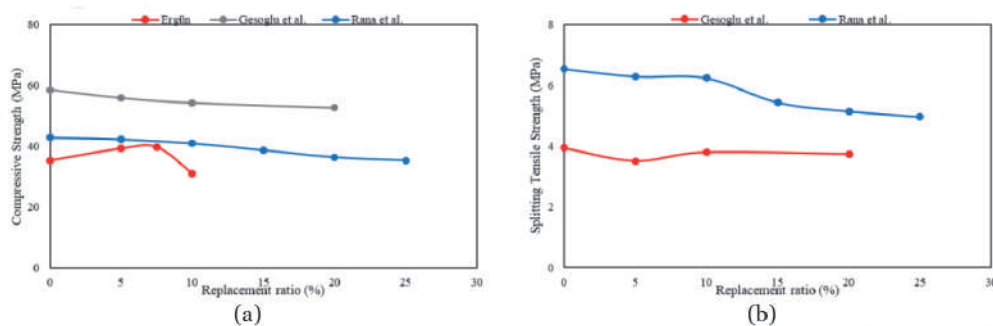


Figure 5.
An example of some mechanical properties of concrete utilizing marble waste as cement replacement
(a) compressive strength, (b) splitting tensile strength.

5. Prediction of concrete compressive strength

In this section, a prediction model for the compressive strength of concrete incorporating marble wastes as partial replacement of cement will be addressed.

5.1 Collected data

The collected dataset for generating the prediction models in this study are displayed in **Tables 3** and **4**. First of all, the papers that discussed the utilization of marble dust were collected. Thereafter, those studies that investigated the compressive and flexural strength of concrete utilizing marble waste as cement replacement were shortlisted, and their data were obtained using GetData graph digitizer software [36].

Several parameters are going to be used in developing the estimation model for marble dust compressive strength (f_{cm}) and its flexural strength (f_{tm}). These parameters are the control compressive strength (f_{cc}) or flexural strength (f_{tc}), marble dust content (MD_C), its CaO content (MD_{CaO}), and its specific gravity (MD_{SG}). The last three inputs are basically used to take the effect of marble waste properties on concrete behavior. Because this material does not have a standardized characteristic in which its properties depend on the type of rocks being processed in the factories.

5.2 Multiple linear regression

As mentioned previously, the multiple linear regression method will be used for building the mathematical expression of the estimation model. In general, it is a statistical way to establish a linear relationship between a dependent variable and two or more independent predictors [37]. The mathematical model that describes this method of estimation was discussed by Achen [38], as written in (Eq. (1)).

$$y_i = \beta_0 + \beta_1 x_{1i} + \dots + \beta_k x_{ki} + \varepsilon_i \quad (1)$$

where y_i is the i^{th} observation on the dependent variable; x_{1i}, \dots, x_{ki} are the i^{th} observations on the independent variables; β_0 is an intercept term; β_1, \dots, β_k are the coefficients to be estimated; and ε_i is a random error component of the i^{th} observation, also known as the residual.

After creating a prediction model, it is essential to test its goodness-of-fit. On this matter, the coefficient of determination (Eq. (2)) was adopted in this study in which values closer to one represents a good fitting model.

$$R^2 = 1 - \frac{\sum (y_i - \hat{y}_i)^2}{\sum (y_i - \bar{y})^2} \quad (2)$$

where y_i is the actual value, \hat{y}_i is the predicted one, and \bar{y} is the mean of the actual values.

Thereafter, the adequacy of the prediction model is evaluated by conducting a residual analysis through first plotting the residuals, (Eq. (3)), against one of the independent variables and then scaling these values using the standardized residuals method (Eq. (4)) to obtain potential outliers.

$$e_i = (y_i - \hat{y}_i) \quad (3)$$

Author/s	Marble waste properties			Compressive strength		
	Content (kg)	CaO (%)	Specific Gravity	f _{cc} (MPa)	f _{cm} (MPa)	Δf _c (%)
Ergün [3]	15	51.7	2.68	35.4	39.4	-10.15
Ergün [3]	22.5	51.7	2.68	35.4	39.9	-11.28
Ergün [3]	30	51.7	2.68	35.4	31.1	13.83
Gesoğlu et al. [16]	26	52.45	2.71	58.57	55.94	4.70
Gesoğlu et al. [16]	52	52.45	2.71	58.57	54.34	7.78
Gesoğlu et al. [16]	104	52.45	2.71	58.57	52.75	11.03
Rana et al. [32]	20.25	65.2	2.87	43	42.4	1.42
Rana et al. [32]	40.5	65.2	2.87	43	41.1	4.62
Rana et al. [32]	60.75	65.2	2.87	43	38.8	10.82
Rana et al. [32]	81	65.2	2.87	43	36.44	18.00
Rana et al. [32]	101.25	65.2	2.87	43	35.4	21.47
Sardinha et al. [34]	15.4	54.2	2.73	39.2	37.3	5.09
Sardinha et al. [34]	30.7	54.2	2.73	39.2	34.3	14.29
Sardinha et al. [34]	61.4	54.2	2.73	39.2	28	40.00
Sardinha et al. [34]	15.4	54.2	2.73	52.1	46.2	12.77
Sardinha et al. [34]	30.7	54.2	2.73	52.1	44.4	17.34
Sardinha et al. [34]	61.4	54.2	2.73	52.1	35.8	45.53
Sardinha et al. [34]	15.4	54.2	2.73	53.6	53.5	0.19
Sardinha et al. [34]	30.7	54.2	2.73	53.6	47.95	11.78
Sardinha et al. [34]	61.4	54.2	2.73	53.6	37.4	43.32
Singh et al. [20]	42.2	26.63	2.67	38.54	39.88	-3.36
Singh et al. [20]	63.3	26.63	2.67	38.54	41.35	-6.80
Singh et al. [20]	84.4	26.63	2.67	38.54	35.09	9.83
Singh et al. [20]	105.5	26.63	2.67	38.54	33.12	16.36
Singh et al. [20]	39.4	26.63	2.67	31.37	32.44	-3.30
Singh et al. [20]	59.1	26.63	2.67	31.37	33.65	-6.78
Singh et al. [20]	78.8	26.63	2.67	31.37	27.01	16.14
Singh et al. [20]	98.5	26.63	2.67	31.37	25.74	21.87
Singh et al. [20]	35.1	26.63	2.67	23.54	24.65	-4.50
Singh et al. [20]	52.65	26.63	2.67	23.54	23.08	1.99
Singh et al. [20]	70.2	26.63	2.67	23.54	20.42	15.28
Singh et al. [20]	87.75	26.63	2.67	23.54	20.03	17.52
Aliabdo [1]	20	83.22	2.5	39.93	37.3	7.05
Aliabdo [1]	30	83.22	2.5	39.93	38.4	3.98
Aliabdo [1]	40	83.22	2.5	39.93	38.8	2.91
Aliabdo [1]	60	83.22	2.5	39.93	34.6	15.40
Aliabdo [1]	20	83.22	2.5	48.73	51.76	-5.85
Aliabdo [1]	30	83.22	2.5	48.73	52.64	-7.43
Aliabdo [1]	40	83.22	2.5	48.73	53.12	-8.26

Author/s	Marble waste properties			Compressive strength		
	Content (kg)	CaO (%)	Specific Gravity	f_{cc} (MPa)	f_{cm} (MPa)	Δf_c (%)
Aliabdo [1]	60	83.22	2.5	48.73	48.44	0.60
Bostanci [35]	25	43.5	2.86	46	41.33	11.30
Bostanci [35]	50	43.5	2.86	46	38.44	19.67
Uysal & Yilmaz [25]	55	55.49	2.71	75.9	76.2	-0.39
Uysal & Yilmaz [25]	110	55.49	2.71	75.9	77.5	-2.06
Uysal & Yilmaz [25]	165	55.49	2.71	75.9	70.8	7.20
Kumar & Kumar [2]	22.28	55.09	2.63	33.18	34.67	-4.30
Kumar & Kumar [2]	44.56	55.09	2.63	33.18	35.85	-7.45
Kumar & Kumar [2]	66.84	55.09	2.63	33.18	30.22	9.79
Kumar & Kumar [2]	89.12	55.09	2.63	33.18	29.19	13.67

Table 3.
Collected data for the compressive strength estimation model.

Generally, a good fit is observed when the residuals of the estimation model are scattered randomly along the independent variable axis by representing positive and negative values. Furthermore, a potential outlier is identified when a value in standardized residuals exceeds approximately 3 [39, 40].

$$d_i = \frac{e_i}{\sqrt{MS_E}} \quad (4)$$

where MS_E is the mean squared error.

5.3 Compressive strength regression model

In this section, a prediction model for the compressive strength of concrete incorporating marble dust as a cement replacement will be discussed. In general, to overcome the dependency of the prediction model on the size of the testing specimen, the compressive strength of the control mixture will be used as an input to the model in which the output will represent the compressive strength of marble dust concrete specimen that has the same size as the inputted one. The analysis of variance of the predicted model is collected in **Table 5**, and the estimation model is depicted in (Eq. (6)) with an R^2 value of 0.9 representing a reasonably good fitting indicator. As recorded in **Table 5**, the p-value of the input parameters was below 5% for the cases of Marble dust content and its specific gravity and the control compressive strength. In comparison, the CaO content had a higher value. Although this observation does not give a very solid conclusion to what is the most influencing parameter on the compressive strength, it can supply a rough idea that marble specific gravity has a higher effect on the compressive strength than the marble content and its CaO. A similar conclusion is derived using the simple linear regression approach, **Figure 6**, between these factors and the change in the compressive strength (Eq. (5)), where higher R^2 values refer to the better correlation and consequently the more considerable effect.

$$\Delta f_c = \frac{f_{cc} - f_{cm}}{f_{cc}} \times 100 \quad (5)$$

$$f_{cm} = 51.6 + 1.0123f_{cc} - 0.0468MD_c - 0.0473MD_{CaO} - 18.6MD_{SG} \quad (6)$$

Author/s	Marble waste properties			Flexural strength		
	Content (kg)	CaO (%)	Specific Gravity	f_{tc} (MPa)	f_{tm} (MPa)	Δf_t (%)
Ergün [3]	15	51.7	2.68	5.3	5.3	0.00
Ergün [3]	22.5	51.7	2.68	5.3	5.1	3.92
Ergün [3]	30	51.7	2.68	5.3	5	6.00
Rana et al. [32]	20.25	65.2	2.87	6.55	6.3	3.97
Rana et al. [32]	40.5	65.2	2.87	6.55	6.25	4.80
Rana et al. [32]	60.75	65.2	2.87	6.55	5.44	20.40
Rana et al. [32]	81	65.2	2.87	6.55	5.14	27.43
Rana et al. [32]	101.25	65.2	2.87	6.55	5	31.00
Singh et al. [20]	42.2	26.63	2.67	7.8	8.17	-4.53
Singh et al. [20]	63.3	26.63	2.67	7.8	8.15	-4.29
Singh et al. [20]	84.4	26.63	2.67	7.8	7.32	6.56
Singh et al. [20]	105.5	26.63	2.67	7.8	7.1	9.86
Singh et al. [20]	39.4	26.63	2.67	6.83	7	-2.43
Singh et al. [20]	59.1	26.63	2.67	6.83	7.02	-2.71
Singh et al. [20]	78.8	26.63	2.67	6.83	6.16	10.88
Singh et al. [20]	98.5	26.63	2.67	6.83	6.08	12.34
Singh et al. [20]	35.1	26.63	2.67	5.7	5.803	-1.77
Singh et al. [20]	52.65	26.63	2.67	5.7	5.905	-3.47
Singh et al. [20]	70.2	26.63	2.67	5.7	5.408	5.40
Singh et al. [20]	87.75	26.63	2.67	5.7	5.12	11.33
Kumar & Kumar [2]	22.28	55.09	2.63	5.33	5.43	-1.84
Kumar & Kumar [2]	44.56	55.09	2.63	5.33	5.63	-5.33
Kumar & Kumar [2]	66.84	55.09	2.63	5.33	5.73	-6.98
Kumar & Kumar [2]	89.12	55.09	2.63	5.33	4.7	13.40

Table 4.
 Collected data for the flexural strength estimation model.

Analysis of variance					
Source	DF	Adj SS	Adj MS	F-Value	P-Value
Regression	4	6838.16	1709.54	98.05	0
Marble dust content	1	86.85	86.85	4.98	0.031
CaO	1	22.52	22.52	1.29	0.262
Specific gravity of marble dust	1	149.57	149.57	8.58	0.005
Control compressive strength	1	5249.81	5249.81	301.11	0
Error	44	767.15	17.44		
Total	48	7605.31			

Table 5.
 Analysis of variance for the compressive strength model.

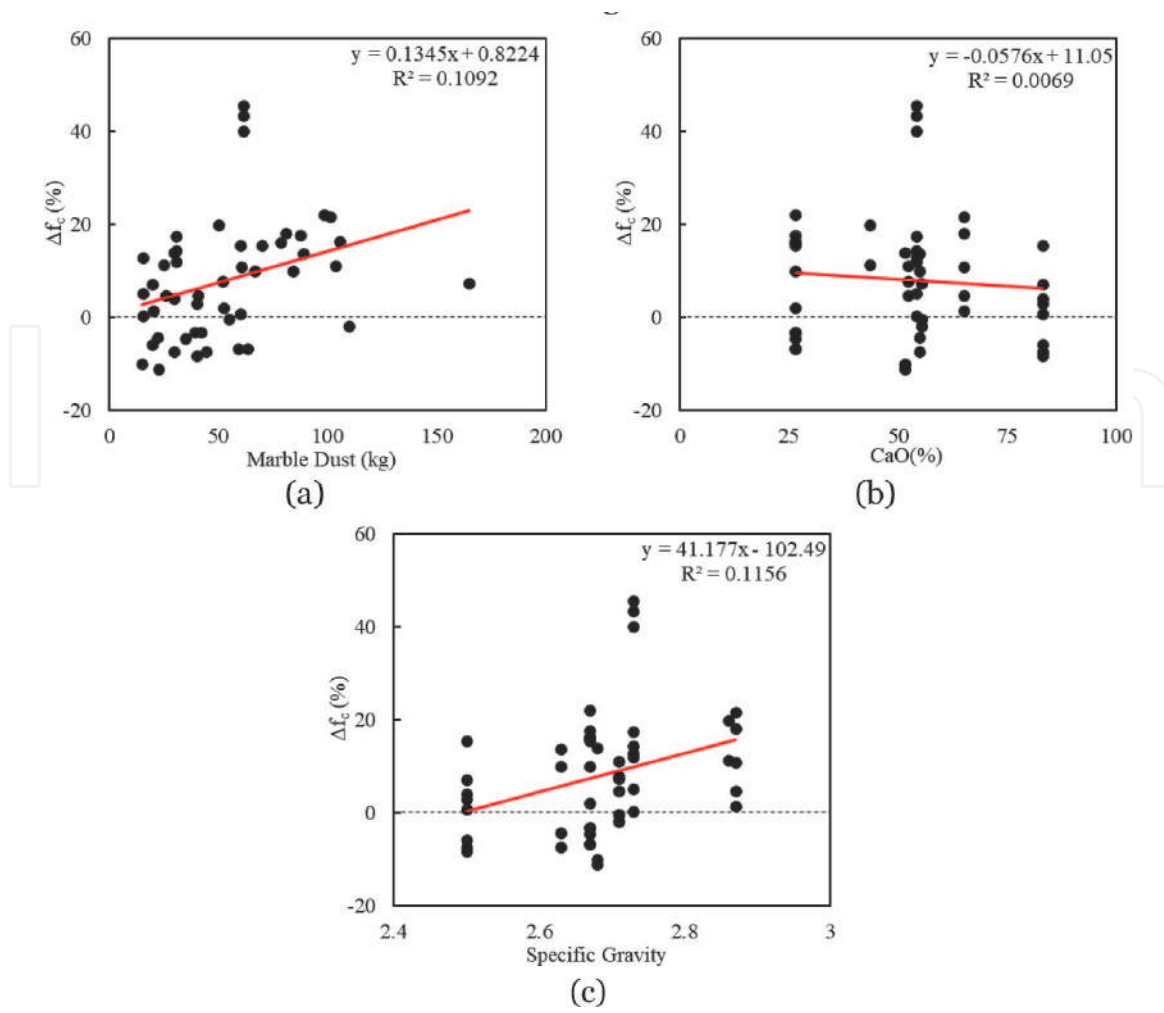


Figure 6. Influence of marble dust properties on the change in the compressive strength (a) marble dust conten, (b) CaO in the marble dust, (c) specific gravity of the marble dust.

The performance of the interpolation model is represented in **Figure 7**. It is seen that the regression line between the measured and predicted values is mainly lying over the equality line, and the points are distributed all over it, which represents a good fitting model. The residuals of this predictor are seen in **Figure 8**, and these

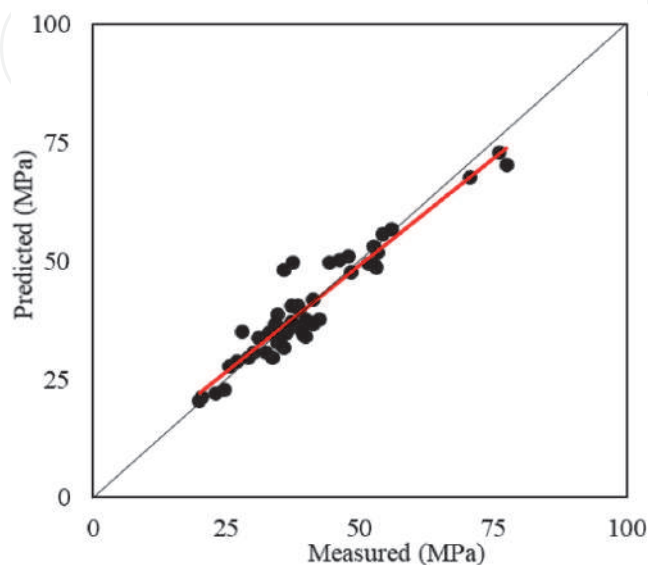


Figure 7. Performance of the proposed compressive strength prediction model.

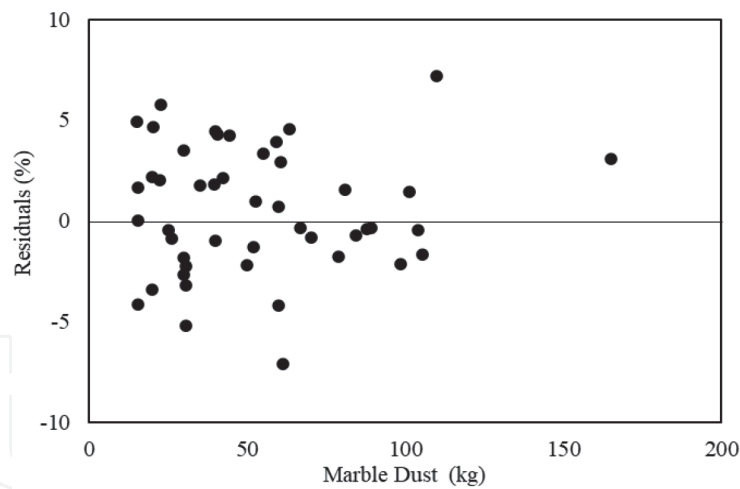


Figure 8.
Residuals obtained from the compressive strength prediction model.

values follow the basic requirements of being randomly scattered along the dependent variable axis, which is the marble dust content, in this case, meaning that the proposed model is appropriate for the given dataset.

The standardized residuals were obtained to determine the outliers, **Figure 9**, which their values more than three. Hence, it can be noticed that almost no outliers has occurred in this study, which indicates a good fitting capability. Another check on the prediction model is shown in **Figure 10**, in which the distribution on the predicted values is compared to this of the experimental one. Indeed, the histograms are slightly changed in the case of estimation; however, the general distribution is conserved after prediction.

Finally, it can be observed that the proposed prediction model delivers a useful capability for estimating the compressive strength of concrete mixtures utilizing marble dust as a replacement of cement.

5.4 Flexural strength regression model

The analysis of variance of the predicted model is summarized in **Table 6**, and the prediction model is stated in Eq. (8) with an R^2 value of 0.93 representing a

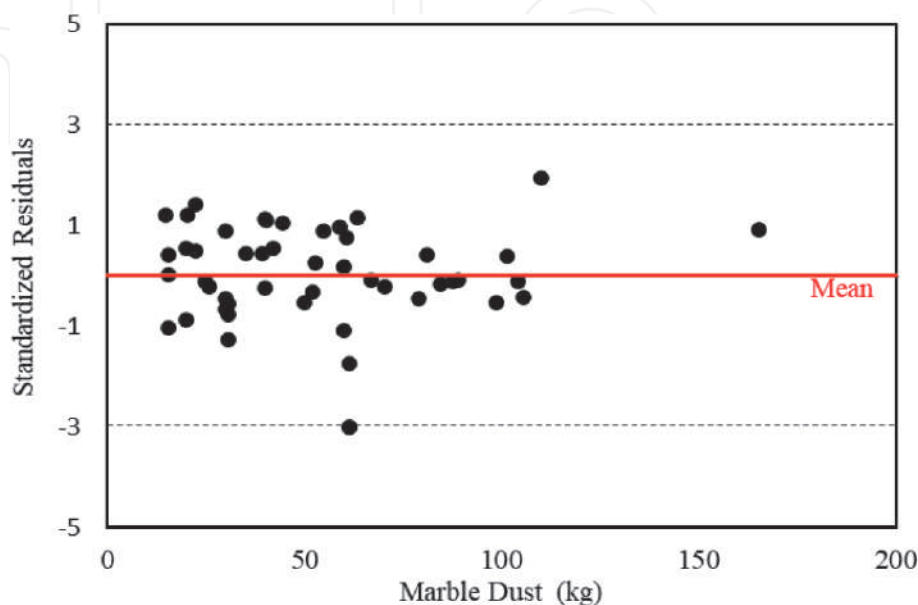


Figure 9.
Standardized residuals of the proposed compressive strength prediction model.

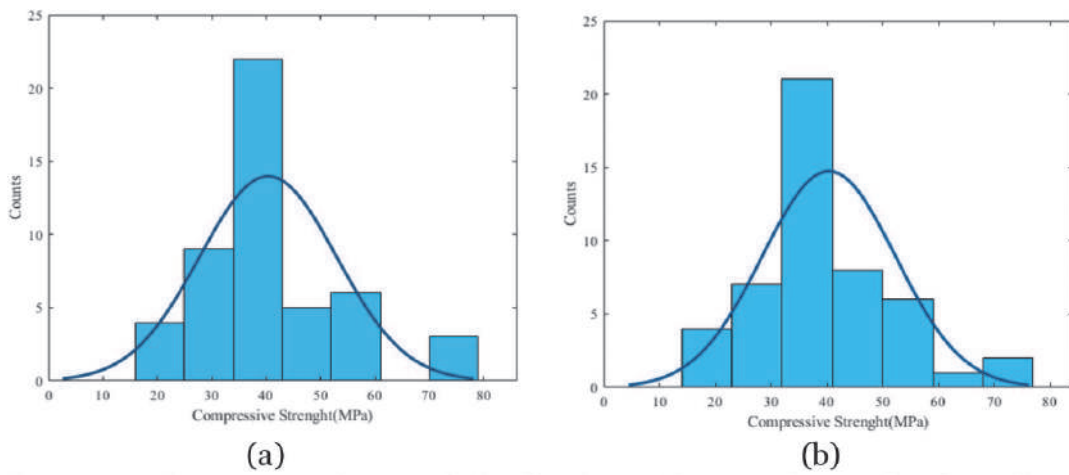


Figure 10. Histogram and normal distribution for the compressive strength (a) experimental dataset, and (b) predicted values.

Analysis of variance					
Source	DF	Adj SS	Adj MS	F-Value	P-Value
Regression	4	20.66	5.16	61.27	0
Marble dust content	1	2.77	2.77	32.86	0
CaO	1	0.00	0.00	0.04	0.837
Specific gravity of marble dust	1	1.00	1.00	11.85	0.003
Control compressive strength	1	11.62	11.62	137.85	0
Error	19	1.60	0.08		
Total	23	22.26			

Table 6. Analysis of variance for the flexural strength model.

reasonable good fitting indicator. In similar to the compressive strength, the specific gravity of the marble dust has the most influence on the flexural strength as compared to the CaO and effect. Also, the same conclusion can be acquired using the simple linear regression approach, **Figure 11**, between these factors and the change in the flexural strength (Eq. (7)).

$$\Delta f_t = \frac{f_{tc} - f_{tm}}{f_{tc}} \times 100 \quad (7)$$

$$f_{tm} = 10.29 + 1.1452f_{tc} - 0.0137MD_c - 0.00133MD_{CaO} - 3.93MD_{SG} \quad (8)$$

The performance of the estimation model is described in **Figure 12**. It can be seen that good fitting is obtained for the given dataset with a reasonably high R^2 value in comparison to the compressive strength. The residuals of this model are placed in **Figure 13**. It can be discovered that these values are randomly scattered along the marble dust content axis, which represents that the proposed model fits the given dataset.

The standardized residuals approach was used to investigate the occurrence of potential outliers, as indicated in **Figure 14**. In general, it can be observed that no points have exceeded 3, which means no outliers have existed. In addition, the

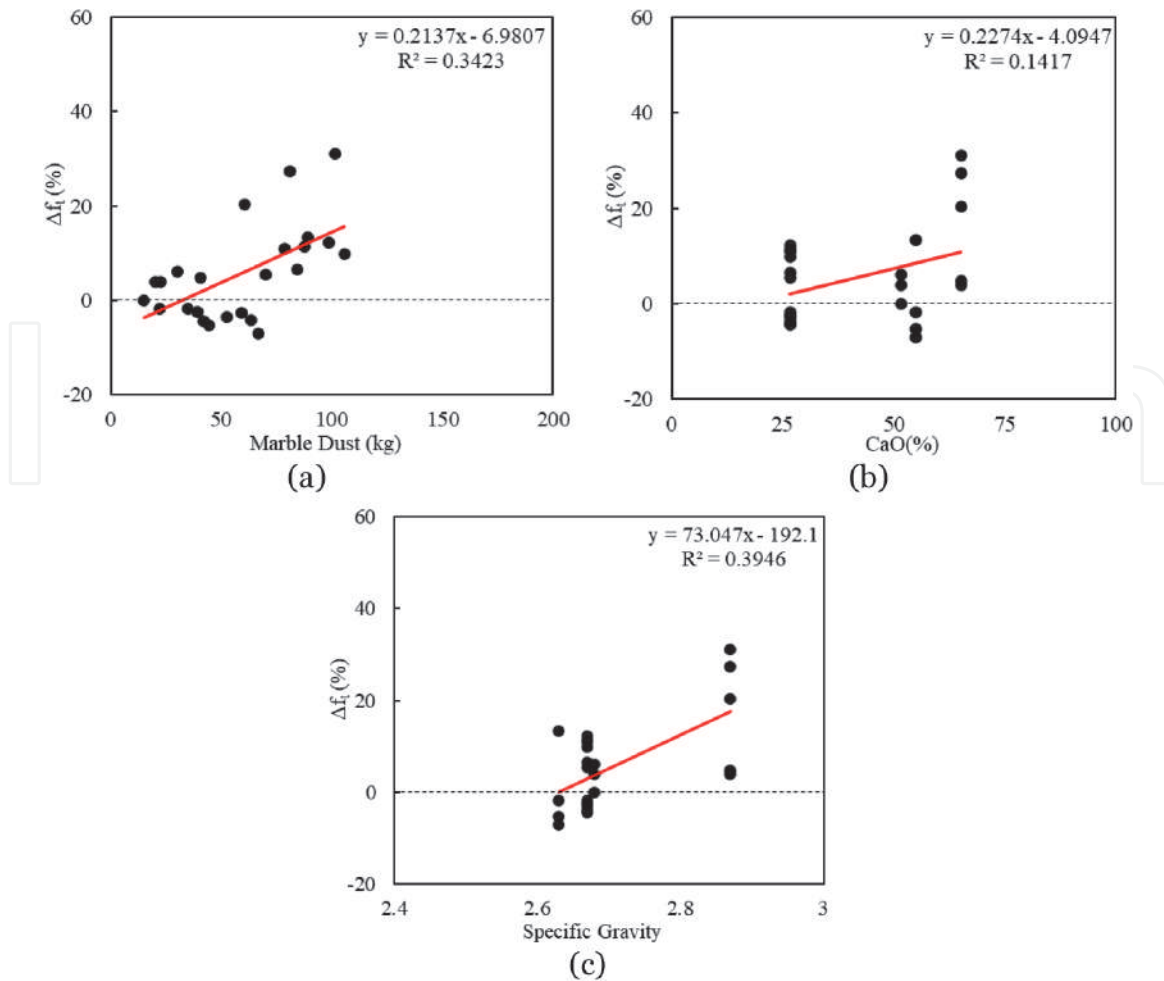


Figure 11. Influence of marble dust properties on the change in the flexural strength (a) marble dust conten, (b) CaO in the marble dust, (c) specific gravity of the marble dust.

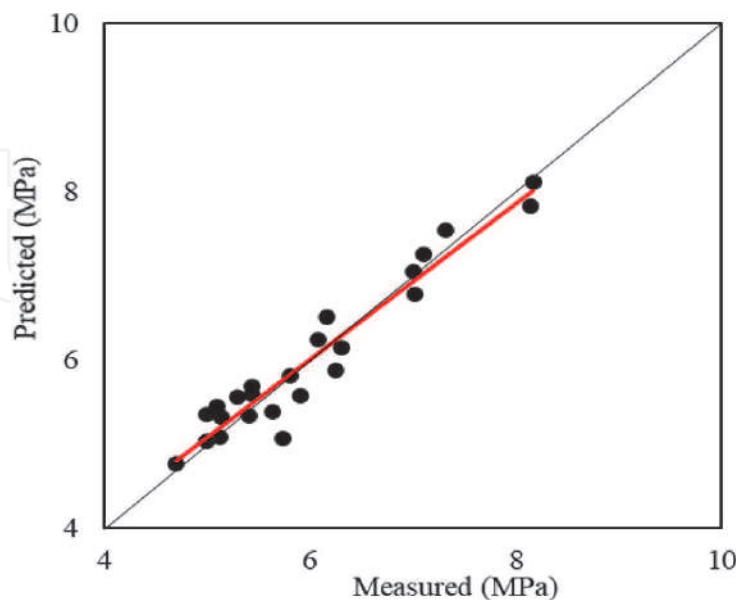


Figure 12. Performance of the proposed flexural strength prediction model.

distribution of the predicted values as compared to the experimental one can be found in **Figure 15**. A slight variation can be seen, although the behavior is generally conserved in both cases, reflecting a suitable fitting capability for the dataset.

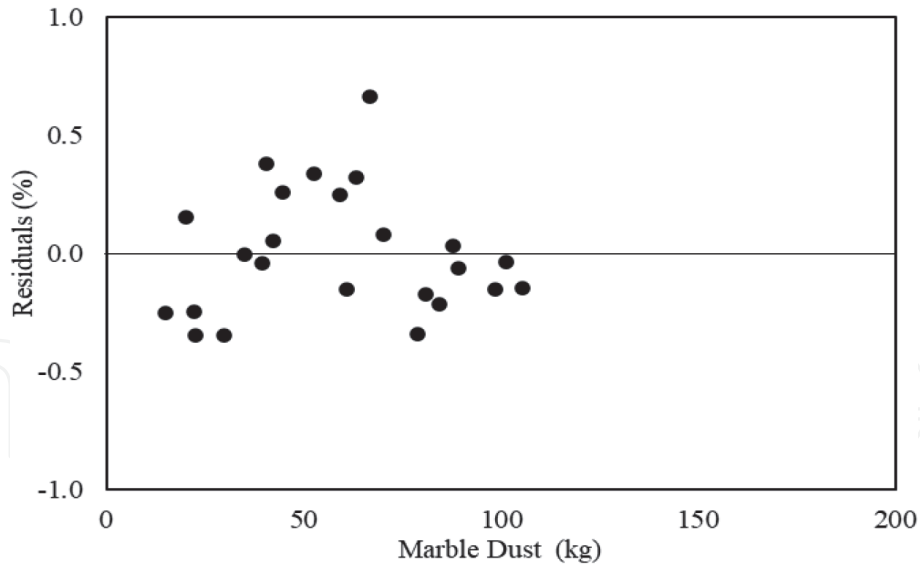


Figure 13.
Residuals obtained from the flexural strength prediction model.

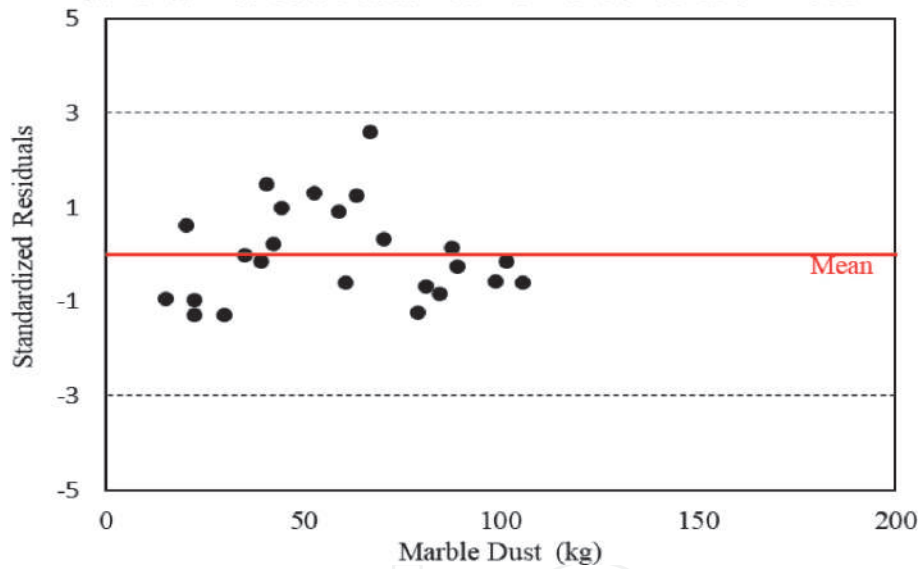


Figure 14.
Standardized residuals of the proposed flexural strength prediction model.

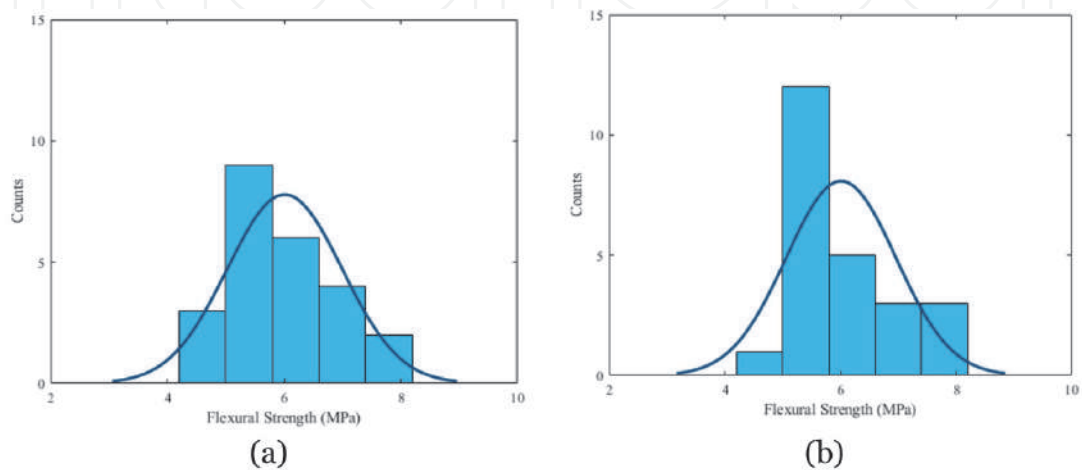


Figure 15.
Histogram and normal distribution for the flexural strength (a) experimental dataset, and (b) predicted values.

6. Future trends

Many efforts were focused on the influence of marble dust on the properties of several types of cement-based materials. However, it was observed that the literature is still in need of some comprehensive studies that can help the scientific community to understand the influence of using marble dust as a filler in sustainable concrete mixtures that incorporate recycled aggregates such as plastic or rubber. Such a mixture might provide a promising sustainable solution for ultimate waste management plans in developing countries where such materials are highly available. Another research gap is mainly related to the dynamic properties of mixtures incorporating marble dust, as such studies are minimal. Moreover, it is essential to display some numerical studies that can propose prediction models based on the marble dust content in the concrete mixture.

7. Conclusion

This chapter has focused on briefly reviewing the utilization and mechanical properties of cement-based materials incorporating marble dust with emphasis on concrete mixtures with marble wastes cement replacement. In addition, it aimed to propose two estimation models using multiple regression analysis for the compressive and flexural strengths of marble dust concrete. On the base of the statements above, the following points are drawn:

- It is quite challenging to narrow down the ranges of marble dust properties and to standardize them due to the massive variate in the origin of the rocks being processed while obtaining this material.
- Marble dust can be used as a filler material in concrete to improve the microstructure of the mix.
- Up to a certain replacement ratio, generally considered as 10% in several studies, the incorporation of marble waste can positively influence the compressive strength capacity of the mixture.
- Several potential applications of marble dust in the construction industry have already been considered in the literature, including its utilization as a filler in cement-based materials, a partial replacement of concrete constituents, and a substitute of limestone in various industrial applications.
- The specific gravity of marble dust can be considered as one of the main characteristics that affect the strength properties of the investigated concrete mixtures.
- The proposed estimation models can reliably be used to predict the compressive and flexural strengths of concrete utilizing marble dust as a partial replacement of cement.

Further research efforts are still needed in this field to cover some of the gaps in the literature on the behavior of recycled aggregate concrete incorporating this material to develop the understanding of both scientists and engineers working in the construction industry. It is also recommended to comprehensively study the influence of marble dust chemical properties on the performance of the produced

cement-based material can to come up with detailed mathematical relationships similar to the ones presented in this study due to the inconsistency in the experimental results due to the wide variety in the natural waste properties.

IntechOpen

Author details

Ahed Habib^{1*} and Maan Habib²

1 Eastern Mediterranean University, Famagusta, North Cyprus, via Mersin 10, Turkey

2 Al-Balqa Applied University, Amman, Jordan

*Address all correspondence to: ahed.habib@cc.emu.edu.tr

IntechOpen

© 2020 The Author(s). Licensee IntechOpen. This chapter is distributed under the terms of the Creative Commons Attribution License (<http://creativecommons.org/licenses/by/3.0>), which permits unrestricted use, distribution, and reproduction in any medium, provided the original work is properly cited. 

References

- [1] A. A. Aliabdo, M. Abd Elmoaty and E. M. Auda, "Re-use of waste marble dust in the production of cement and concrete," *Construction and building materials*, vol. 50, pp. 28-41, 2014
- [2] R. Kumar and S. K. Kumar, "Partial replacement of cement with marble dust powder," *International Journal of Engineering Research and Applications*, vol. 5, no. 8, pp. 106-114, 2015
- [3] A. Ergün, "Effects of the usage of diatomite and waste marble powder as partial replacement of cement on the mechanical properties of concrete," *Construction and building materials*, vol. 25, no. 2, pp. 806-812, 2011
- [4] R. Rodrigues, J. De Brito and M. Sardinha, "Mechanical properties of structural concrete containing very fine aggregates from marble cutting sludge," *Construction and Building Materials*, vol. 77, pp. 349-356, 2015
- [5] O. Gencel, C. Ozel, F. Koksall, E. Erdogmus, G. Martínez-Barrera and W. Brostow, "Properties of concrete paving blocks made with waste marble," *Journal of cleaner production*, vol. 21, no. 1, pp. 62-70, 2012
- [6] V. Corinaldesi, G. Moriconi and T. R. Naik, "Characterization of marble powder for its use in mortar and concrete," *Construction and building materials*, vol. 24, no. 1, pp. 113-117, 2010
- [7] E. T. Tunc, "Recycling of marble waste: A review based on strength of concrete containing marble waste," *Journal of environmental management*, vol. 231, pp. 86-97, 2019
- [8] M. Galetakis and A. Sultana, "A review on the utilisation of quarry and ornamental stone industry fine by-products in the construction sector," *Construction and Building Materials*, vol. 102, pp. 769-781, 2016
- [9] H. Y. Aruntaş, M. Gürü, M. Dayı and I. Tekin, "Utilization of waste marble dust as an additive in cement production," *Materials & Design*, vol. 31, no. 8, pp. 4039-4042, 2010
- [10] B. Demirel, "The effect of the using waste marble dust as fine sand on the mechanical properties of the concrete," *International journal of physical sciences*, vol. 5, no. 9, pp. 1372-1380, 2010
- [11] H. Ş. Arel, "Recyclability of waste marble in concrete production," *Journal of Cleaner Production*, vol. 131, pp. 179-188, 2016
- [12] H. E. Elyamany, M. Abd Elmoaty and B. Mohamed, "Effect of filler types on physical, mechanical and microstructure of self compacting concrete and Flow-able concrete," *Alexandria Engineering Journal*, vol. 53, no. 2, pp. 295-307, 2014
- [13] M. G. H. Education, *Dictionary of Geology & Mineralogy*, McGraw-Hill, 2003
- [14] P. Julphunthong and P. Joyklad, "Utilization of Several Industrial Wastes as Raw Material for Calcium Sulfoaluminate Cement," *Materials*, vol. 12, no. 20, p. 3319, 2019
- [15] B. Demirel and K. E. Alyamaç, "Waste marble powder/dust," in *Waste and Supplementary Cementitious Materials in Concrete*, Woodhead Publishing, 2018, pp. 181-197
- [16] M. Gesoğlu, E. Güneyisi, M. E. Kocabağ, V. Bayram and K. Mermerdaş, "Fresh and hardened characteristics of self compacting concretes made with combined use of marble powder, limestone filler, and fly ash," *Construction and Building Materials*, vol. 37, pp. 160-170, 2012

- [17] K. Vardhan, S. Goyal, R. Siddique and M. Singh, "Mechanical properties and microstructural analysis of cement mortar incorporating marble powder as partial replacement of cement," *Construction and Building Materials*, vol. 96, pp. 615-621, 2015
- [18] D. K. Ashish, "Concrete made with waste marble powder and supplementary cementitious material for sustainable development," *Journal of cleaner production*, vol. 211, pp. 716-729, 2019
- [19] N. Bilgin, H. A. Yeprem, S. Ö. N. M. E. Z. Arslan, A. Bilgin, E. Günay and M. Marşoglu, "Use of waste marble powder in brick industry," *Construction and Building Materials*, vol. 29, pp. 449-457, 2012
- [20] M. A. Singh and D. Bhunia, "An investigation on effect of partial replacement of cement by waste marble slurry," *Construction and Building Materials*, vol. 134, pp. 471-488, 2017
- [21] L. G. Li, Z. H. Huang, Y. P. Tan, A. K. H. Kwan and H. Y. Chen, "Recycling of marble dust as paste replacement for improving strength, microstructure and eco-friendliness of mortar," *Journal of Cleaner Production*, vol. 210, pp. 55-65, 2019
- [22] T. Uygunoğlu, İ. B. Topçu and A. G. Çelik, "Use of waste marble and recycled aggregates in self-compacting concrete for environmental sustainability," *Journal of cleaner production*, vol. 84, pp. 691-700, 2014
- [23] M. Uysal and M. Sumer, "Performance of self-compacting concrete containing different mineral admixtures," *Construction and Building materials*, vol. 25, no. 11, pp. 4112-4120, 2011
- [24] I. B. Topcu, T. Bilir and T. Uygunoğlu, "Effect of waste marble dust content as filler on properties of self-compacting concrete," *Construction and Building Materials*, vol. 23, no. 5, pp. 1947-1953, 2009
- [25] M. Uysal and K. Yilmaz, "Effect of mineral admixtures on properties of self-compacting concrete," *Cement and Concrete Composites*, vol. 33, no. 7, pp. 771-776, 2011
- [26] A. Talah, F. Kharchi and R. Chaid, "Influence of marble powder on high performance concrete behavior," *Procedia Engineering*, vol. 114, pp. 685-690, 2015
- [27] F. Gameiro, J. De Brito and D. C. da Silva, "Durability performance of structural concrete containing fine aggregates from waste generated by marble quarrying industry," *Engineering Structures*, vol. 59, pp. 654-662, 2014
- [28] N. Toubal Seghir, M. Mellas, Ł. Sadowski, A. Krolicka, A. Żak and K. Ostrowski, "The utilization of waste marble dust as a cement replacement in air-cured mortar," *Sustainability*, vol. 11, no. 8, p. 2215, 2019
- [29] A. O. Mashaly, B. A. El-Kaliouby, B. N. Shalaby, A. M. El-Gohary and M. A. Rashwan, "Effects of marble sludge incorporation on the properties of cement composites and concrete paving blocks," *Journal of Cleaner Production*, vol. 112, pp. 731-741, 2016
- [30] M. Singh, A. Srivastava and D. Bhunia, "Potential applications of marble dust in industrial use by characterization techniques—A review," *International Journal of Advanced Structures and Geotechnical Engineering*, vol. 5, no. 3, pp. 99-106, 2016
- [31] M. J. Munir, S. M. S. Kazmi and Y. F. Wu, "Efficiency of waste marble powder in controlling alkali-silica reaction of concrete: A sustainable

approach," *Construction and Building Materials*, vol. 154, pp. 590-599, 2017

[32] A. Rana, P. Kalla and L. J. Csetenyi, "Sustainable use of marble slurry in concrete," *Journal of Cleaner Production*, vol. 94, pp. 304-311, 2015

[33] N. M. Soliman, "Effect of using marble powder in concrete mixes on the behavior and strength of RC slabs," *International Journal of Current Engineering and Technology*, vol. 3, no. 5, pp. 1863-1870, 2013

[34] M. Sardinha, J. de Brito and R. Rodrigues, "Durability properties of structural concrete containing very fine aggregates of marble sludge," *Construction and building materials*, vol. 119, pp. 45-52, 2016

[35] S. C. Bostanci, "Use of waste marble dust and recycled glass for sustainable concrete production," *Journal of Cleaner Production*, vol. 251, 2020

[36] S. Fedorov, "GetData graph digitizer (2.26)," www.getdata-graph-digitizer.com, 2013

[37] D. J. Olive, *Multiple Linear and 1D Regression*, 2010

[38] C. H. Achen, *Interpreting and using regression*, vol. 29, Sage, 1982

[39] D. C. Montgomery, E. A. Peck and G. G. Vining, *Introduction to linear regression analysis*, John Wiley & Sons, 2012

[40] D. C. Montgomery, *Design and analysis of experiments*, John Wiley & sons, 2012

Applications of Cement in Pavement Engineering

*Sarella Chakravarthi, Galipelli Raj Kumar
and Sabavath Shankar*

Abstract

Recycled materials primarily Reclaimed Asphalt Pavement (RAP), and Recycled Concrete Aggregate (RCA) are produced from pavement rehabilitation and construction-demolition activities. Generally, these materials are utilized for landfills, parking lots, shoulders, and other places that are not environmentally friendly. The top layers of the pavement and concrete structures are constructed using superior qualities of aggregates that satisfy the specification. During their service life, the aggregates present in these structures undergo deterioration due to environmental and traffic factors. After reaching the end of their service life, the deteriorated structures are dismantled and considered as waste. Nevertheless, these recycled materials will have some retain value which can be used in different layers of the pavements in different percentages. The reuse of these materials in place of conventional aggregates preserves the environment and become a sustainable construction practice. Further, the direct utilization of these materials in the pavements may not satisfy the mechanical characteristics. To fulfill these gaps, cement stabilization of recycled materials is the best option. With this background, the proposed book chapter will highlight the usage of cement in pavement application, and a few types of research works carried in cement treated pavement layers will be discussed in a detailed and scientific manner.

Keywords: cement concrete pavement, granular layers, cement treated bases and performance of pavements

1. Introduction

Recycled materials primarily Reclaimed Asphalt Pavement (RAP), and Recycled Concrete Aggregate (RCA) are produced from pavement rehabilitation and construction-demolition activities. Generally, these materials are utilized for landfills, parking lots, shoulders, and other places that are not environmentally friendly. The top layers of the pavement and concrete structures are constructed using superior qualities of aggregates that satisfy the specification. During their service life, the aggregates present in these structures undergo deterioration due to environmental and traffic factors. After reaching the end of their service life, the deteriorated structures are dismantled and considered as waste. However, these recycled materials have some retain value which can be used in different layers of the pavements in different percentages. The reuse of these materials in place of conventional aggregates preserves the environment and become a sustainable construction practice. However, the direct utilization of these materials in the pavements may not achieve

acceptable mechanical characteristics. To fulfill these mechanical properties with recycled materials, stabilization is the best option left to the engineers.

Several stabilization techniques are involved around the world to provide adequate strength to the weak bases or soil materials. The stabilizers include lime, asphalt emulsion, fly ash, and cement are widely used to improve the mechanical properties of recycled materials as a base or subbase courses in pavements. Cement stabilization is advantageous because of rapid gain in strength and its easy availability in the market. To understand the mechanical properties of the recycled materials with cement stabilization, a laboratory study is carried using RAP and RCA in different proportions with Natural Aggregates (NA). The compaction characteristics, Unconfined Compressive Strength (UCS), Indirect Tensile Strength (ITS), and Modulus of Elasticity (E) tests were conducted to assess the performance.

Apart from the recycled aggregates, several hazardous and industrial wastes from the production plants like Electrolyte Manganese Residue (EMR), Red mud, slag, and glass can be efficiently stabilized using cement and can be used in the pavements as a base. Zang et al. (2019) proved that the stabilization of the EMR and Red mud in the road bases achieved adequate strength and make it environmentally friendly [1]. The replacement of conventional aggregates with 50% steel slag stabilized with 4% cement content achieved maximum strength and stiffness along with other economic benefits [2]. At the same time, the use of cement treated recycled glass up to 30% along with the other recycled materials achieved required strength properties [3]. Besides, it is estimated from the study that 26-32% of cost savings with the cement stabilization of the recycled aggregates [4].

The usage of cement in pavement construction is considerable. There are several applications in the construction field that includes bridges, tunnels, safety barriers, pavements, and sound barriers. The benefits of cement-treated bases include high bearing capacity and increased stiffness, and lower deformation under loads. The following are the potential advantages of cement in various construction fields which are listed below.

- Airports for parking aprons, taxiway and runway take-off
- Parking areas for heavy vehicles
- Heavy-duty industrial floors
- Usage of cement and concrete in bridge decks
- Subgrade soil stabilization with cement
- Soil stabilization with lime and cement
- Recycling of pavement with treated and bases and subbases
- Construction of dry lean cement concrete layer
- Debonding layer over stabilized cemented bases
- Construction of concrete pavement
- Construction of interlocking bloc pavement s
- Cell filled pavements.

With this background, the application of the cement in the field of pavement engineering as a base and sub-base layer is presented. This includes evaluation in terms of mechanical properties at various cement stabilization levels and finally compared with the available specifications.

2. Literature review

The potential use of recycled aggregates in pavement bases is investigated around the world. Their utilization in the pavement is limited due to inferior physical and mechanical properties. Reclaimed asphalt pavement (RAP) materials used in the pavements has concerns with the reduction in the strength, more significant permanent deformation, poor distribution of stresses, and durability issues and recommended for stabilization [5, 6]. Besides, the use of recycled concrete aggregates (RCA) above the water table is recommended [7] due to the concerns of groundwater contamination and durability issues [8, 9]. Studies suggested that the properties of the recycled materials can be enhanced with the addition of additives or blending with superior quality materials [10]. The stiffness of the base increases with the cement stabilization, which reduces the deflections and increases the pavement life at higher traffic loads and serves better than NA bases [8, 9]. With this background, there is a stressing need for chemical stabilization of recycled materials to improve their mechanical properties. Some of the previous studies were presented in **Table 1**, which shows the benefits of the cement stabilization on various recycling materials.

Author, year	Conclusions
Arulrajah et al. 2020 [11]	Stabilization of construction and demolition wastes containing a little amount of polyethylene terephthalate with 3% cement satisfied the requirements of pavement base and subbases.
Kasu et al. 2020 [4]	Cement content in the mix has a significant influence on the mechanical and durability properties compared with recycled aggregate contents.
Arshad, 2020 [12]	Addition of cement content in the range of 1.5-4.5% improved the mechanical properties and reduced the strains in the recycled aggregate blends
Yan et al. 2020 [13]	The addition of recycled aggregate content from the construction and demolition waste into the stabilized bases improves the mechanical and durability properties. However, the residual strength is maximum at 30% of the recycled aggregate content in the mix.
Chakravarthi et al. 2019 [14]	Concluded that cement stabilization of the RCA is more pronounced than RAP and improvement in the mechanical properties is observed.
Faysal et al. 2016 [15]	Strength and stiffness characteristics are significantly improved with cement content.
LaHucik et al. 2016 [16]	Cement stabilization on a small scale for the bases with recycled materials like RAP and Quarry by-products is feasible for no freeze zones.
Behiry, 2013 [17]	Revealed that the performance of cement treated recycled materials depends on cement content, curing time and dry density.
Xuan et al. 2012 [18]	Stated that an increase in the cement content and decreasing the masonry content improves the strength and modulus of the bases.
Taha et al. 2002 [19]	Replacement of cement stabilization of RAP-virgin aggregate mixes in place of conventional bases considered a viable alternative.

Table 1.
Previous studies on cement stabilization of recycled bases.

3. Objectives and methodology of the study

The current study aims at laboratory evaluation of the cement stabilized bases consists of recycled materials like RAP and RCA as a partial and full replacement with natural Aggregates (VA) with the following goals.

- To determine the influence of the cement content and recycled aggregates content on the stabilized base mixes in terms of various mechanical properties.
- To optimize the cement content, recycled aggregates, and VA combination for road bases based according to the standard specifications.
- Stiffness characterization of the given recycled aggregates and VA combinations at different stabilization levels.

The required materials such as conventional aggregate, RAP, RCA, and ordinary Portland cement of 53 grade are collected locally. Aggregate gradations for the test mixtures were determined and compared with the requirements following the Ministry of Road Transport and Highways (MoRTH, 2013) specifications, Government of India (GoI) [20]. Initially, bitumen was extracted from the collected RAP material, followed by physical tests like Sieve analysis, impact test, Flakiness, and Elongation index were performed on RAP and RCA according to the standards as shown in **Figure 1**. From the physical properties, the flakiness and elongation index for RAP is higher than the specification limits, and the water absorption of the RCA is more than 2%. The flakiness and elongation index of RAP aggregates is due to the formation of fracture surfaces during its service life. The crushing process and the water absorption of the RCA are more compared with the VA because of the presence of cement mortar around its surface. Although the recycled materials did not satisfy the required specifications, they are used in the study. This is the main motivation of the study to improve their mechanical properties through the process of stabilization. After physical characterization, the materials are blended in the ratio of RAP/RCA and conventional aggregate content (0/100, 25/75, 50/50, 75/25) as shown in **Figure 2** with an increment of cement from 0%, 2%, 4%, 6%. The next step involves the determination of compaction characteristics of the mixes such as Optimum moisture content

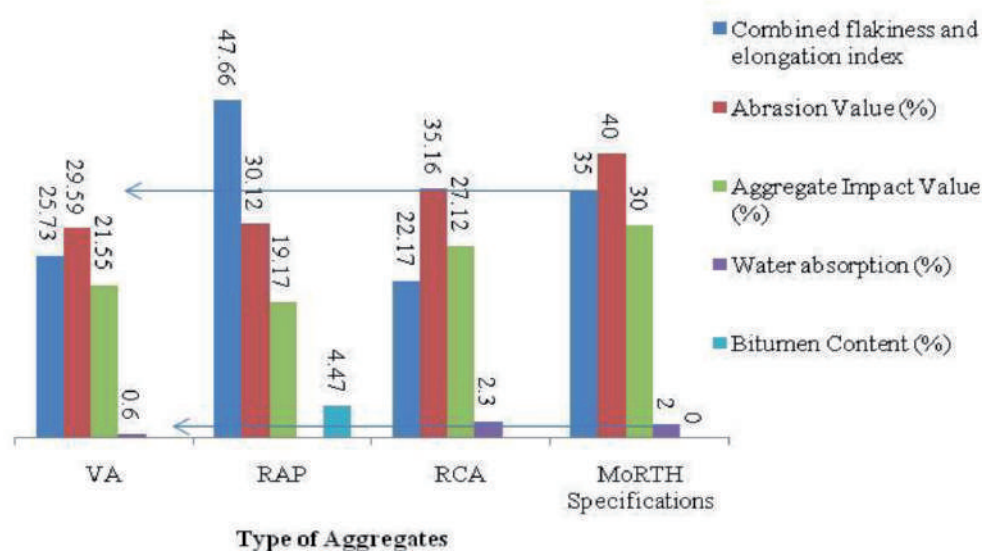


Figure 1.
Physical properties of aggregates.

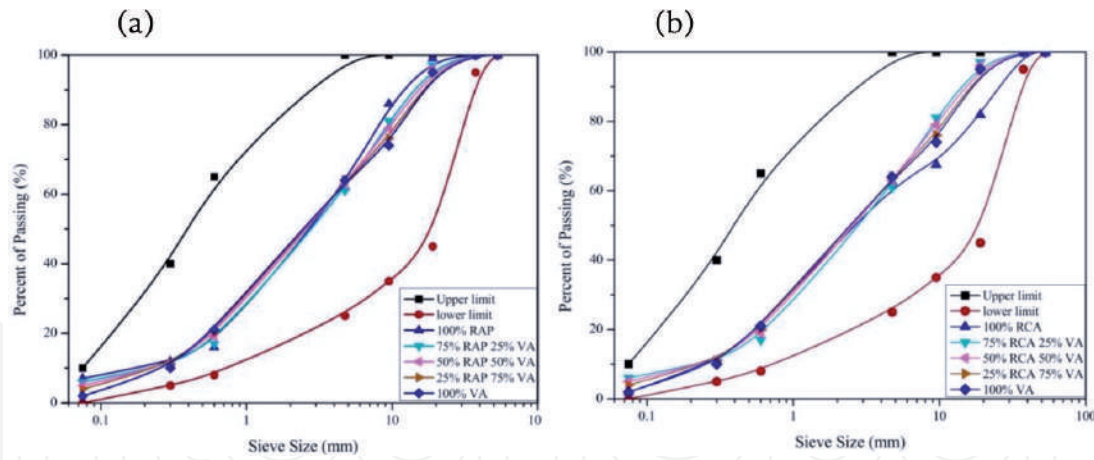


Figure 2.
 (a) Gradation curve for RAP blends; (b) gradation curve for RCA blends.

(OMC) and maximum dry density (MDD) using the Modified Proctor Test. The obtained OMC values from the modified Proctor test are used in the preparation of the samples for further tests and cured for 7 days as suggested by the researchers. The strength parameters like UCS, ITS, and stiffness parameters like Modulus of elasticity and Resilient Modulus were evaluated for the specimens prepared at OMC.

4. Compaction characteristics

Modified Proctor's test was performed according to the Indian Standards (IS 2720-part 8-1985) on all the mixes proportions of RAP and RCA with VA. The test is repeated three times to check the repeatability and accuracy. Modified Proctor compaction is achieved using a hammer of weight 4.5 kg falling from a height of 457 mm in the mold of dimensions 102 mm in diameter and 127 mm in height. All particle sizes greater than 19 mm were replaced with the same amount of particles less than 19 mm from the mix as a mold correction.

The obtained OMC and MDD results for different blending mixes are shown in **Tables 2** and **3**. It is revealed that the required amount of OMC is reduced with the increase in the percentage of RAP due to the low moisture absorption capacity of bitumen coated RAP. While the MDD is low at 100% RAP and increases with VA content due to the low specific gravity of the RAP aggregates which agrees with the previous research study [21] and MDD increases with the cement content. The addition of the cement to the mix improves the compaction capacity due to good aggregate packing. In the case of RCA blends, there is no proper trend observed with the addition of RCA due to the indifferences in mortar on the surface of RCA. The same is verified by conducting a water absorption test on two samples of the

% of cement	100% RAP		75% RAP		50% RAP		25% RAP	
	OMC (%)	MDD (g/cc)	OMC (%)	MDD (g/cc)	OMC (%)	MDD (g/cc)	OMC (%)	MDD (g/cc)
0	7.06	1.93	7.44	2.03	7.61	2.13	7.16	2.20
2	7.13	2.08	7.52	2.08	7.72	2.14	7.38	2.22
4	7.24	2.11	7.64	2.10	7.89	2.15	7.67	2.22
6	7.45	2.21	7.88	2.11	7.95	2.16	8.09	2.23

Table 2.
 Optimum moisture content and maximum dry density results for RAP blends.

% of cement	100% RCA		75% RCA		50% RCA		25% RCA	
	OMC (%)	MDD (g/cc)	OMC (%)	MDD (g/cc)	OMC (%)	MDD (g/cc)	OMC (%)	MDD (g/cc)
0	9.7	2.14	9.2	2.13	12.3	2.02	9.44	2.13
2	8.2	2.1	10.2	1.98	7.93	2.16	10.06	2.2
4	11.1	2.06	9.2	2.01	9.28	2.17	9.44	2.22
6	9.5	2.09	11.5	1.97	10.92	2.2	10.35	2.25

Table 3.
Optimum moisture content and maximum dry density results for RCA blends.

same gradation with the difference in the mortar presence. This variation of mortar percentage in the sample causes significant variations in the OMC and MDD at high percentages of RCA in the mix (100%RCA and 75% RCA). The MDD values of RAP and RCA blends ranges between 1.93 and 2.25 g/cc.

5. Unconfined compressive strength test (UCS) and elastic modulus

The Unconfined Compressive Strength (UCS) is used to determine the bonding strength or cohesion of a stabilized material. The samples are prepared at corresponding OMC according to ASTM D 1632. The dimensions of the cylindrical mold are of size 101.6 mm diameter, and 200 mm height is chosen. The samples are compacted and cured in closed plastic bags to prevent the escape of moisture. They tested at the end of the 7 days curing period. The UCS is calculated from the maximum load at the failure divided by the cross-sectional area of each specimen gives the compressive strength (**Figure 3**).

There is a surge in the UCS with cement content, as observed in **Figure 4**. Besides, the rate of increase in strength declines with the addition of recycled aggregates content. Higher RAP content slows down the rate of strength gain in the mixtures. For example, the mixes with increased recycled aggregates content have low strength at given cement content. The increase in asphalt coated surface area requires more amount of the stabilizing agent to form bonds with the other aggregates. Besides, the RCA stabilized bases do not show any particular trend with RCA content.

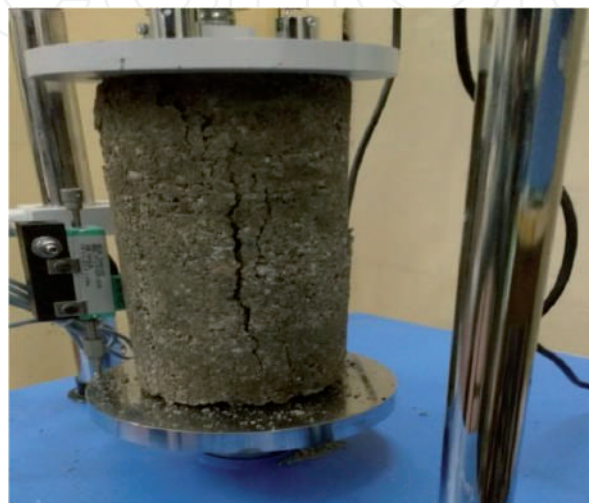


Figure 3.
Sample testing of UCS.

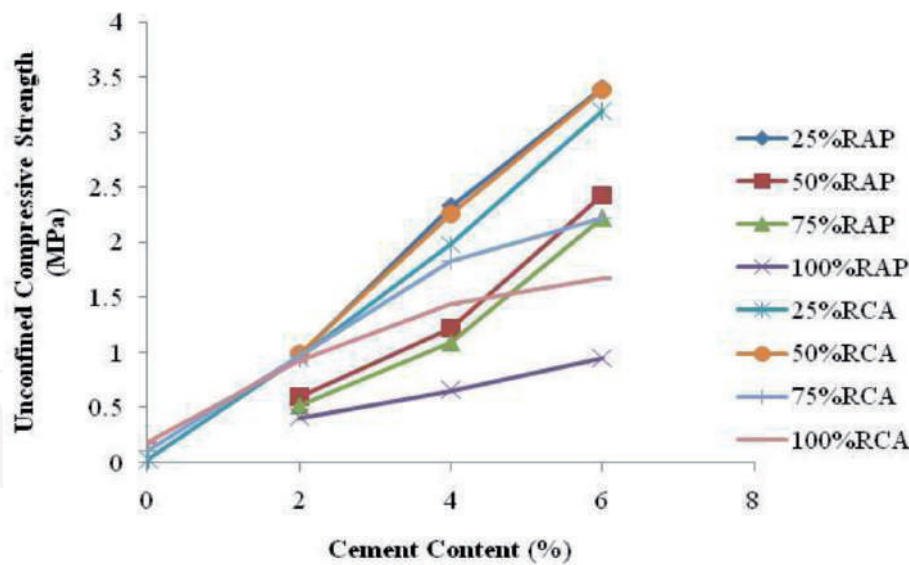


Figure 4.
 Unconfined compressive strengths of RAP - VA and RCA - VA blends of varying cement percentages.

Further, 50% of RCA shows higher strength irrespective of the cement content; this is due to the better interlocking of RCA with the NA, which increases the strength. At 6% cement content, all the mixes exhibit higher strengths. The obtained results are compared with the low volume road standards for cement-treated bases, as shown in **Table 4**.

From the observations, the majority of the blends at 4% cement satisfied the specifications as a subbase layer for low volume roads. However, RAP/RCA blends with 25% RAP and 6% cement content have UCS of 3.4 MPa/3.19 MPa and 50% RCA with 6% cement with UCS of 3.37 MPa satisfied the Ministry of Rural Development (MoRD) specification, i.e., 2.76 MPa and can be used as a base layer for low volume roads and as a subbase layer for high volume roads. To extend their utilization as a base layer in the high-volume roads requires an increase in stabilization levels and curing period.

Further, RCA blends show more strength compared with RAP blends. For instance, at constant cement content, 100% RCA mix show almost double strength compared with 100% RAP mix. The reason behind this phenomenon is due to the existence of a strong bond between RCA, VA, and cement. Besides, the mortar which is coated with the RCA aggregates contributes to the development of strength. The RCA blends without stabilization exhibited retained strength at 7 days of curing. This clearly explains the self-cementing property of the RCA in agreement with the previous studies where the mortar present in the RCA helps in bonding [23].

Besides, the untreated RAP mixes are weak and collapsed while removing from the split mold, which represents the weak bonding between the aggregates. The strength development in the blends depends on the blended aggregate proportions, stabilization level, and the residual cement present in the existing RCA. However,

UCS (MPa)			
Low volume road (traffic <2 msa) [22]		High volume road (traffic >2 msa) [20]	
Sub-base	Base	Sub-base	Base
1.70	2.76	1.5-3.0	4.5-7.0

Table 4.
 UCS as per Indian specifications.

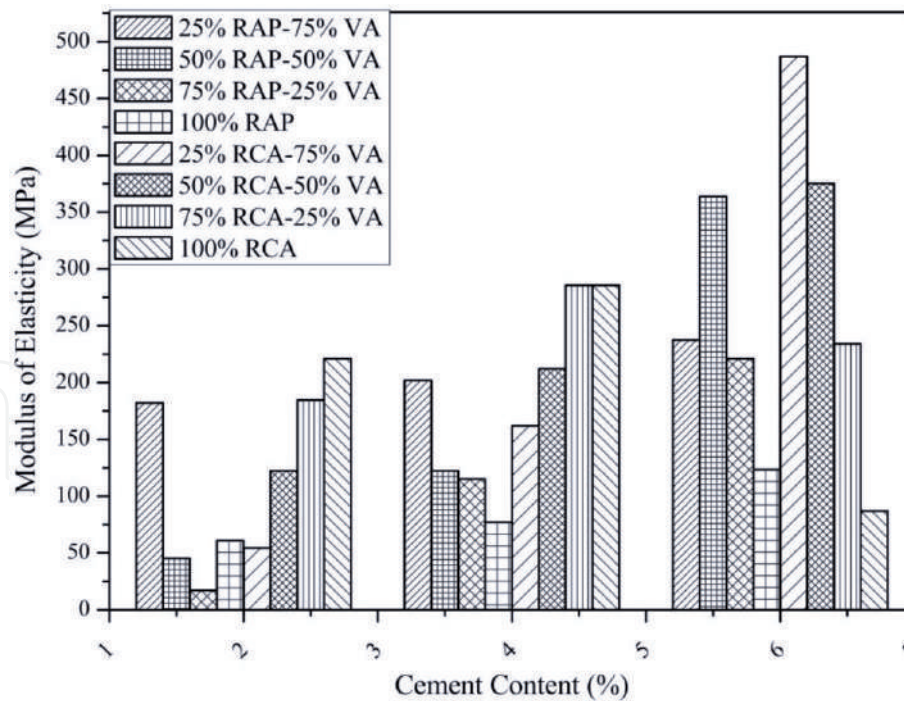


Figure 5. Modulus of elasticity of RAP VA and RCAVA mixes at 7 days curing period.

RAP did not have a contribution to strength development [24]. A linear relationship is noticed between the UCS and the cement content irrespective of the type of mix. Out of which 25% RAP-75% VA and 50% RCA - 50% VA blends show a rapid gain in strength. This is due to the existence of the unhydrated mortar in RCA, less asphalt coated surface area, and presence of high-quality aggregates, and better interlocking between the aggregates along with the stabilization.

Elastic modulus is the ratio of applied stress to corresponding strain within the elastic limit. This property is used to characterize the materials and to analyze the stresses and strains in different pavement layers. With the continuous application of loads, the recoverable character of these materials will be declined, and the plastic deformation is accumulated. This repeated application of load property is measured using Resilient Modulus (M_R) (Figure 5).

The elastic modulus of RAP/VA and RCA/VA blends at different cement contents after 7 days of curing period is calculated. The elastic modulus of RCA blends ranges from 11.95 MPa at 100% RCA with 0% cement content to 486.96 MPa at 25% RCA at 6% cement content. In contrast, the elastic modulus of RAP blended mixes ranges from 60.99 MPa at 100% RAP at 2% cement content to 363.78 MPa at 50% RAP at 6% cement content.

There is a linear increase in the elastic modulus with an increase in the cement content in each mix. However, 100% RCA and 75% RCA-25% VA at 6% cement content there is a tremendous decrease. This is due to the overdosage of the cement to the mix in addition to the existing residual mortar surrounding the aggregates, which makes the material more brittle.

Blending with VA improved the modulus of all RAP mixes as the elastic modulus increased with the increase in the percentage of VA in the combination. The scenario is completely reverse in the case of RCA blends where the elastic modulus increases with the increase in the RCA. This trend is observed up to a smaller dosage of cement contents that is 4%. Whereas at 6% cement, the scenario is completely different for RCA mixes, further addition of the RCA to the mix lowers the modulus values. This clearly shows the effect of blending, in addition to the cement content, equally impacts the overall performance of the mix.

6. Indirect tensile strength test (ITS)

The tensile strength of the cement-treated bases is important as cement-treated materials generally weak in tensile. The developed tensile cracks extend to the top of the pavement layers and weaken the pavement structure makes it susceptible to moisture. Generally, the tensile strain at the bottom of the bituminous layer is considered for analysis which also represents the top of the cement-treated base. The higher the tensile strength represents is more resistance to the tensile stresses that cause in the base. To determine the tensile strength characteristics, the ITS test is carried out on RAP, and RCA blends at different cement contents curing for 7 days. The samples are compacted at the obtained OMC to reach the maximum density with dimensions of the internal diameter of 101.60 mm and 63.5 ± 2.5 mm in height and then extracted after 24 hours followed by curing for 7 days. Then cured samples are tested for ITS as per ASTM D6931 at a loading rate of 50.8 mm per minute, and the failure load is noted. The Indirect Tensile Strength is determined by using the following formula:

$$S_T = \frac{2000P}{\pi Dt} \quad (1)$$

Here, S_T is the Indirect Tensile Strength in N/mm^2 , D is the Diameter of the Specimen in mm, t is the thickness of the specimen in mm, and P is the Ultimate Failure Load in kN (**Figure 6**).

From **Figure 6**, it is observed that ITS value decreases as the RAP content increases with constant cement; this is due to weak bonding between the RAP and conventional aggregates. 25% RAP with 6% cement shows more ITS value and 50% RCA with 6% cement content have higher ITS in case of RCA blends. The ITS values

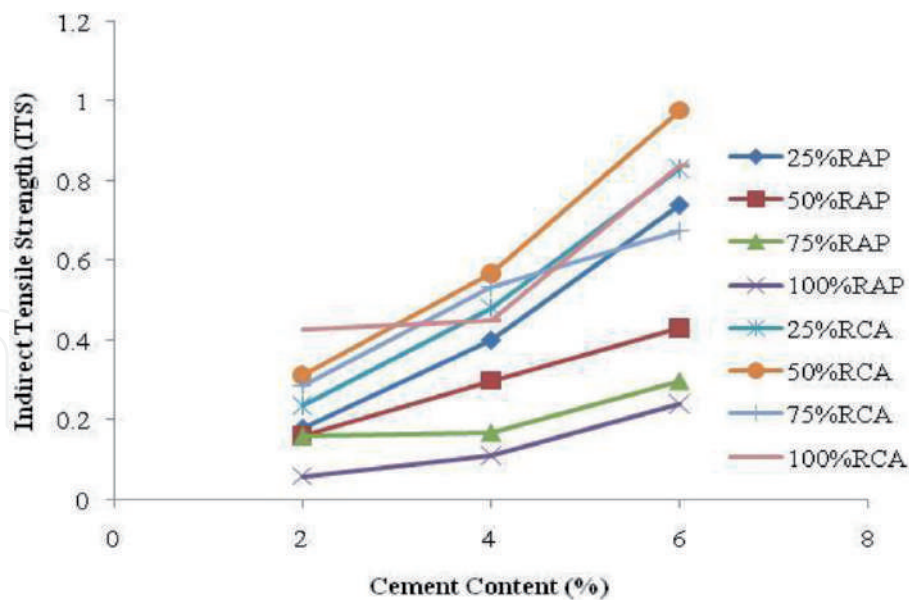


Figure 6. Indirect tensile strengths of RAP-VA and RCA-VA blends of varying cement percentages [14].

Country/code	ITS (MPa)
Italy [25]	0.32-0.60 (gyratory compaction) > 0.25 (proctor compaction)
South Africa [25]	>0.25 for cement 1.5-3% >0.20 for cement 3-5%

Table 5. ITS of different countries specifications.

increase with the increase in the amount of cement. The RCA blends show more strength compared with RAP blends as observed in UCS. 50% RCA blends followed by 25% of RCA blends show higher strength compared with remaining blends. This is due to the existence of proper interlocking between RCA and VA and the self-cementing behavior of RCA. In contrast, the RAP blended mixes have a weak bond compared with RCA due to the existing bitumen coating. It is observed that at an average the ITS value is 0.2 times that of the UCS value of RAP treated bases and 0.32 times that of UCS value in case of RCA treated bases for a 7-day curing period.

The ITS value of the present study is compared with other country's specifications. Moreover, it is observed that the acceptable UCS is around 0.20 MPa from **Table 5**. All the recycled aggregate blends achieve this value except 100% RAP at 3% cement content. However, RCA blends achieved the required ITS at 2% cement content.

7. Resilient modulus

Resilient Modulus (M_R) is the ratio of deviator stress to the recoverable strain under the application of repeated loading. It is one of the important stiffness parameters and used as input in the pavement design by most of the transportation departments. The samples were prepared according to ASTM D 1632 and ASTM D 6926 using a cylindrical metal specimen with an interval diameter of 101.60 mm and 63.5 ± 2.5 mm in height. The repeated-load indirect tension test is used to determine the resilient modulus of the mixtures according to ASTM D 4123 by applying compressive loads with a waveform at 25°C temperature and 1 Hz for loading frequencies (the recommended load range can be 10 to 20% of the indirect tensile strength). The Poisson's ratio for the calculation of resilient modulus was assumed as 0.2. The resilient modulus is calculated using the following equation.

$$ERT = \frac{P(\mu + 0.27)}{\Delta H * t} \quad (2)$$

where P is the repeated load, μ is the Poisson's ratio, ΔH is the horizontal deformation, and t is the thickness of the specimen.

Figure 7 shows that M_R value increases with the cement content and decreases with the RAP content. The maximum stiffness values were observed for 25% RAP mixes

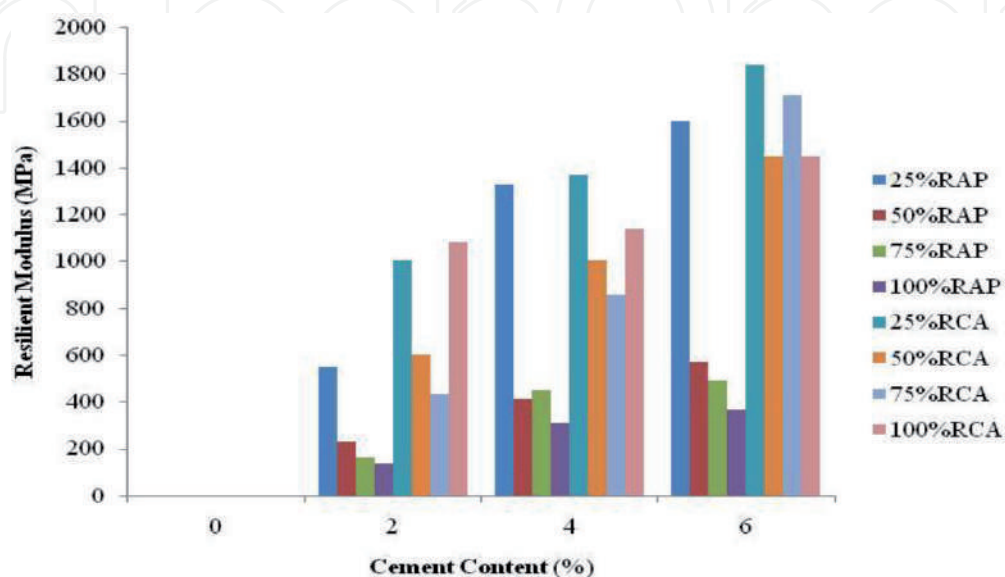


Figure 7. Resilient Modulus of RAP-VA and RCA-VA mix at 7 days curing period.

and 75% RCA as well. However, there is no appropriate trend that is observed in the RCA blends. However, there is an increase in the stiffness of the mixture independent of the RCA content. As the test is conducted at 7 days of the curing period, more curing periods might be required to gain sufficient stiffness for the cement-treated RAP bases.

8. Applications of the cement-treated recycled bases

The motive of the utilization of the cement-treated recycled bases is to improve the bearing capacity of the base layer with already used aggregates which is a conservative method. It is one of the sustainable construction practices and economical. The selection of the optimum amount of the cement stabilizer is necessary to detrimental overdosage effects like shrinkage. Besides, there is an increase in carbon footprints with a high amount of cement content. The cement-treated recycled bases can be served as a base and subbase layer in the low volume and high-volume roads as well. The Full-depth reclamation, along with cement stabilization, is advantageous when the pavement condition Index is low with poor hydro planning. It will create a strong base layer that can be covered with a thin asphalt layer. Further, the RCA can be used in the base and subbase layers, which is a locally available source. Stabilization of RCA leads good results in decreasing the leachate problems and to improve the mechanical properties.

9. Conclusions

After a thorough investigation of the strength and stiffness properties of the cement-treated recycled materials, the following conclusions are drawn:

- Cement Stabilization of the recycled materials improved the strength and stiffness of the mixes. However, the recycled material content in the mix plays a critical role in the strength development for RAP mixes.
- Maximum strength is achieved at 50% RCA and 25%RAP blended mixes which are measured in terms of ITS and UCS.
- The relation between the ITS and UCS of the cement-treated based is established. On average, the ITS value is 0.2 times that of the UCS value for RAP treated bases and 0.32 times that of UCS value in the case of RCA treated bases at 7 days of curing period.
- Cement stabilization of RCA blends is more effective compared with RAP blends in terms of mechanical properties.
- Based on the experimental results, cement stabilized recycled materials require more curing period to achieve adequate strength and stiffness. All the stabilized bases achieved the target strength at 6% cement content for low volume roads subbases except 100% RAP mix.

IntechOpen

IntechOpen

Author details

Sarella Chakravarthi, Galipelli Raj Kumar and Sabavath Shankar*
Department of Civil Engineering, National Institute of Technology, Warangal, India

*Address all correspondence to: ss@nitw.ac.in

IntechOpen

© 2020 The Author(s). Licensee IntechOpen. This chapter is distributed under the terms of the Creative Commons Attribution License (<http://creativecommons.org/licenses/by/3.0>), which permits unrestricted use, distribution, and reproduction in any medium, provided the original work is properly cited. 

References

- [1] Zhang Y, Liu X, Xu Y, Tang B, Wang Y, Mukiza E. Preparation and characterization of cement-treated road base material utilizing electrolytic manganese residue. *Journal of Cleaner Production*. 2019; 232:980-92.
- [2] Liu J, Yu B, Wang Q. Application of steel slag in cement-treated aggregate base course. *Journal of Cleaner Production*. 2020:121733.
- [3] Arulrajah A, Disfani MM, Haghghi H, Mohammadinia A, Horpibulsuk S. Modulus of rupture evaluation of cement stabilized recycled glass/recycled concrete aggregate blends. *Construction and Building Materials*. 2015; 84:146-55.
- [4] Kasu SR, Manupati K, Muppireddy AR. Investigations on design and durability characteristics of cement-treated reclaimed asphalt for base and subbase layers. *Construction and Building Materials*. 2020; 252:119102.
- [5] Guthrie, W. Spencer, Dane Cooley, and Dennis L. Eggett. Effects of reclaimed asphalt pavement on mechanical properties of base materials. *Transportation Research Record*. 2005; 1: 44-52. DOI: 10.3141/2005-06
- [6] Puppala, Anand J., Laureano R. Hoyos, and Ajay K. Potturi. Resilient moduli response of moderately cement-treated reclaimed asphalt pavement aggregates. *Journal of Materials in Civil Engineering*. 2011; 23(7): 990-998. DOI: 10.1061/(ASCE)mt.1943-5533.0000268
- [7] Murray Reid, J., Khaled E. Hassan, Okan Sirin, and Ramzi A. Taha. Demonstrating the Worth of Recycled Aggregates—A Case Study from Qatar. In *Geo-Chicago 2016*. p. 534-545. DOI: 10.1061/9780784480137.051
- [8] Pérez, Pablo, Francisco Agrela, Rosario Herrador, and Javier Ordoñez. Application of cement-treated recycled materials in the construction of a section of road in Malaga, Spain. *Construction and Building Materials*. 2013; 44: 593-599. DOI: 10.1016/j.conbuildmat.2013.02.034
- [9] Eren, Ş. and Filiz, M. Comparing the conventional soil stabilization methods to the consolid system used as an alternative admixture matter in IspartaDaridere material. *Construction and Building Materials*. 2009; 23 (7): 2473-2480. DOI: 10.1016/j.conbuildmat.2009.01.002. Available from: <http://www.sciencedirect.com/science/article/pii/S0950061809000038>.
- [10] Arulrajah, A., Piratheepan, J., Disfani, M. M., & Bo, M. W. Geotechnical and environmental properties of recycled construction and demolition materials in pavement subbase applications. *Journal of Materials in Civil Engineering*. 2013; 25(8), 1077-1088. DOI: 10.1061/(ASCE)MT.1943-5533.0000652
- [11] Arulrajah, Arul, SahanPerera, Yat Choy Wong, SuksunHorpibulsuk, and FarshidMaghool. Stiffness and flexural strength evaluation of cement stabilized PET blends with demolition wastes. *Construction and Building Materials*. 2020; 239: 117819. DOI: 10.1016/j.conbuildmat.2019.117819
- [12] Arshad M. Laboratory investigations on the mechanical properties of cement-treated RAP-natural aggregate blends used in base/subbase layers of pavements. *Construction and Building Materials*. 2020; 254:119234.
- [13] Yan K, Li G, You L, Zhou Y, Wu S. Performance assessments of open-graded cement stabilized macadam containing recycled aggregate. *Construction and Building Materials*. 2020; 233:117326.

- [14] Chakravarthi, S., Anusha Boyina, Arun Kumar Singh, and S. Shankar. Evaluation of cement-treated reclaimed asphalt pavement and recycled concrete pavement bases. *International Journal of Pavement Research and Technology*. 2019; 12 (6): 581-588. DOI: 10.1007/s42947-019-0069-1
- [15] Faysal, M., Mahedi, M., Aramoon, A., Thian, B., Hossain, M. S., Khan, M. A., & Khan, M. S. Determination of the structural coefficient of different combinations of cement-treated/untreated recycled base materials. In *Geotechnical and Structural Engineering Congress*; 2016. p. 1198-1208. DOI: 10.1061/9780784479742.100
- [16] LaHucik, Jeffrey, Scott Schmidt, Erol Tutumluer, and Jeffery Roesler. Cement-treated bases containing reclaimed asphalt pavement, quarry by-products, and fibers. *Transportation Research Record*, 2580. 2016; (1): 10-17. DOI: 10.3141/2580-02
- [17] Behiry, Ahmed Ebrahim Abu El-Maaty. Utilization of cement treated recycled concrete aggregates as base or subbase layer in Egypt. *Ain Shams Engineering Journal*. 2013; 4 (4): 661-673. DOI: 10.1016/j.asej.2013.02.005
- [18] Xuan, D. X., L. J. M. Houben, A. A. A. Molenaar, and Z. H. Shui. Mixture optimization of cement treated demolition waste with recycled masonry and concrete. *Materials and structures* 45. 2012; 1-2: 143-151. DOI: 10.1617/s11527-011-9756-3
- [19] Taha, Ramzi, Ali Al-Harthy, Khalid Al-Shamsi, and Muamer Al-Zubeidi. "Cement stabilization of reclaimed asphalt pavement aggregate for road bases and subbases." *Journal of materials in civil engineering* 14, no. 3 (2002): 239-245. DOI: 10.1061/(asce)0899-1561(2002)14:3(239)
- [20] Ministry of Road Transport and Highways, Specifications for Road and Bridgeworks, Fifth Revision, Ministry of Road Transport and Highways, New Delhi, 2013.
- [21] Guthrie WS, Brown AV, Eggett DL. Cement stabilization of aggregate base material blended with reclaimed asphalt pavement. *Transportation Research Record*. 2007; 2026(1): 47-53. DOI: 10.3141/2026-06
- [22] MORD. Ministry of Rural Development: Specifications for Rural Roads. New Delhi: The Indian Roads Congress, 2014.
- [23] Poon CS, Chan D. Feasible use of recycled concrete aggregates and crushed clay brick as unbound road sub-base. *Construction and building materials*. 2006; 20(8): 578-585. DOI: 10.1016/j.conbuildmat.2005.01.045
- [24] Yuan D, Nazarian S, Hoyos LR, Puppala AJ. Evaluation and mix design of cement-treated base materials with a high content of reclaimed asphalt pavement. *Transportation Research Record*. 2011; 2212 (1):110-119. DOI: 10.3141/2212-12
- [25] Autelitano, F., & Giuliani, F. Electric arc furnace slags in cement-treated materials for road construction: Mechanical and durability properties. *Construction and Building Materials*. 2016; 113: 280-289. DOI: 10.1016/j.conbuildmat.2016.03.054

Cementitious Grouts Containing Irradiated Waste Polyethylene Terephthalate

*Muhammad Imran Khan, Muslich Hartadi Sutanto,
Madzlan Bin Napiah and Salah E. Zoorob*

Abstract

This chapter describes a review of the design and formulation of various cementitious grouts for semi-flexible pavement surfaces. Additionally, the authors also conducted extensive experimental work on the possibility of using a most effective and innovative way of recycling waste polyethylene terephthalate (PET) by exposing to gamma radiation and using as a replacement of Ordinary portland cement in the formulation of cement grouts for semi-flexible pavement surfaces. In the current study, cement in the grouts was replaced with PET (regular and irradiated), fly ash and silica fume and was evaluated for flowability and strength properties. The study concludes that normal PET causes a significant reduction in compressive strength, however, some of the strength is restored when irradiated PET was used. The recycling of waste PET, as a cement replacement in the cementitious grouts for semi-flexible pavement surfaces, with the irradiation process can be doubled as compared to utilizing normal/regular PET.

Keywords: cementitious grout, irradiated waste polyethylene terephthalate, fly ash, silica fume, compressive strength

1. Introduction

Generally, pavements are classified into two types: flexible pavements and rigid pavements. Conventional flexible pavements are constructed from bituminous materials and are widely used as a highway, expressway/freeway, and airport pavements due to their satisfactory performance against distresses and better riding quality, good serviceability, high skid resistance, low cost and easy maintenance [1–3]. However, due to recent exponential increase in traffic load and extreme adverse environmental conditions, the flexible pavements are exposed to many distresses (such as rutting, cracking, corrugation, shoving, stripping etc.) which can badly affect its service life and performance [4, 5]. On the other hand, rigid pavements are constructed from cement concrete with or without reinforcement. Rigid pavements have better durability, high compressive strength but have some disadvantages such as; provision of joints, rough-riding quality, slow setting time, high susceptibility to thermal stresses, high initial cost and maintenance efforts, cannot simply be ignored [6–8]. Taking into consideration the disadvantages of both flexible and rigid pavements there was a need for an alternative pavement

design that can combine the positive attributes of conventional flexible and rigid pavements with a view of the improvement in serviceability and performance. One such alternative is the design of semi-flexible pavement surfaces (SFPS) [9–13].

2. Semi-flexible pavement surfaces

Semi-flexible pavement surface (SFPS) material (also known as grouted macadam) is designed as an open-graded asphalt mixture (OGAM) with 25–35% air voids and then cement grout is infused into the voids [2, 7, 14–17]. However, few researchers advised the range of air voids to be 20–35% [18, 19]. It is a well-known fact that the major demerits of rigid pavements are extended construction time and provision of joints to allow thermal expansion as compared to flexible pavements. Therefore, the semi-flexible pavements are gaining popularity from last few decades and are devised as a jointless pavement with reduced time of construction, easy to repair and construct as well as offers good serviceability and riding quality as compared to rigid pavements [18, 20, 21]. This new type of pavements possesses both flexibility and rigidity which depends on characteristics of the bituminous mixture and cement grout, respectively. Moreover, SFPS provides superior resistance to rutting and are not susceptible to permanent deformation [18]. Semi-flexible pavements have been constructed in various countries as a highway intersection, bus lanes in urban areas, tunnels roads, the pavement in industrial area for the movement of heavy machinery, airport taxiways and aprons as fuel and spillage resistance [15, 16, 21–27].

3. History of the construction of semi-flexible pavement

The first construction of SFPS was carried out in the 1950s, in France and was given the name as Salviacim. It was proposed to provide resistance against oil and fuel attack on the surface and was constructed as a protective layer over conventional asphalt concrete pavement [28]. However, further development of Salviacim was processed by Lefebvre Enterprises, a French construction company, as a replacement to rigid pavements to provide cost-effective construction [29, 30]. Later, this type of pavement construction spread in different countries including South Africa, Saudi Arabia, Australia, UK and Japan as a heavy-duty surface construction [31]. Some other brand names also become popular in Europe based on the type of designed materials such as Hardicrete Heavy-duty surfacing, Densiphalt (or confalt) and Worthycim Heavy-duty surfacing [32–35]. In the USA the semi-flexible pavement is called as Resin Modified Pavement (RMP) and in Japan, it was given name as Rut-proof Pavement (RP-Pavement) [20, 29]. Moreover, the construction of SFPS spread throughout Europe, Various states of Africa, North America, South Pacific and Far East [36].

4. Composition of semi-flexible pavement surfaces

The construction of semi-flexible pavement surfaces (SFPS) is performed in two stages. In the first stage, the open-graded asphalt mixture (OGAM) is prepared, laid, and compacted to achieve the target air voids of 25–35%. The compaction is accomplished by a light application of roller compactor without vibration to avoid disintegration of course aggregates and tracks in the mixture. In the second stage, the cementitious grouts are prepared and poured on the surface of OGAM and

allowed to infiltrate into the voids. The construction is normally carried out in two consecutive days, the reason is to allow the OGAM to cool down before applying the cement grouts. Rubber scraper can be used to spread the grout on the surface [18, 20]. The schematic representation of this process is demonstrated in **Figure 1**. Hence the major constituents of semi-flexible surfaces are a selection of open-graded asphalt mixture and formulation of cement grouts.

4.1 Selection of open graded asphalt mixture

The major constituent in constructing semi-flexible pavement surfaces are the aggregates. Consequently, it needs careful attention while selecting gradation of aggregate for mix designing of semi-flexible mixtures. Typically, semi-flexible pavement surfaces comprise of open-graded asphalt skeleton with air voids ranging from 25 to 35% above which highly flowable cementitious grouts are spread and allowed to penetrate [35, 37, 38]. The key parameters for the selection and design of OGAM for semi-flexible pavements are the consideration of air voids and binder drainage. The air voids of final compacted OGAM shall be in the range of 25 to 35%. In case if air voids are less than 25%, the mixture may not have interconnected voids and would be difficult for the cement grout to penetrate through the depth of OGAM [39]. As a result, adequate strength and homogeneous properties will not be attained to withstand traffic load and environmental stresses as shown in **Figure 2** [18]. On the other hand, if air voids are more than 35%, a large amount of cement grout will be required, and the final mix will more be likely a rigid pavement and may lead to fatigue failure. Similarly, binder drainage (or draindown) of bitumen in the final mixture shall not be more than 0.3% as per AASHTO T 305 or ASTM D6390 standards [40, 41].

Therefore, few studies have been conducted for the selection of suitable aggregate gradation that fulfills the requirement of air voids and binder drainage. Recently, a detailed study has been conducted by Saboo N. et al., (2019) on

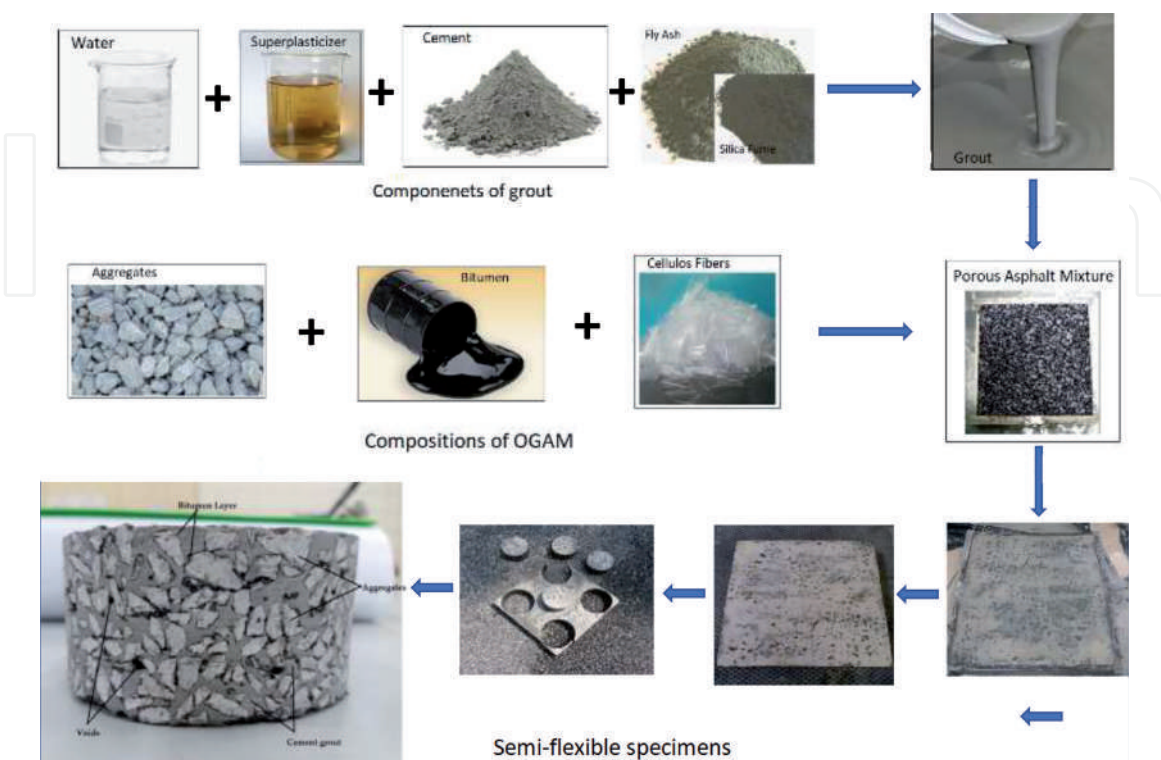


Figure 1.
Schematic representation of the process of preparing semi-flexible surfaces.



Figure 2.
Disconnectivity of internal voids due to low air-voids [18].

evaluating different types of porous aggregate gradations for semi-flexible pavement surfaces. The hierarchical ranking approach was used to reject/select and finally to choose the most desirable gradation system [26]. In this study, seven different porous asphalt mix skeletons were prepared with bitumen contents ranging from 2–5%. The gradations were selected from the previous research that has already been used in various studies and is presented in **Figure 3**.

During the initial elimination process, draindown test, air voids in the compacted mix, voids in the coarse aggregate (VCA), permeability and cantabro loss tests were used. The selected mixtures were further evaluated for Indirect Tensile test (ITS) to rank the gradation system accordingly. It was finally suggested three mixes including BSI with 4% bitumen, Densiphalt-12 with 4% and Densiphalt-12 with 4.5% bitumen were chosen as most desirable porous asphalt mix skeleton to be considered for semi-flexible pavement surfaces as shown in **Table 1** [26].

Similarly, another study was conducted by Hou et al., on the random selection of 22 aggregate gradations by varying percentages of coarse aggregates, fine aggregates, and fillers. The effect of grouting on these gradations was evaluated by volumetric analysis, cantabro and binder drainage test as well as wheel tracking and bending tests [42]. It was revealed that grouting ability of OGAM is not only influenced by initial air voids but also on void interconnectivity, morphological characteristics, and size of pores. The comparison of air voids before and after grouting is demonstrated in **Figure 4** and can be seen that grouting ability is not

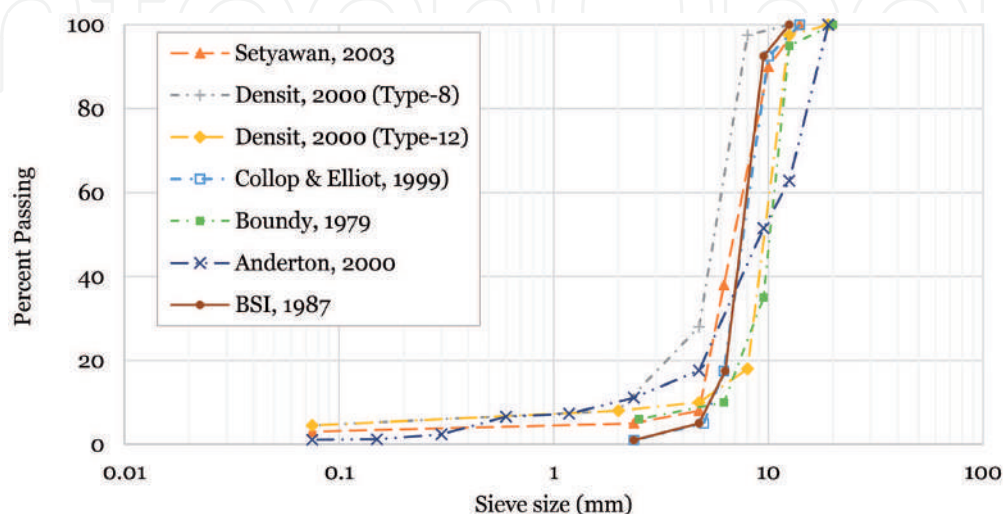


Figure 3.
Porous asphalt gradation curves.

Gradation	Draindown (%) <0.30	Air voids (%) >25%	VCA ratio < 1	Permeability (m/day) >100 m/day	Cantabro loss (%) <50%	ITS(kPa)
BSI with 4% bitumen	0.30	33.05	0.95	362.90	33.20	113.35
Densiphalt-12 with 4%	0.19	33.56	0.93	332.90	34.91	114.42
Densiphalt-12 with 4.5%	0.30	32.08	0.91	247.69	34.91	136.80

Table 1.
 Final selection criteria for porous aggregate gradation.

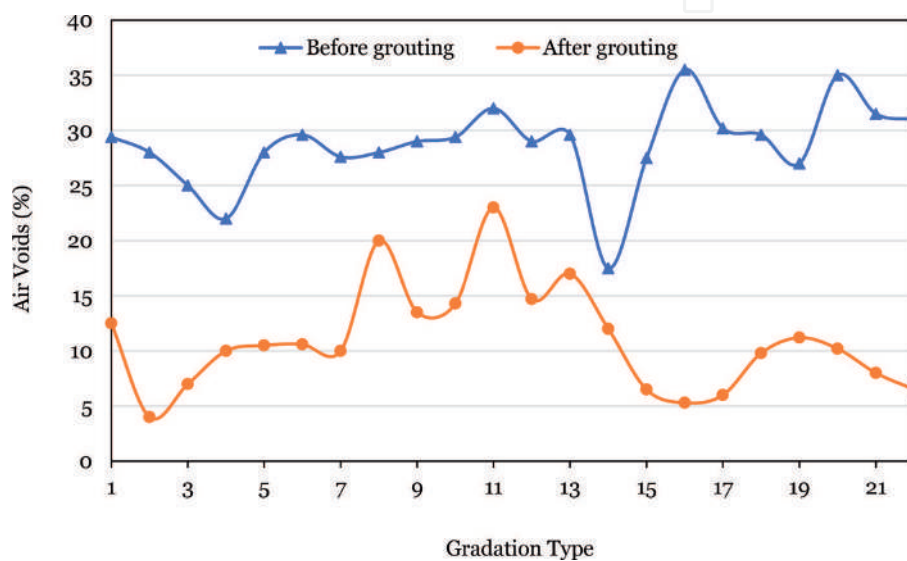


Figure 4.
 Air voids before and after grouting [42].

only influenced by initial air voids. The grouting ability can also be enhanced by increasing the percentage of coarse aggregates and reducing binder content (3.8% in this study was used) which can improve the interconnectivity of voids.

4.2 Cement grouts

Cement grout or cement slurry is an essential part of semi-flexible pavement surfaces, which contributes to the rigidity of pavement. The design and formulation of grouts for semi-flexible pavement surfaces differ from traditional cement past and cement mortars used in the concrete industry. The constituents of the grouts are formulated in such a way that can easily be penetrated the voids of OGAM. Additionally, the grouts should have enough strength to withstand the stresses induced due to traffic and the environment. Therefore, the flowability (fluidity), workability, and strength of cement grouts play a key role in the performance of semi-flexible pavement surfaces. In a scenario, if the fluidity of cement grout is insufficient it would not fill properly the air voids of OGAM and as a result, the designed SFP mixtures would not provide sufficient strength and durability. The fluidity of grouts is usually determined by flow-cone, however, the flow-out time depends on the geometry of the cone. Ordinary Portland cement (OPC), water (different ratios), and/or sand, fillers, and other supplementary cementing materials (such as fly ash and silica fume)

are normally used to formulate the compositions of cement grouts. Furthermore, superplasticizer can be used to improve the fluidity at a relatively low w/c ratio. Various studies have been conducted on designing the constituents of cement grouts for semi-flexible pavements surfaces and are listed in the following section.

5. Design parameters of cement grouts for SFPS

5.1 Flowability of the cement grouts

One of the primary considerations to formulate the compositions of cementitious grouts for semi-flexible pavement surfaces is the flow or fluidity of grouts. The grouts are required to be sufficiently flowable that can easily penetrate the voids of the porous asphalt skeleton. The flowability/fluidity of grouts highly depends on w/c ratio, superplasticizer as well as other additives and supplementary cementing materials. Traditionally, the flowability/fluidity is measured by flow-cone apparatus in which the desired quantity of grout is poured and the flow-out time of grout from the flow-cone is measured in seconds. Higher the time of flow, lower is the fluidity and hence less workability. On the other hand, a lower time taken by grout to flow-out indicates high flowability and higher workability.

However, the standard requirement of flow-out time of cement grout depends on the geometry and size of the flow-cone, as three different flow-cones are being frequently used in literature. Which are; (a) Malaysian flow-cone, (b) Marsh flow-cone and (c) ASTM flow-cone and their schematic representation are shown in **Figure 5(a-c)**. According to the Malaysian standards, the flow-out time of 1000 mL of grout using Malaysian flow-cone (**Figure 5(a)**) shall be in the range of 11 sec to 16 sec [43, 44]. The cement grouts with the flow of 11–16 sec will have sufficient fluidity and suitable for grouting SFP surfaces. Similarly, the quantity of grout required for Marsh flow-cone (**Figure 5(c)**) is also 1000 mL, however, due to change in geometry the time of flow-out shall be in the range of 8 to 10 sec [38]. Nevertheless, the flow-cone used in ASTM C939 have different geometry as shown in **Figure 5(b)** and hence the requirement of flow-out time. According to the standard, recommended fluidity of cement grout is 10 to 14 sec while allowing a grout quantity of 1725 mL to flow-off the funnel.

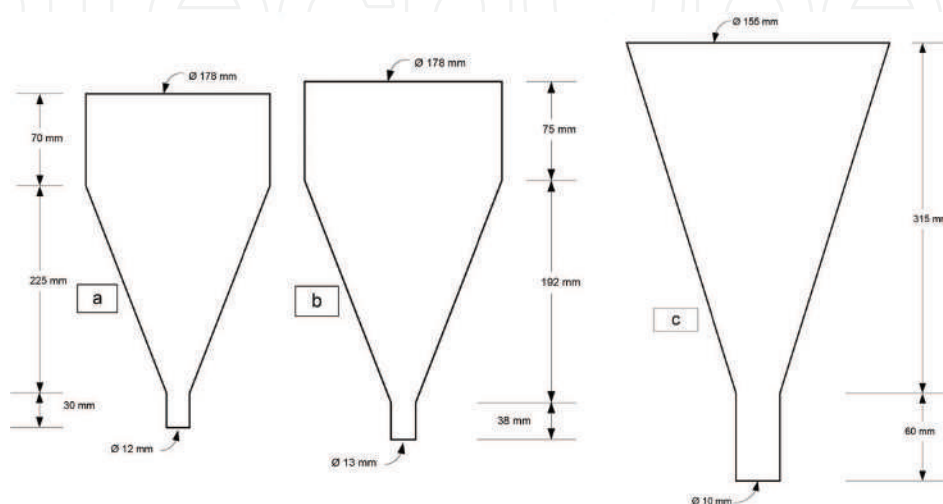


Figure 5. Flow cones used in literature to measure the fluidity of grouts: (a) Malaysian flow-cone, (b) ASTM flow-cone and (c) marsh flow-cone (dimensions not-to-scale).

Various studies have been conducted on evaluating the fluidity of cement grout by varying water content as well as inclusion superplasticizer, other additives and supplementary cementing materials. However, increasing w/c ratio causes a reduction in strength properties of grout and therefore it shall be carefully selected. To overcome the issues related to high w/c ratio, superplasticizer plays a key role in improving the fluidity of grouts at relatively low w/c ratio. It is always recommended to use superplasticizer in designing cement grouts for SFP surfaces at low w/c ratio in order to achieve the desired strength properties at high flowability of grouts [15, 45]. A study concluded that increasing w/c ratio causes a significant increase in fluidity with a considerable reduction in compressive strength. However, the addition of superplasticizer up to 1% (by weight of cement) causes improvement in fluidity as well as compressive strength. Moreover, increasing superplasticizer beyond 1.5% can cause a bleeding problem in grouts [46].

The incorporation of high w/c ratio and plasticizing action of styrene-butadiene admixtures produces highly flowable cement grout however with low strength properties and gives weaker grouts [15]. On the other hand, stronger grouts with desired fluidity can be achieved by the addition of milled glass and polycarboxylate superplasticizer at relatively low w/c ratio [15]. The highest fluidity presented by the weaker grout group could be explained by their higher water/cement ratio and the styrene-butadiene admixture plasticizing action. In the stronger grouts group, increasing the content of milled glass significantly reduces the flow time values. Incorporating milled glass particles with their impermeable and low specific surface areas indicates that at the same water/cement ratio water is available to fluidize the grouts.

Similarly, in a study different w/c ratio (0.48–0.63), fly ash content (0–20%) and mineral powder (0–20%) were used to design cement paste and to analyze the fluidity of grouts using flow-cone shown in **Figure 5(b)**. Increasing w/c ratio causes a significant increase in the fluidity of cement paste. Similarly, the increase in fluidity was also observed with increase in the dose of fly ash. However, the addition of mineral powder initially causes a reduction in fluidity and then increased was witnessed. Based on fluidity, drying shrinkage and strength properties, 0.56–0.58 w/c ratio, 10% fly ash and 10% mineral powder were recommended as a suitable combination of grouts for SFP mixtures [47].

5.2 Strength properties of grouts

The second most important parameter for selection of cement grout for SFP surfaces is the compressive strength of grouts. The compressive strength largely depends on w/c ratio and other supplementary cementing materials and additives. Various materials have been used so far including, fly ash, silica fume, ground granulated blast furnace slag (GGBS), gypsum and mineral powders for designing cement grouts suitable for SFP surfaces requirements. A study has shown that increase in w/c ratio from 0.48 to 0.63 causes a significant reduction in 7 and 28-days compressive strength, however, flexural strength was slightly reduced [47]. Therefore, there is need to introduce the addition of other admixtures and supplementary cementing materials, such as superplasticizer, fly ash, silica fume which can contribute in improving the strength properties at relatively low w/c ratio while achieving the desired flowability.

The combination of silica fume additionally with superplasticizer can produce grouts with sufficient fluidity and strength properties that can be recommended for semi-flexible pavement surfaces. Hence, silica fume with 5% replacement of OPC and 2.0% polycarboxylate based superplasticizer at 0.30 w/c ratio gives fluidity of 15 sec (as determined by Malaysian flow-cone) and 28-days compressive

strength of 92.5 MPa [48]. Therefore, this grout can be recommended to produce high-strength cement grouts for semi-flexible pavement surfaces that can be used in heavy-loaded pavements.

6. Formulation of cement grouts for SFPS

It is necessary to optimize the constituents of cement grouts that can be used as a grouting material for semi-flexible surfaces. The constituents are but not limited to water, cement, superplasticizer, sand, and/or other supplementary cementing materials (SCM). The optimization is normally evaluated based on fluidity and compressive strength (at different curing period). The Authors also conducted a related study to optimize the constituents of cement grout using a statistical tool known as response surface methodology (RSM). In this study, w/c ratio (0.25 to 0.45) and Polycarboxylate-ether type superplasticizer (0 to 2%) were selected as factors (dependent variables) whereas flow-value and compressive strength (1-day, 7-days, and 28-days) were considered as responses (dependent) variables to conduct statistical analysis and optimization in RSM. The ANOVA and multi-objective optimization techniques were utilized to formulate the optimum combination of w/c ratio and dosage of superplasticizer [46].

A study conducted by [49] utilizing latex modified cement mortar to investigate the performance SFPS. The composition of cement grouts was selected as; 0.70 w/c ratio, 20% sand, 10% limestone filler, and latex with 0, 1.2, and 2.4%. The results indicate that an increasing percentage of latex improved the compressive and flexural strength, however, a negative effect on fluidity. Moreover, SFP mixtures with latex-modified grout showed better moisture resistivity, rutting resistance, and fatigue life as compared to conventional asphalt mixture [49]. In another study, three different interface optimizers (silane coupling agent, carboxyl styrene-butadiene latex, and cationic emulsified asphalt) were used with various percentages in cement grouts to improve the interfacial connection between the cement grout and asphalt in SFP mixtures. The results indicate that interface optimizers despite causing a reduction in strength properties of grout, greatly improves the interfacial connection of cement grout with asphalt as observed from microstructural analysis of mixtures as shown in **Figure 6** [50]. These interface optimizers also show a positive effect in terms of crack resistance at low temperature, stability at high temperature, and moisture stability, particularly by cationic emulsified asphalt.

A similar study was conducted to evaluate the adhesion of cement grout with porous asphalt mixture and the mechanical properties of SFP mixtures. In this study a modified cement grout containing; cement, w/c ratio (0.40), silica fume (10%), superplasticizer (2%), aluminum powder (0.04%), viscosity modifying agent (0.2%), and asphalt emulsion (20%, 40% and 60%) were used to produce SFP mixtures. The results indicate that asphalt emulsion modified grouts have better adhesion with porous asphalt mixture as compared to control grouts. This phenomenon may overcome fatigue problems in semi-flexible pavements. The overall performance of semi-flexible pavement mixtures using asphalt emulsion modified grouts showed better performance in terms of rutting resistance, moisture damage resistance, and low-temperature crack resistance as compared to control grout and conventional HMA [1].

An analytical approach using mathematical programming was used to optimize the constituents of cement grouts. Various combinations of grouts were prepared using w/c (0.40, 0.50, 0.60), naphthalene based superplasticizer (0%, 2%, 4%, 6%),

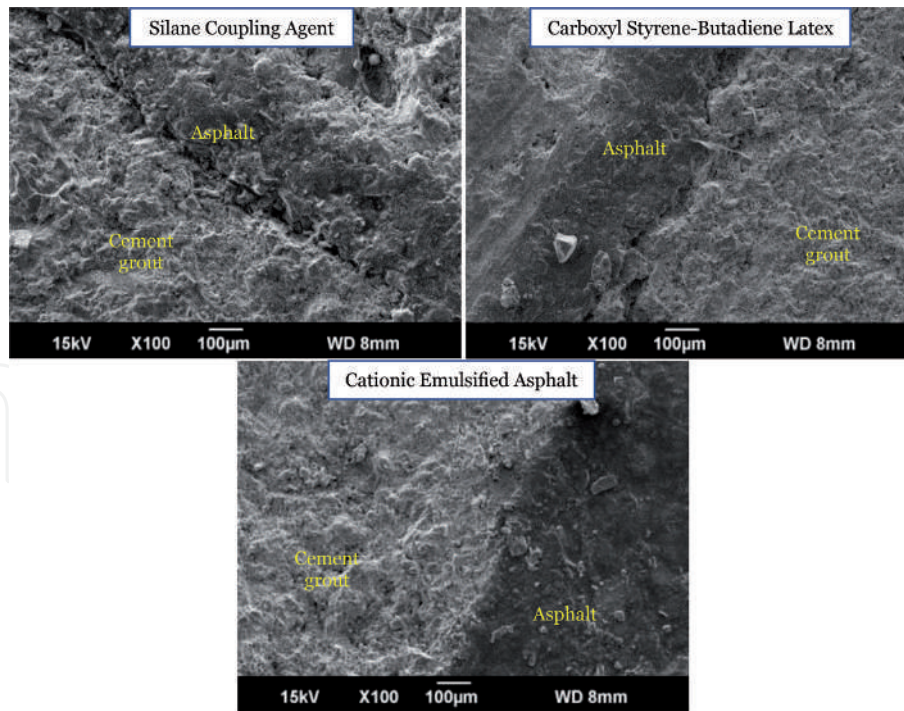


Figure 6. Microstructure of cement-asphalt interface modified with a silane coupling agent, carboxyl styrene-butadiene latex, and cationic emulsified asphalt [50].

sand with 23% by weight of cement (size <2.36 mm, <1.18 mm, <0.6 mm) to optimize the composition of grouts by evaluating flow and compressive strength properties. The results indicate that flow was significantly improved by increasing the dose of naphthalene superplasticizer from 0 to 6% and the w/c ratio from 0.40 to 0.60. The optimal combination of grouts obtained using mathematical programming was 0.54 w/c ratio, 2% superplasticizer, and 1.66 mm sand size. The flow time and compressive strength at this combination are 14 sec and 24.25 MPa respectively. Similarly, another group of grouts was prepared using polycarboxylate superplasticizer. The compositions were w/c ratio (0.40, 0.45, 0.50), polycarboxylate superplasticizer (0%, 0.5%, 1.0%, 1.5%, 2.0%), sand with 23% by weight of cement (size <2.36 mm, <1.18 mm, <0.6 mm). Interestingly, the compressive strength of grouts increased with an increasing dose of SP from 0 to 1.0% and then starts decreasing again. Moreover, the flow time was significantly decreased with increasing SP and w/c ratio. The optimal doses of ingredients using the analytical approach were 0.48 w/c ratio, 1.0% SP and 0.6 mm sand particle size with flow time of 14 sec and compressive strength of 23.46 MPa [27].

Latex powder (0%, 1.2% and 2.4% by weight of cement) was used to modify cement grout with 0.72 w/c ratio, 20% sand, and 10% filler and to use for semi-flexible pavement mixtures. The addition of latex powder showed improved compressive and flexural strength of cement grout, while causes reduction in fluidity. The latex powder with 1.2% was considered as optimum based on strength and fluidity and was used to produce SFP mixtures. SFP mixtures with 1.2% latex-modified grout showed better resistance to high-temperature performance while higher moisture susceptibility, while weaker fatigue resistance and low-temperature performance. However, the moisture damage and low-temperature behavior of SFP mixtures were still in good agreement [51]. Similarly, cement grout was formulated using 0.63 w/c ratio, 10% mineral filler, 20% sand and 0–12% Carboxyl Latex. The substitution of carboxyl latex to grout causes a reduction in compressive strength both at 7-days and 28-days curing.

However, flexural strength was increased with increasing dose of carboxyl latex. Hence, 8% of carboxyl latex was considered as optimum dosage. The performance of SFP mixtures filled with carboxyl latex-modified grout was improved in terms of rutting resistance, low-temperature crack resistance, moisture damage and fatigue resistance [52]. Moreover, various studies have been conducted on the selection of compositions of cement grouts for semi-flexible pavement surfaces as described in **Table 2**.

Composition of grouts	Strength Properties of grouts	Concluding remarks	References
w/c ratio = 0.50, fly-ash = 23%, superplasticizer = 2%	Not determined	SFP mixtures demonstrate higher resistance against rutting and moisture damage as compared to HMA mixtures. SFP mixtures showed lower fatigue life as compared to HMA mixtures. SFP mixtures showed better thermal cracking resistance at low temperatures than HMA mixture using fracture work property.	[53]
w/c ratio = 0.31 Cement grouting was JGM-301 (factory produced)	Compressive Strength: 3-days = 34.5 MPa 28-dyas = 42.3 MPa	It was recommended that semi-flexible pavement surfaces with this grout can be used for heavily loaded pavements.	[19, 54]
Water: cement: sand: filler = 720:1000:497:249 Means: w/c ratio = 0.72, sand =20%, filler = 10% Latex = 0, 1.2%, 2.4%	Compressive Strength: 7-days = 21.6 MPa to 24.1 MPa Flexural Strength: 7-days = 1.65 MPa to 3.54 MPa	Latex in cement mortar has a positive effect on compressive and flexural strength while negative impact on fluidity. SFP mixtures show better moisture resistance, high rutting resistance, and better fatigue life as compared to dense asphalt mixtures. However, SFP mixtures showed poor performance in terms of brittle cracking resistance as compared to dense asphalt mixtures.	[49]

Composition of grouts	Strength Properties of grouts	Concluding remarks	References
Three interface optimizers were used 1. Control grout (OPC) 2. Silane coupling agent (0.25%, 0.50%, 0.75%) 3. Carboxyl styrene-butadiene latex (5%, 10%, 15%) 4. Cationic emulsified asphalt (5%, 10%, 15%) w/c ration = not known	7-days compressive Strength: 1. 42.98 MPa for OPC 2. 34.65 MPa, 36.85 MPa, 33.61 MPa for Silane coupling agent 3. 25.70 MPa, 29.70 MPa, 26.15 MPa for Carboxyl styrene-butadiene latex 4. 37.79 MPa, 33.82 MPa, 31.53 MPa for Cationic emulsified asphalt	The interface optimizers improve the drying shrinkage resistance but cause a reduction in strength properties. The interfacial connection of cationic emulsified asphalt modified grout with bitumen was proved to be best whereas worst for silane coupling agent. These interface optimizers also deliver satisfactory results in terms of crack resistance at low temperature, stability at high temperature, and moisture stability.	[50]
w/c ratio = 0.40 silica fume = 10% SP = 2% aluminite powder (AP) = 0.04% viscosity modifying agent (VMA) = > VMA/C = 0.2% Asphalt Emulsion (AE)/cement binder AE/C = 20%, 40%, 60%	7-days compressive Strength: CP = 26 MPa CAEP20% = 13 MPa CAEP40% = 11.3 MPa CAEP60% = 10.5 MPa 28-days compressive Strength: CP = 28.5 MPa CAEP20% = 19 MPa CAEP40% = 17.8 MPa CAEP60% = 17 MPa	The compressive strength of grout reduces with the addition of asphalt emulsion. The asphalt emulsion improves the adhesion between cement grout and porous asphalt mixture. SFP with asphalt emulsion-based grouts has better rutting resistance as compared to conventional HMA. However, the rutting resistance decrease with increasing percentages of asphalt emulsion in the grouts. The overall performance of SFP mixtures based on asphalt emulsion modified grouts have better performance in terms of rutting resistance, moisture damage resistance, and low-temperature crack resistance as compared to control grout and conventional HMA.	[1]

Composition of grouts	Strength Properties of grouts	Concluding remarks	References
Naphthalene based superplasticizer = 0, 2%, 4%, 6% w/c ratio = 0.4, 0.5, 0.6 Sand = 23% by weight of cement	7-days compressive Strength: 10.22 MPa to 31.65 MPa (for sand size <0.6 mm) 13.15 MPa to 33.75 MPA ((for sand size <1.18 mm) 16.48 MPa to 36.69 MPA ((for sand size <2.36 mm)	An analytical approach was used for optimization using mathematical programming. The optimal composition of grout: w/c ratio = 0.54, SP = 2% with compressive strength of grout = 24.25 MPa	[27]
Polycarboxylate superplasticizer = 0, 0.5%, 1%, 1.5%, 2% w/c ratio = 0.4, 0.45, 0.50 Sand = 23% by weight of cement	7-days compressive Strength: 13.15 MPa to 29.10 MPa (for sand size <0.6 mm) 16.38 MPa to 30.39 MPA ((for sand size <1.18 mm) 18.45 MPa to 31.20 MPA ((for sand size <2.36 mm)	An analytical approach was used for optimization using mathematical programming. The optimal composition of grout: w/c ratio = 0.48, SP = 1% with compressive strength of grout = 23.46 MPa	[27]
w/c ratio = 0.72, sand =20%, filler = 10% Latex powder (LP) = 0, 1.2%, 2.4%	7-days Compressive Strength: 23.5 MPa (0% LP), 24.1 MPa (1.2% LP), 21.6 MPa (2.4% LP) 7-days Flexural Strength: 1.65 MPa (0% LP), 2.81 MPa (1.2% LP), 3.54 MPa (2.4% LP)	Fluidity decreases with increasing latex powder. The cement grout with 1.2% latex powder has higher compressive strength as compared to control and 2.4% latex powder. However, the flexural strength of grouts increased with increasing latex powder. SFP mixtures with latex-modified grout showed better resistance to high-temperature performance and moisture susceptibility, while weaker fatigue resistance and low-temperature performance.	[51]

Composition of grouts	Strength Properties of grouts	Concluding remarks	References
w/c ratio = 0.63, mineral filler = 10% and sand = 20% Carboxyl Latex = 0–12%	7-days Compressive Strength: 20.76 MPa to 11.20 MPa 28-days Compressive Strength: 31.43 MPa to 18.56 MPa 7-days Flexural Strength: 1. MPa to 4.95 MPa 28-days Flexural Strength: 5.74 MPa to 6.49 MPa	The substitution of carboxyl latex to grout causes a reduction in compressive strength both at 7-days and 28-days curing. However, flexural strength was increased with increasing dose of carboxyl latex. 8% carboxyl latex was considered as optimum dosage. The performance of SFP mixtures filled with carboxyl latex-modified grout was improved in terms of rutting resistance, low-temperature crack resistance, moisture damage and fatigue resistance.	[52]
w/c ratio = 0.60 cement: sand = 1: 0.5	3-days compressive strength = 10.4 MPa 28-dyas compressive strength = 30.7 MPa 3-days Flexural Strength = 3.3 MPa 28-days Flexural Strength = 7.3 MPa	The semi-flexible mixtures show better high-temperature performance while maintaining its flexibility. It also demonstrates better results of low-temperature cracking resistance as compared to conventional HMA. However, the split tensile strength was lowered. The SFP mixtures showed significant improvement in moisture resistance and present great advantages over conventional HMA.	[55]

Composition of grouts	Strength Properties of grouts	Concluding remarks	References
<p>Cement paste: w/c ratio = 0.48, 0.53, 0.58, 0.63 fly ash = 0%, 10%, 20% mineral powder (ground granulated blast furnace slag) = 0%, 10%, 20%</p> <p>Cement mortar: w/c ratio = 0.55, 0.60, 0.65 fly ash = 0%, 10%, 20% mineral powder (ground granulated blast furnace slag) = 0%, 10%, 20% Sand = 10%, 15%, 20%</p>	<p>Optimal Combinations: Cement paste: 0.56–0.58 w/c ratio, 10% fly ash and 10% mineral powder Cement mortar: 0.61–0.63 w/c ratio, 10% fly ash and 15% mineral powder</p>	<p>The overall performance of cement paste was observed to be better than cement mortar in terms of fluidity and strength and recommended more suitable for grouting semi-flexible pavement surfaces with the following combinations; w/c ratio = 0.58, fly ash = 10 and mineral powder = 10%</p>	[47]
<p>w/c ratio = 0.30, 0.35, 0.40, 0.45, 0.50 SP (Polycarboxylate) = 0 to 2.5% Silica fume = 0%, 5% and 10% Optimum combination of 0.30 w/c ratio, 2.0% SP and 5% silica fume</p>	<p>1-day compressive strength = 57.5 MPa 28-days compressive strength = 92.5 MPa 7-days Flexural strength = 6.7 MPa 28-days Flexural strength = 9.1 MPa</p>	<p>Grout with 5% replacement of SF and 2.0% SP produces cement grouts with desirable flowability and compressive strength required for SFP surfaces.</p>	[48]

Table 2.
Summary of the various types of cement grouts used in literature.

7. Irradiated polyethylene terephthalate (PET) based cement grouts

The authors utilized an innovative and effective way of recycling waste PET in cement grouts for semi-flexible pavement surfaces. This was done by exposing waste PET to gamma rays, which, in fact, improve the crystallinity and chain-scission properties of PET. The waste PET was obtained from Plastic Recycling Factory, Ipoh, Malaysia. The initial particle size was in the range of 0.075 mm to 0.85 mm. After exposing to gamma rays, the PET was further sieved on 0.015 mm sieve to obtain a fine powder.

Utilizing regular PET in cement grouts causes a significant reduction in strength properties, however, some of the lost strength can be recovered back while using irradiated PET instead of regular PET. Similarly, silica fume and fly ash were also added for the purpose to achieve high strength cement grouts. The elemental and chemical composition of cement (OPC), silica fume and fly ash are given in **Table 3**. Initially, cement grouts were produced by varying water-cement (w/c) ratio (0.25 to 0.45) and superplasticizer (0–2%) and were evaluated for flowability using Malaysian flow cone and compressive strength at 1-day, 7-days and 28-days curing. Based on flowability in the range of 11 sec to 16 sec, maximizing compressive strength and taking into account the bleeding problem, w/c ratio of 0.35 and superplasticizer of 1% were selected. Further grouts were produced by replacing OPC with regular PET, Irradiated PET, fly ash and silica fume. The compositions are demonstrated in **Table 4**.

Material	SiO ₂	Al ₂ O ₃	Fe ₂ O ₃	CaO	MgO	K ₂ O	SO ₃	TiO ₂	P ₂ O ₅	Na ₂ O	Others
Cement	22.65	4.63	2.34	61.72	4.23	1.14	2.24	0.20	0.12	0.11	0.62
Silica Fume	92.5	0.92	0.8	0.93	1.6	0.5	0.82	—	—	0.2	1.73
Fly Ash	36.4	13.72	18.24	19	3.26	2.2	2.5	1.45	1.2	1.73	0.3

Table 3.
 Elemental and chemical composition of cement, silica fume and fly ash.

Grout symbol	PET % (regular/irradiated)	Fly ash %	Silica fume %	Other constitutes
G1	0	0	0	0.35 w/c ratio 1% SP
G2	2.5	10	—	
G3	5	10	—	
G4	7.5	10	—	
G5	10	10	—	
G6	2.5	—	5	
G7	5	—	5	
G8	7.5	—	5	
G9	10	—	5	

Table 4.
 Constitutes of PET based cement grouts.

7.1 Flow properties of PET-based grouts

The flowability/fluidity of cement grouts was determined by measuring the flow-out time of 1-liter grout using Malaysian flow-cone. The results of fluidity are demonstrated in **Figure 7**. It can be seen that increasing PET content tends to increase the flow-out time and hence causes a reduction in fluidity. However, no

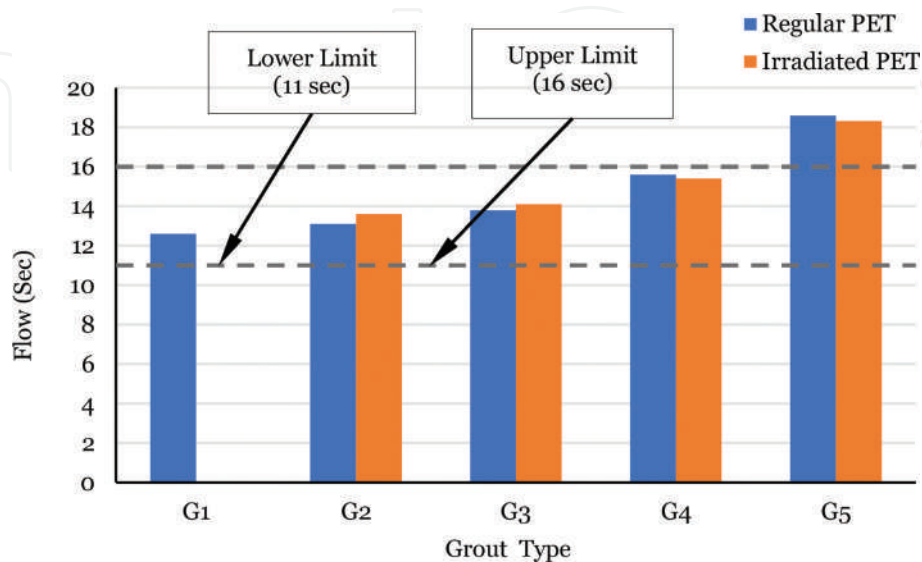


Figure 7.
 Fluidity of cement grouts containing PET and FA.

significant change occurs due to the irradiation of the PET. Moreover, the fluidity of all grouts is within the range of 11 sec to 16 sec except grout containing 10% PET (regular and irradiated). The reduction in the fluidity of grout containing PET is due to the relatively large particle size of PET as compared to cement which restricts the free movement of a particle in the grouts.

Similar behavior is also noticed in grouts containing PET and silica fume as illustrated in **Figure 8**. The fluidity decreased with increasing PET content in the presence of silica fume as compared to controlled grouts. However, the fluidity of grouts containing silica fume is quite lower than that of grouts containing fly ash at the same PET contents. In this case, the fluidity of grouts containing 7.5% PET and 10% PET does not lie within the required range and hence cannot be recommended for SFP surfaces.

7.2 Strength of grouts containing irradiated PET

The compressive strength of grouts was determined by fabricating cube specimens of dimension 50 mm *50 mm *50 mm. After demolding, the specimens were cured in water and tested for compression test at 7-days and 28-days curing age. The results are illustrated in **Figures 9–12**.

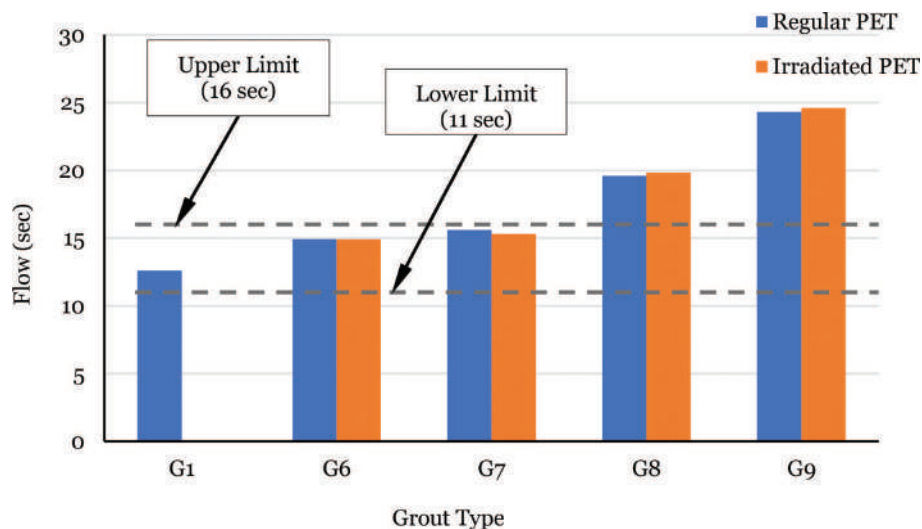


Figure 8.
Fluidity of cement grouts containing PET and SF.

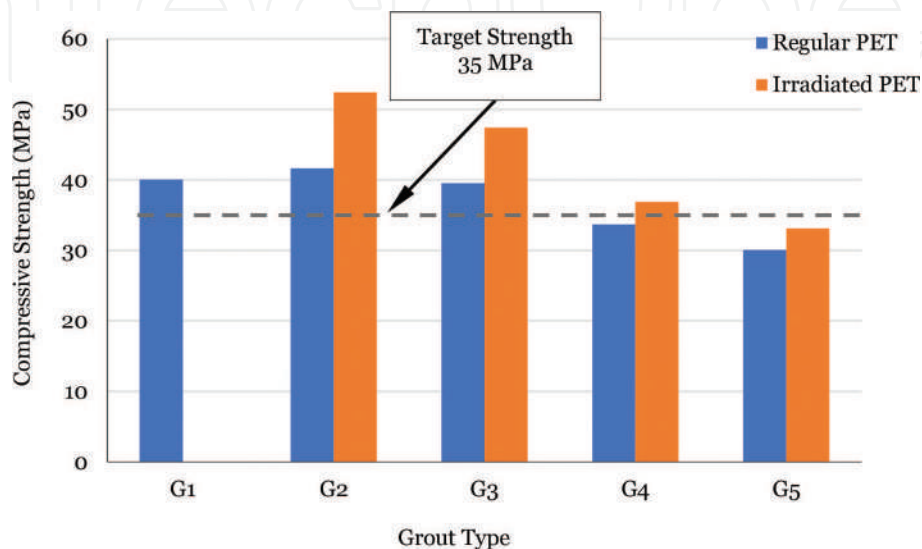


Figure 9.
Compressive strength (7-days) of grouts containing PET and FA.

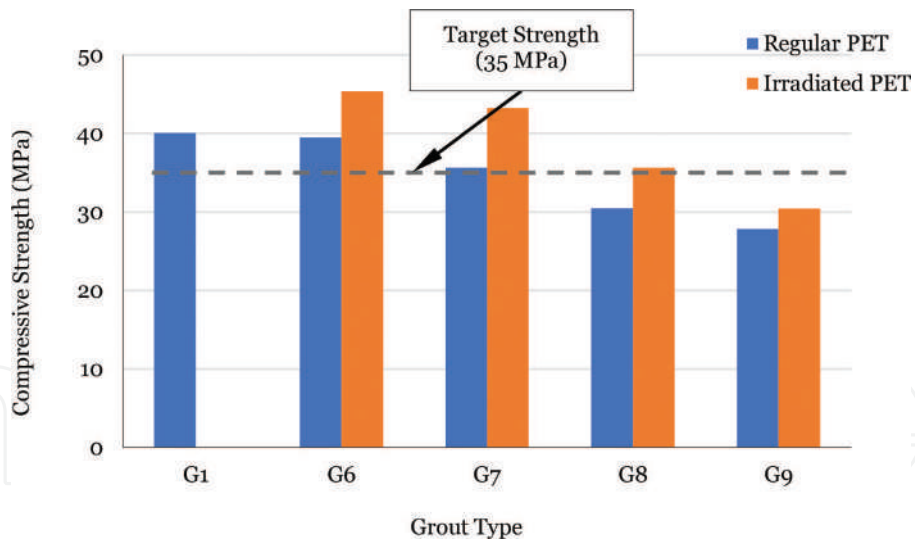


Figure 10.
Compressive strength (7-days) of grouts containing PET and SF.

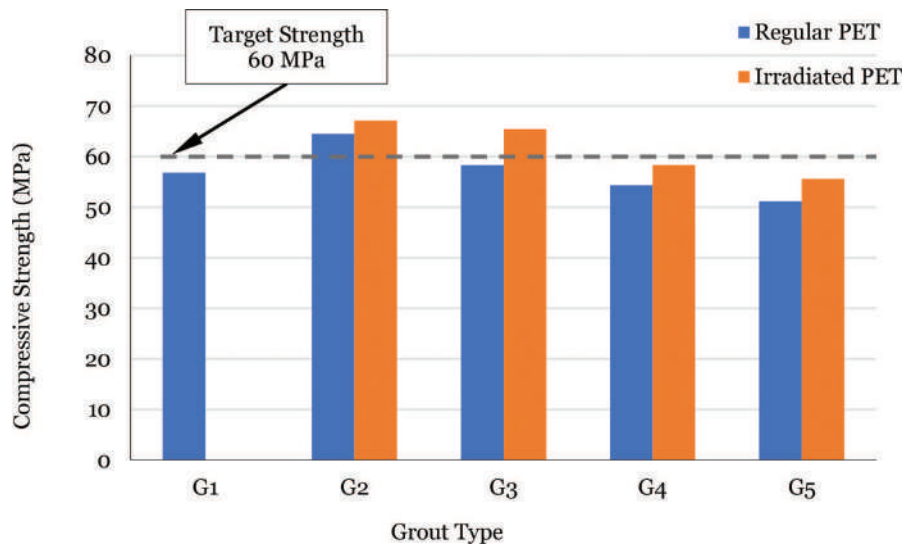


Figure 11.
Compressive strength (28-days) of grouts containing PET and FA.

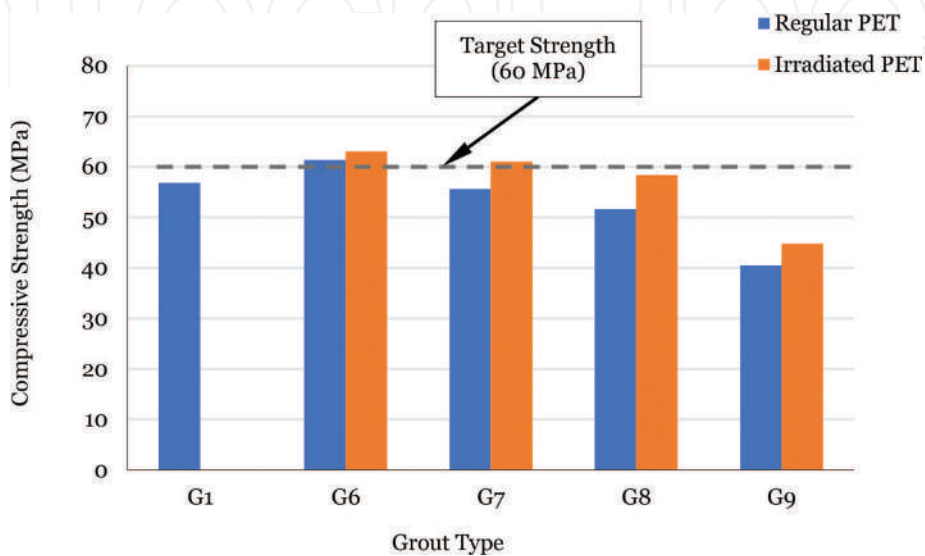


Figure 12.
Compressive strength (28-days) of grouts containing PET and SF.

It is a well-known fact that replacing cement with PET causes a significant reduction in strength properties. On the other hand, compressive strength is improved while using 10% FA as a cement replacement and in combination with a superplasticizer. It can be seen from **Figure 9**, grout containing 2.5% regular PET and 10% FA (G2) has slightly higher 7-days compressive strength compared to controlled grout (G1). Despite 10% FA, all other grouts containing regular PET (i.e 5%PET, 7.5%PET, and 10%PET) have 7-days compressive strength lower than that of control grout. It is due to the loss in compressive strength while replacing cement with PET. Interestingly, a significant amount of strength has been recovered while using irradiated PET instead of regular PET as shown in G2 to G5. The strength recovery is higher at a lower percentage of PET (i.e 2.5% and 5%) and lower at higher percentages. The purpose of this study was to recycle the maximum percentage of waste PET while achieving the target 7-days compressive strength of 35 MPa. Hence, it can be seen that the cement grout containing 7.5% regular PET does not achieve the target strength, however, with the irradiation the same dosage of PET replacement reached the target strength. Similar behavior is noticed in the grouts containing silica fume and PET as shown in **Figure 10**. However, the 7-days compressive strength of all grouts containing regular PET (G6 to G9) is lower than controlled grout (G1).

Moreover, 28-days compressive strength gives a more clear picture to decide the final maximum percentage of PET that can replace cement in the grouts. **Figure 11** depicts that grout with 2.5% PET (both regular and irradiated) achieved the target strength of 60 MPa. However, grout containing 5% of regular PET does not reach the target line. Interestingly, 5% of irradiated PET recovered the strength loss and reached the target strength. Furthermore, 7.5% PET and 10% PET (both regular and irradiated) have lower compressive strength than the target value and hence cannot be recommended. The very similar behavior is also witnessed in the grouts containing silica fume in addition to regular and irradiated PET as shown in **Figure 12**. Grout containing 5% irradiated PET just achieved the target strength of 60 MPa while the strength of 5% regular PET is quite lower than the target line. Moreover, the overall strength of grouts containing FA is higher than that of grouts containing SF.

8. Conclusion

In the current study, cement in the grouts was replaced with PET (regular and irradiated), fly ash and silica fume and were evaluated for flowability and strength properties. Following conclusions are summarized from this study.

The air voids content in the range of 25–35% is generally required in mix designing the open-graded asphalt mixtures for semi-flexible pavement surfaces. These voids are required to ensure the interconnectivity of voids in the mixture to allow grout infiltration.

Highly flowable cement grouts are required to properly fill the voids in the open graded asphalt mix. Utilization of superplasticizer not only reduce the water-cement ratio but also improve strength properties up to some extent. Similarly, the pozzolanic reaction of fly ash and silica fume is also enhanced by using superplasticizer and help in improving 7-days and 28-days compressive strength as compared to controlled grout.

Utilizing regular PET causes a significant reduction in the compressive strength of grout. However, the irradiation process of PET (by exposing to gamma rays) recovers some strength which was lost due to regular PET. Similarly, the compressive strength was also improved by additional replacement of cement with fly ash and silica fume.

In achieving the target fluidity of 11–16 sec and 28-days compressive strength of 60 MPa, a maximum of 2.5% regular PET can be used as a cement replacement in addition to fly ash and silica fume. Interestingly, the same range of fluidity and target strength was achieved with 5% irradiated PET. Hence, the irradiation of PET can be used as an effective way to recycle a relatively large amount of plastics in the construction industry to achieve sustainability.

Finally, 0.35 w/c ratio, 1% superplasticizer, 5% irradiated PET in addition to 10% fly ash or 5% silica fume are recommended as a composition of cement grouts that can be used in designing semi-flexible pavement surfaces with an aim of sustainability and reducing greenhouse gas emission.

Author details

Muhammad Imran Khan^{1*}, Muslich Hartadi Sutanto¹, Madzlan Bin Napiah¹ and Salah E. Zoorob²

1 Department of Civil and Environmental Engineering, Universiti Teknologi PETRONAS, Malaysia

2 Construction and Building Materials Program, Kuwait Institute for Scientific Research, Kuwait

*Address all correspondence to: muhammad_17007177@utp.edu.my

IntechOpen

© 2020 The Author(s). Licensee IntechOpen. This chapter is distributed under the terms of the Creative Commons Attribution License (<http://creativecommons.org/licenses/by/3.0>), which permits unrestricted use, distribution, and reproduction in any medium, provided the original work is properly cited. 

References

- [1] Zarei, S., et al., Experimental analysis of semi-flexible pavement by using an appropriate cement asphalt emulsion paste. *Construction and Building Materials*, 2020. **230**: p. 116994.
- [2] Cai, J., et al., Comprehensive service properties evaluation of composite grouting materials with high-performance cement paste for semi-flexible pavement. *Construction and Building Materials*, 2017. **153**: p. 544-556.
- [3] Abedini, M., et al., Low-temperature adhesion performance of polymer-modified Bitumen emulsion in chip seals using different SBR latexes. *Petroleum Science and Technology*, 2017. **35**(1): p. 59-65.
- [4] Moghaddam, T.B., M.R. Karim, and M. Abdelaziz, A review on fatigue and rutting performance of asphalt mixes. *Scientific Research and Essays*, 2011. **6**(4): p. 670-682.
- [5] Xu, T. and X. Huang, Investigation into causes of in-place rutting in asphalt pavement. *Construction and Building Materials*, 2012. **28**(1): p. 525-530.
- [6] Hou, S., T. Xu, and K. Huang, Investigation into engineering properties and strength mechanism of grouted macadam composite materials. *International Journal of Pavement Engineering*, 2016. **17**(10): p. 878-886.
- [7] Ling, T.-Q., et al., The Application of Semi-Flexible Pavement on Heavy Traffic Roads. *International Journal of Pavement Research and Technology*, 2009. **2**(5).
- [8] Oliveira, J.R.M., N.H. Thom, and S.E. Zoorob, Design of Pavements Incorporating Grouted Macadams. *Journal of Transportation Engineering*, 2008. **134**(1): p. 7-14.
- [9] Disfani, M.M., et al., Performance evaluation of semi-flexible permeable pavements under cyclic loads. *International Journal of Pavement Engineering*, 2020. **21**(3): p. 336-346.
- [10] Pratelli, C., et al., Preliminary In-Situ Evaluation of an Innovative, Semi-Flexible Pavement Wearing Course Mixture Using Fast Falling Weight Deflectometer. *Materials (Basel, Switzerland)*, 2018. **11**(4): p. 611.
- [11] Tran, T.N., et al. Semi-flexible material: The sustainable alternative for the use of conventional road materials in heavy-duty pavement. in *Congrès International de Géotechnique–Ouvrages–Structures*. 2017. Springer.
- [12] LING, T.-q., et al., Research on performance of water-retention and temperature-fall semi-flexible pavement material. *China Journal of Highway and Transport*, 2010. **2**.
- [13] Al-Qadi, I.L., H. Gouru, and R. Weyers, Asphalt Portland cement concrete composite: laboratory evaluation. *Journal of transportation engineering*, 1994. **120**(1): p. 94-108.
- [14] Pei, J., et al., Design and performance validation of high-performance cement paste as a grouting material for semi-flexible pavement. *Construction and Building Materials*, 2016. **126**: p. 206-217.
- [15] Afonso, M.L., et al., Development of a semi-flexible heavy duty pavement surfacing incorporating recycled and waste aggregates – Preliminary study. *Construction and Building Materials*, 2016. **102**: p. 155-161.
- [16] Yang, B. and X. Weng, The influence on the durability of semi-flexible airport pavement materials to cyclic wheel load test. *Construction and Building Materials*, 2015. **98**: p. 171-175.

- [17] Hirato, T., M. Murayama, and H. Sasaki, Development of high stability hot mix asphalt concrete with hybrid binder. *Journal of Traffic and Transportation Engineering (English Edition)*, 2014. **1**(6): p. 424-431.
- [18] Hassani, A., M. Taghipoor, and M.M. Karimi, A state of the art of semi-flexible pavements: Introduction, design, and performance. *Construction and Building Materials*, 2020. **253**: p. 119196.
- [19] Cai, X., et al., Interlocking property evaluation of dual skeleton in semi-flexible pavement material by micromechanical model and X-ray computed tomography. *Construction and Building Materials*, 2020. **254**: p. 118934.
- [20] Oliveira, J.R., Grouted macadam: material characterisation for pavement design. 2006, University of Nottingham: Nottingham.
- [21] Corradini, A., et al., Improved understanding of grouted mixture fatigue behavior under indirect tensile test configuration. *Construction and Building Materials*, 2017. **155**: p. 910-918.
- [22] An, S., et al., Laboratory and Field Evaluation of a Novel Cement Grout Asphalt Composite. *Journal of Materials in Civil Engineering*, 2018. **30**(8): p. 04018179.
- [23] Gong, M., et al., Evaluation on the cracking resistance of semi-flexible pavement mixture by laboratory research and field validation. *Construction and Building Materials*, 2019. **207**: p. 387-395.
- [24] Hassan, K., A. Setyawan, and S. Zoorob. Effect of cementitious grouts on the properties of semi-flexible bituminous pavements. in *Proceedings of the 4th European Symposium on Performance of Bituminous and Hydraulic Materials In Pavements, Bitmat 4*, 11-12 April 2002, Nottingham, UK. 2002. Routledge.
- [25] Cihackova, P., et al., Performance characteristics of the open-graded asphalt concrete filled with a special cement grout. *Baltic Journal of Road and Bridge Engineering*, 2015. **10**(4): p. 316-324.
- [26] Saboo, N., et al., Development of hierarchical ranking strategy for the asphalt skeleton in semi-flexible pavement. *Construction and Building Materials*, 2019. **201**: p. 149-158.
- [27] Saboo, N., et al., Optimal proportioning of grout constituents using mathematical programming for semi flexible pavement. *International Journal of Pavement Research and Technology*, 2019. **12**(3): p. 297-306.
- [28] Van de Ven, M. and A. Molenaar, Mechanical Characterization of Combi-layer. *Asphalt paving technology*, 2004. **73**: p. 1-22.
- [29] Anderton, G.L., Engineering properties of resin modified pavement (RMP) for mechanistic design. 2000: U.S. Army Corps of Engineers, Engineer Research and Development Center.
- [30] Setyawan, A., Development of semi-flexible heavy-duty pavements. 2006, University of Leeds.
- [31] Ahlrich, R.C. and G.L. Anderton, Construction and Evaluation of Resin Modified Pavement. 1991, Army Engineer Waterways Experiment Station Vicksburg MS Geotechnical Lab: Army Engineer Waterways Experiment Station Vicksburg MS Geotechnical Lab.
- [32] British Board of Agreement (BBA), Hardicrete Heavy Duty Surfacing. 1994, British Board of Agreement (BBA), Agreement Certificate No 88/1969. Watford.
- [33] British Board of Agreement (BBA), Worthycim Heavy Duty Paving. 1996, British Board of Agreement (BBA), Agreement Certificate 87/1900. Watford.

- [34] ApS, C. A Jointless Wearing Course with High Strength for High Loads. 2018 [cited 2018 December]; Available from: <http://www.confalt.com/confaltr.html>.
- [35] Densit-a/s, "Densiphalt Handbook". 2000, Aalborg,.
- [36] Ahlrich, R.C. and G.L. Anderton. Resin Modified Pavement in Airfield Applications. in Airport Pavement Innovations. Theory to Practice. Proceedings of Conference Held Sept 8-10, 1993, Vicksburg, Mississippi, USA. 1993.
- [37] Ricci, R., Laboratory study of grouted macadams impregnated with mine waste geopolymeric binder. 2012, University Di Bologna.
- [38] Anderton, G.L., Engineering properties of resin modified pavement (RMP) for mechanistic design. 2000: Engineer Research and Development Center Vicksburg MS Geotechnical Lab.
- [39] Vavrik, W.R., et al., The bailey method of gradation evaluation: the influence of aggregate gradation and packing characteristics on voids in the mineral aggregate (with discussion). Journal of the Association of Asphalt Paving Technologists, 2001. **70**.
- [40] AASHTO T 305, Standard method of test for determination of draindown characteristics in uncompacted asphalt mixtures. 2005, American Association of State Highway and Transportation Officials.
- [41] ASTM D6390, Standard Test Method for Determination of Draindown Characteristics in Uncompacted Asphalt Mixtures, in ASTM International, West Conshohocken, PA. 2017, ASTM International, West Conshohocken, PA: ASTM International, West Conshohocken, PA.
- [42] Hou, S., T. Xu, and K. Huang, Aggregate Gradation Influence on Grouting Results and Mix Design of Asphalt Mixture Skeleton for Semi-Flexible Pavement. Journal of Testing and Evaluation, 2017. **45**(2): p. 591-600.
- [43] REAM, Road Engineering Association of Malaysia, "Specification of Semi-Rigid Wearing Course". 2007, Road Engineering Association of Malaysia (REAM).
- [44] P.W.D, Public Works Department "Description of Workmanship and Materials (Semi-Rigid Pavement), Section E" City Hall Kuala Lumpur, Kuala Lumpur, Malaysia, 2003. 2003.
- [45] Anagnostopoulos, C.A., Effect of different superplasticisers on the physical and mechanical properties of cement grouts. Construction and Building Materials, 2014. **50**: p. 162-168.
- [46] Imran Khan, M., et al., Optimization of Cementitious Grouts for Semi-Flexible Pavement Surfaces Using Response Surface Methodology. IOP Conference Series: Earth and Environmental Science, 2020. **498**: p. 012004.
- [47] Zhang, J., et al., Formulation and performance comparison of grouting materials for semi-flexible pavement. Construction and Building Materials, 2016. **115**: p. 582-592.
- [48] Koting, S., et al., Effects of Using Silica Fume and Polycarboxylate-Type Superplasticizer on Physical Properties of Cementitious Grout Mixtures for Semiflexible Pavement Surfacing. The Scientific World Journal, 2014. **2014**: p. 7.
- [49] Zhong, K., et al., Interfacial and mechanical performance of grouted open-graded asphalt concrete with latex modified cement mortar. Construction and Building Materials, 2020. **234**: p. 117394.
- [50] Xu, Y., et al., High-Performance Semi-Flexible Pavement Coating Material with the Microscopic Interface

Optimization. *Coatings*, 2020. **10**(3):
p. 268.

[51] Luo, S., et al., Open-graded asphalt concrete grouted by latex modified cement mortar. *Road Materials and Pavement Design*, 2018. **21**(1): p. 1-17.

[52] Wang, D., et al., Impact analysis of Carboxyl Latex on the performance of semi-flexible pavement using warm-mix technology. *Construction and Building Materials*, 2018. **179**: p. 566-575.

[53] Zhang, W., et al., Performance Characterization of Semi-Flexible Composite Mixture. *Materials*, 2020. **13**(2): p. 342.

[54] Cai, X., et al., Identification of microstructural characteristics in semi-flexible pavement material using micromechanics and nano-techniques. *Construction and Building Materials*, 2020. **246**: p. 118426.

[55] Zhang, H., et al., Study on the mechanical performance and application of the composite cement-asphalt mixture. *International Journal of Pavement Engineering*, 2019. **20**(1): p. 44-52.